Unit Commitment with Uncertainty

by

Chao Li

A Dissertation Presented in Partial Fulfillment
of the Requirements for the Degree
Doctor of Philosophy

Approved November 2016 by the
Graduate Supervisory Committee:

Kory W. Hedman, Co-Chair
Muhong Zhang, Co-Chair
Pitu B. Mirchandani
Teresa Wu

ARIZONA STATE UNIVERSITY

December 2016

ABSTRACT

This dissertation carries out an inter-disciplinary research of operations research, statistics, power system engineering, and economics. Specifically, this dissertation focuses on a special power system scheduling problem, a unit commitment problem with uncertainty. This scheduling problem is a two-stage decision problem. In the first stage, system operator determines the binary commitment status (on or off) of generators in advance. In the second stage, after the realization of uncertainty, the system operator determines generation levels of the generators. The goal of this dissertation is to develop computationally-tractable methodologies and algorithms to solve large-scale unit commitment problems with uncertainty.

In the first part of this dissertation, two-stage models are studied to solve the problem. Two solution methods are studied and improved: stochastic programming and robust optimization. A scenario-based progressive hedging decomposition algorithm is applied. Several new hedging mechanisms and parameter selections rules are proposed and tested. A data-driven uncertainty set is proposed to improve the performance of robust optimization.

In the second part of this dissertation, a framework to reduce the two-stage stochastic program to a single-stage deterministic formulation is proposed. Most computation of the proposed approach can be done by offline studies. With the assistance of offline analysis, simulation, and data mining, the unit commitment problems with uncertainty can be solved efficiently.

Finally, the impacts of uncertainty on energy market prices are studied. A new component of locational marginal price, a marginal security component, which is the weighted shadow prices of the proposed security constraints, is proposed to better represent energy prices.

ACKNOWLEDGMENTS

TABLE OF CONTENTS

LIST OF TABLES

LIST OF FIGURES

Chapter 1

INTRODUCTION

1.1 Overview

Operations Research (OR) has long been known as a mathematical and analytical tool to help decision makers make better decisions. In this dissertation, the state-of-art OR-based methodologies are studied, improved and applied into the field of electric power system scheduling problems.

The National Academy of Engineering ranks the electrification as the greatest achievement of the 20th century (National Academy of Engineering, 2015). Electric power industry is an $840-billion industry in the U.S., which represents approximately 3% of the real gross domestic product (Edison Electric Institute, 2013). Each year, electric power utilities spend roughly $200-billion in their planning and operation (Energy Information Administration, 2015).

Specifically, this dissertation focuses on a special power system scheduling problem, a unit commitment (UC) problem with uncertainty. The problem is of interests in two folds. First, practically, electric power industry is one of the biggest sectors in the U.S., and a slight improvement in decision-making can lead to huge savings for social welfares. Second, theoretically, the UC problem with uncertainty is formulated as large-scale mixed integer programming, which is one of the most challenging optimization problems to solve.

This dissertation is built upon three projects as follows:

- Stochastic unit commitment with intermittent resources (supported by Sandia National Laboratory, 1/2013-6/2013)

- Mathematical frameworks for dynamic reserve policies (supported by National Science Foundation, 8/2013-12/2014)

- Markets for ancillary services in the presence of stochastic resources (supported by Power System Engineering Research Center, 1/2015-8/2016)

The goal of this dissertation is to develop computationally-tractable OR methodologies and algorithms to solve large-scale UC problems with uncertainty; thus, to improve the reliability and economic efficiency of the power systems.

1.2   Research Focus

This dissertation carries out an inter-disciplinary research of operations research, statistics, power system engineering, and economics. Specifically, this dissertation focuses on a special power system scheduling problem, a unit commitment problem with uncertainty. This scheduling problem is a two-stage decision problem. In the first stage, system operator determines the binary commitment status (on or off) of generators in advance. In the second stage, after the realization of uncertainty, the system operator determines generation levels of the generators.

In general, the power system is a special type of network, with nodes (buses) and arcs (transmission lines). However, electricity differs from ordinary products in several ways: the demand is close to perfectly inelastic; the supplies and demands must be in balance to maintain system frequency continuously under high uncertainty; the electricity travels in the power grids (network) following the Kirchhoff's laws; the storage of bulk energy is considered too expensive with current technologies. Therefore, there are more challenges in electric power system scheduling than in other standard network or supply chain problems.

If everything in the system is certain, then the UC problem can be formulated as a deterministic mixed integer program. The problem can be solved efficiently

with commercial software, even for real-world large-scale power systems. However, uncertainty in the system may result in the inefficiency of the solution obtained from the deterministic models. The uncertainty complicates the scheduling decision-making; thus, advanced tools and methodologies are desired to make better decisions.

Currently, there are three prevalent methodologies to solve the UC problem with uncertainty: stochastic programming, robust optimization, and deterministic approximation (modeling reserves). The first two methods are limited due to the computational challenges. System operators are not convinced to implement the models yet. Industrial practice adopts modeling reserves (extra capacities that generators can deliver) to hedge uncertainty in the power systems. However, the procured reserves may not be deliverable due to post-contingency system congestion. Many ad-hoc reserve determination rules have been applied. There is a lack of systematic and mathematical approaches to determine the reserves in the system.

In the first part of this dissertation, improvements for stochastic programming and robust optimization are proposed in order to make the methodologies scalable and less conservative. In the second part of this dissertation, the focus is on replacing the two-stage UC models by a stochastic equivalent deterministic model with a set of constraints. In order to do so, the potential constraints to be included are analyzed. A necessary and sufficient condition to ensure a feasible dispatch is given. Then, a set of security constraints are explicitly described. Since the number of potential constraints is exponential, an offline simulation and data mining procedure is proposed to reduce the number of constraints to be included. In the last part of this dissertation, the market implications of the proposed security constraints are analyzed.

1.3   Summary of Chapters

Chapter 2 introduces the background of power system scheduling and market models. Basic concepts of power system scheduling are given. The process of unit commitment problem decision is described. Different types of uncertainties in the power systems are illustrated.

Chapter 3 studies the existing literature, and identifies the drawbacks of the existing methodologies. The chapter summaries the three prevalent methodologies: stochastic programming, robust optimization, and deterministic approximation (modeling reserves).

Chapter 4 formulates the problem as two-stage stochastic models. A progressive hedging algorithm is studied and improved to solve the UC problem with single-generator-failure contingency. Hedging on startup and shutdown variables is proposed. Different penalty selection rules are proposed. Finally, the progressive hedging algorithm is used as a pre-solve tool to fix most binary variables, the resulting formulation is solved as mixed integer program.

Chapter 5 proposes a data-driven uncertainty set formulation to reduce the conservativeness of robust optimization. The size of uncertainty set is reduced by decorrelate the temporal and spatial correlations of the data. The solution with the proposed uncertainty set maintains system security and reduce scheduling cost significantly.

Chapter 6 gives the theoretical supports to replace two-stage models with an equivalent deterministic model with a set of security constraints. First, a necessary and sufficient condition to ensure a feasible dispatch in the power system is explicitly given. The condition is based on a polyhedral structure. The extreme rays of the polyhedron are explicitly characterized. Then, based on the condition, different security constraints are given to respond to different types of uncertainty. With the

derived security constraints, the two-stage stochastic program is able to be replaced by an equivalent deterministic program.

Chapter 7 proposes a framework to reduce the number of constraints to be included, with the assists of offline simulation and data mining. With the proposed framework, the program can be solved efficiently with a reliable solution.

Chapter 8 studies shadow prices of the UC problem with uncertainty, and the impacts of security constraints on energy markets. With the security constraints, the prices are a better reflection of the quality of service provided by the generators.

Finally, Chapter 9 concludes this dissertation and proposes several future research directions.

Chapter 2

BACKGROUND

2.1 Electric Power System

Electric power systems can be divided into four sub-systems: the generation, transmission, distribution, and load systems, as illustrated in Figure 2.1 (U.S.-Canada Power System, 2004).
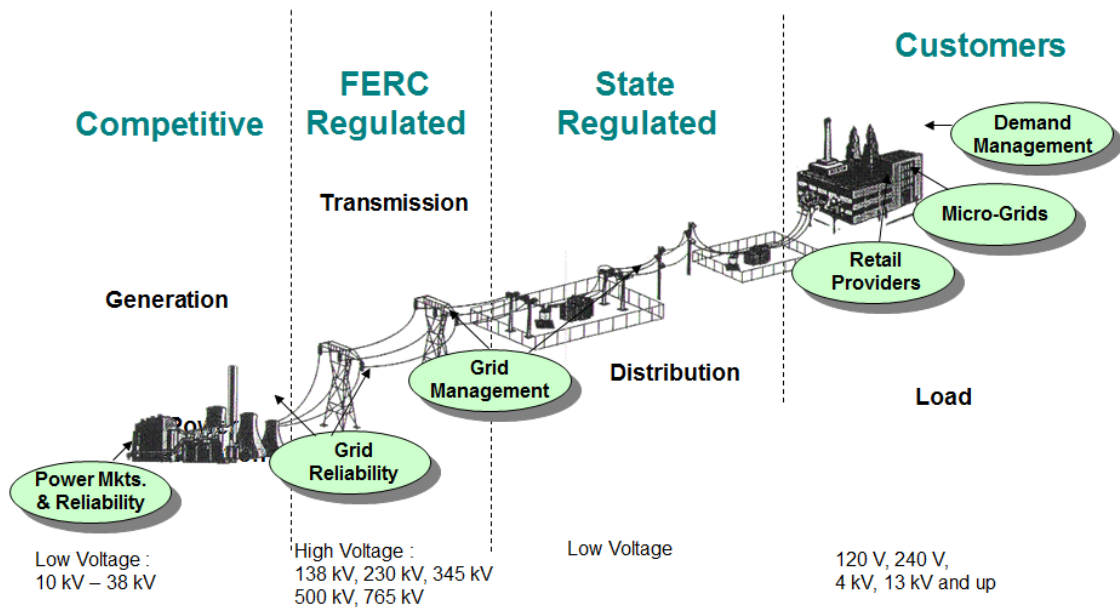
Figure 2.1: Structure of Electric Power Systems

(U.S.-Canada Power System, 2004)

The electric power industry throughout the U.S. was originally operated through vertically integrated public utilities, where the utilities own the generators and transmission lines by themselves and serve certain consumers (California ISO, 2011). As the transmission technology became more efficient, the long-distance power transmission became more viable (California ISO, 2011). This created the possibility for many

utilities to compete over the customer base (California ISO, 2011). The deregulation of the electric power industry in the U.S. was motivated by the growing dissatisfaction of the regulatory structure governing the vertically integrated utilities. This dissatisfaction stemmed from apparent operating inefficiencies, a lack of variety in the products and services available, as well as the potential for exercising market power resulting from the absence of transparency of information regarding the system state and prices. Followed the federal energy policy act in 1992, the concepts of regional transmission organization (RTO) and independent system operator (ISO) were first introduced into public. Currently, two-thirds of the U.S. power systems is served by these independent grid operators, Figure 2.2 illustrates their respective service territories (California ISO, 2011).
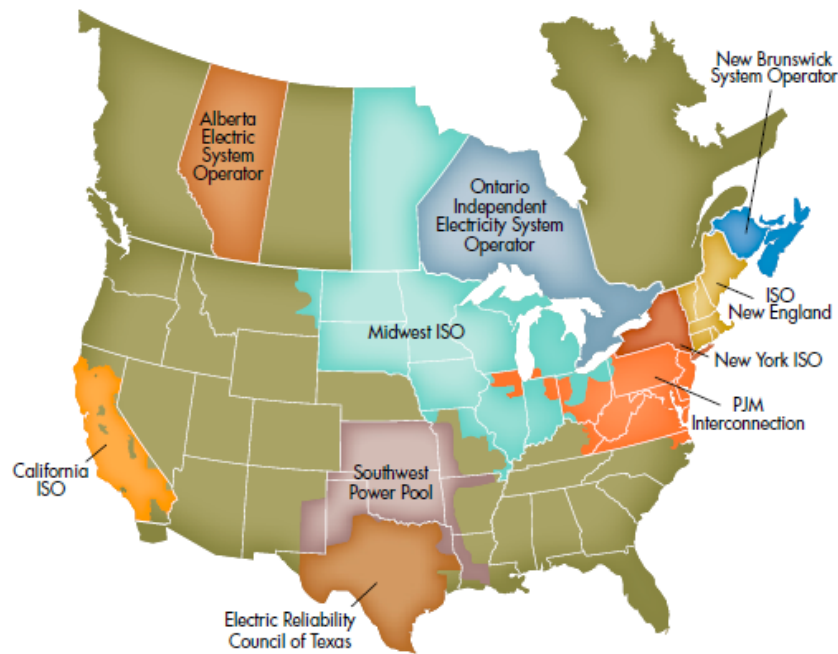
Figure 2.2: RTO/ISOs in the U.S.

(California ISO, 2011)

RTO/ISOs are non-profit independent entities and play a similar role to that of air traffic controllers in air transportation industry. RTO/ISOs focus on the planning and operation of power generation and transmission. RTO/ISOs operate the power system with different markets: including but not limited to energy market, ancillary services market, financial transmission rights market, and capacity market. The function of RTO/ISOs is to ensure transmission reliability and an efficient, competitive market.

One of the most important markets is the energy market. The energy market is a multi-settlement market including mainly day-ahead market (DAM) and real-time market (RTM). The DAM and RTM represent a forward market and a spot market. The forward (financial) market is in advance of the corresponding real-time spot (physical) market where agreements are made based on the future delivery at agreed upon forward contracts. Although different RTO/ISOs have different market clearing processes and terminologies for the processes, there is a general market clearing process describes as follows. In DAM, RTO/ISOs: a) collect bids, b) run security-constrained unit commitment (SCUC) model to determine generator commitments, c) fix commitments, run security-constrained economic dispatch (SCED) model to determine dispatch solution, d) post DAM solution and DAM prices. In RTM, RTO/ISOs: a) run SCED to balance energy supply and demand, b) determine RTM prices. Figure 2.3 (Midcontinent ISO, 2007) illustrate the DAM process in MISO.

2.2 Unit Commitment Problem

One of the most power system challenging problems is the unit commitment (UC) problem. The UC problem refers to the optimization problem that determines the generators (units) on/off status (commitments) in an economical manner. The UC problem is formulated as a mixed integer programing (MIP) due to the discrete nature
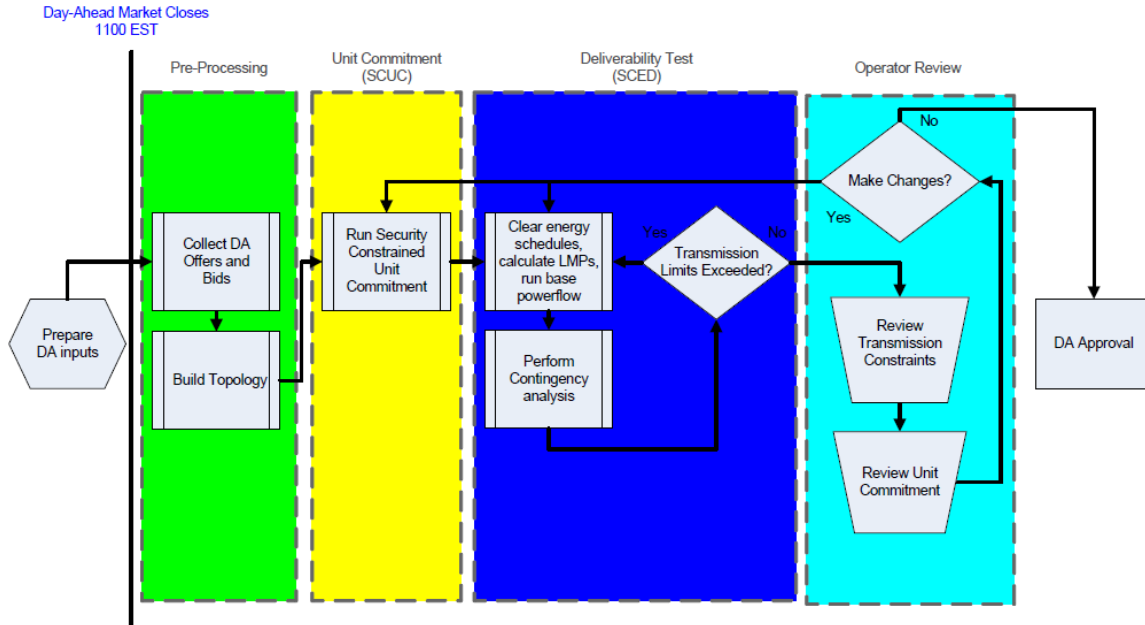
Figure 2.3: DAM Process in MISO

(Midcontinent ISO, 2007)

of the commitment decisions. This results in a non-convex optimization problem, which is a type of difficult problems to solve, known as NP-hard problems (Nemhauser and Wolsey, 1999).

The generation units in the power systems can be categorized as follows:

- Nuclear units
- Coal units
- Petroleum units
- Natural gas turbine units
- Hydro units
- Renewable units (wind, solar, ocean wave, etc.)

For the thermal (nuclear, coal, petroleum, and natural gas) units, it takes some time to start up and shut down the generators. Moreover, once the generators are turned on or off, they need to keep the commitment status for minimum up and

9

down times due to the physical requirements of the generators. Therefore, thermal units' commitment status need to be determined in advance in order to ensure enough supplies will be available during the real-time operation. RTO/ISOs solve the UC problem in their DAMs with the collected supply and demand bids.

2.3 Market Model

In DAM and RTM, RTO/ISOs solve a set of market models to obtain a schedule with the goal of maximizing the social welfare. Power flow problems are non-linear, non-convex problems (Wood and Wollenberg, 1996). RTO/ISOs adopt linearized power flow models to approximate the real power flow in the market models, as known as direct current optimal power flow (DCOPF) models (Federal Energy Regulatory Commission, 2011). A generalized market model is represented as follows:

$$\min \quad C(\mathbf{u}, \mathbf{p}) \tag{2.1}$$

$$\text{s.t.} \quad (\mathbf{u}^g, \mathbf{p}^g) \in \mathbf{X}^g \quad \forall g \qquad \text{resource-level constraints} \tag{2.2}$$

$$K(\mathbf{p}, \mathbf{D}) \leq 0 \qquad \text{system-level constraints} \tag{2.3}$$

where decision variables are commitment status, $\mathbf{u}$, and dispatch quantities, $\mathbf{p}$. Equation (2.1) is objective to minimize total system cost. Equation (2.2) represents a set of resource-level constraints restricting each generator's commitment status, $\mathbf{u}^g$, and generation level output, $\mathbf{p}^g$; where $\mathbf{X}^g, \forall g$, are feasible commitment and dispatch subspaces of each generator. The resource-level constraints include generation bounds constraints, ramping constraints, commitment minimum up/down constraints. Equation (2.3) represents a set of system-level constraints; where $K(\mathbf{p}, \mathbf{D})$ is linear functions of generation level output, $\mathbf{p}$, and forecasted load, $\mathbf{D}$. The system-level constraints usually include system-balance constraint (total generations equal to total loads) and network constraints (power flows are within transmission line limits).

2.4   Uncertainty in Power System

The uncertainty in the power systems can be categorized into discrete or continuous uncertainty. The discrete uncertainty includes the system element failure contingency events. The continuous uncertainty includes the fluctuation of loads and renewable resources.

Power system security refers to the ability to survive potential disturbances (contingencies) without interruption to customer services (Kundur *et al.*, 2004). The North American Electric Reliability Corporation (NERC) requires an N-1 contingency reliability criteria for each RTO/ISO (North American Electric Reliability Corporation, 2007). The N-1 criteria describes that the power systems must be able to withstand the loss of any single element (a generator or a non-radial transmission line or a transformer) without having any involuntary load shedding.

Transmission contingency modeling is handled efficiently today within existing commercial grade SCUC and SCED tools. Transmission contingencies are modeled by including line outage distribution factors (LODFs) to capture the change in line flows from the pre-contingency base case to the post-contingency transmission outage case (Stott *et al.*, 2009; Guo *et al.*, 2009; Davis and Overbye, 2009; Souag *et al.*, 2013; Sood *et al.*, 2014; Bo *et al.*, 2015; Dourbois *et al.*, 2016). With power transfer distribution factors (PTDF) (Wood and Wollenberg, 1996) being used to capture base-case flows, LODFs then allow for the straightforward determination of post-contingency line flows. Existing SCUC and SCED tools are able to manage transmission contingencies efficiently today; however, such tools need assistance in the management of generator contingencies.

Nowadays, more and more renewable energy resources (mainly wind and solar farms) are being built to provide electric power in order to lower generation costs

and reduce environmental pollutions. According to California Renewables Portfolio Standard (California Public Utilities Commission, 2015), the eligible renewable energy resources in California will be increased to 33% of total procurement by 2020, compared with the current 12% nationwide renewable generation (Energy Information Administration, 2014). However, the intermittent and volatile nature of the renewable resources may impact power system characteristics such as voltages, frequency and generation adequacy, which can potentially increase the vulnerability of power systems (Wang *et al.*, 2008). The intermittency refers to the unavailability of renewable for an extended period and the volatility refers to the fluctuations of the renewable within its intermittent characteristics (Wang *et al.*, 2008).

While it brings many benefits both economically and environmentally, on the other hand, the high penetration of the renewable also complicates the power system scheduling due to their uncertain nature. When solving the UC problem in the DAM, the RTO/ISOs need to make the scheduling decisions in advance with the consideration of all kinds of the uncertainty that would happen in the real-time operation. The uncertainty in the power systems complicates the power system scheduling process.

2.5   Locational Marginal Price

Most markets in the U.S. now have a nodal structure and the energy price is given as the term of the locational marginal price (LMP). The LMPs describe the total power system cost changes when consuming one more or less unit of power at a certain location. They are the uniform prices with emphasis on locational perspective. The dual variable of the node-balance constraint in the SCED is corresponding to the LMP. The LMP gives a proper pricing signal for the dispatch.

The LMP captures three components, which include the marginal energy, marginal congestion, and marginal loss components (ISO New England, 2014). The inter-

pretation of the LMP is the system total cost increment/decrement when increasing/decreasing one unit of power at the corresponding location. The shadow prices (dual variables) of the system-level constraints give marginal cost of supplying one more/less MWh of energy, i.e., the LMPs.

Chapter 3

LITERATURE REVIEW

3.1 Introduction

Many OR-based methodologies have been proposed in literature to solve the UC problems with uncertainty. Currently, there are mainly three prevalent methodologies: stochastic programming, robust optimization, and deterministic approximation via modeling reserves.

3.2 Stochastic Programming

In contrast to the deterministic formulation where all data are assumed to be fixed (usually taken as the expected value), the stochastic programming includes the presence of random quantities in the model in order to obtain the optimal decision with uncertainty (Birge and Louveaux, 1997; Shapiro *et al.*, 2009). Based on the different formulation structures, stochastic programming can be categorized as two-stage stochastic programming (TSSP), multi-stage stochastic programming (MSSP), and chance-constrained stochastic programming (CCSP) (Zheng *et al.*, 2015; Tahanan *et al.*, 2014).

3.2.1 Two-Stage Stochastic Programming

In the TSSP, the first-stage decision is made before the realization of the second-stage recourse action data. Let x denote the first-stage decision variables, y denote the second-stage decision variables. The generic linear programming form of the TSSP is described as follows,

$$\min_{x \in \mathbb{R}^n} \quad c'x + \mathbb{E}[Q(x;\xi)] \tag{3.1}$$

$$\text{s.t.} \quad Ax \le b \tag{3.2}$$

$$x \ge 0 \tag{3.3}$$

where $Q(x;\xi)$ is the optimal value of the second-stage problem, and the random vector $\xi := (\tilde{q}, \tilde{h}, \tilde{T}, \tilde{W})$ is corresponding to the data of the second-stage problem.

The second-stage problem is given as follows,

$$\min_{y \in \mathbb{R}^m} \quad \tilde{q}'y \tag{3.4}$$

$$\text{s.t.} \quad \tilde{W}y = \tilde{h} - \tilde{T}x \tag{3.5}$$

$$y \ge 0. \tag{3.6}$$

The second-stage objective is the expectation with respect to the probability distribution of the random vector ξ. Instead of using the distribution of ξ, a series of discrete scenarios that derived from the historical data are included. Each scenario $\xi^s := (\tilde{q}^s, \tilde{h}^s, \tilde{T}^s, \tilde{W}^s)$ of the TSSP is assigned with a probability $\pi^s, s = 1, 2, \cdots, S$. Then by listing all scenarios, the TSSP can be reformulated as its extensive form formulation as follows,

$$\min \quad c'x + \sum_{\forall s} \pi^s (\tilde{q}^s)'y^s \tag{3.7}$$

$$\text{s.t.} \quad Ax \le b \tag{3.8}$$

$$\tilde{W}^s y^s = \tilde{h}^s - \tilde{T}^s x \qquad \forall s \tag{3.9}$$

$$x \ge 0 \tag{3.10}$$

$$y^s \ge 0 \qquad \forall s. \tag{3.11}$$

Most of the literature formulates the UC problems with uncertainty as TSSP (Bouffard *et al.*, 2005), (Shahidehpour *et al.*, 2005), (Wu *et al.*, 2008), and (Hedman

15

et al., 2010). In the formulations, commitment decisions of the generators are put in the first stage; dispatch decisions are pushed to the second stage. The formulations follow the nature of scheduling processes that the commitment status of generators are determined in advance and the dispatch decisions are determined in the real-time operation when uncertainties are revealed. TSSP formulation of the UC problem optimizes the decisions to minimize the total scheduling costs including the day-ahead commitment costs and the expected real-time dispatch costs.

TSSP is a straightforward way to formulate the UC problems with uncertainty. However, the solution quality is dependent on the scenarios and their probability distribution. The scenario selection itself is a very challenging problem. A lot of literature has studied the scenario selection and reduction. Dupačová *et al.* (2003) studied the scenarios reduction algorithms. Papavasiliou and Oren (2013) applied importance sampling algorithm to generate wind scenarios.

The TSSP extensive form formulation by including all scenarios explicitly is computationally intractable to solve within allowable time for real-world electric power systems. Decomposition algorithms are applied in order to solve the problem.

The TSSP has a nice "L-shape" structure, it can be solved by Benders' decomposition (Benders, 1962) and (Nemhauser and Wolsey, 1999). Wang *et al.* (2008) solved the security-constrained UC problem by adding Benders' cuts. Zheng *et al.* (2013) applied a Benders' decomposition-based method to solve the UC problem with discrete decisions in the second stage. However, the drawback of the Benders' decomposition algorithm is that the master problem may grow in size (with the added optimality cuts and feasibility cuts) to the point where it can be as challenging to solve as the original extensive form formulation. Wu and Shahidehpour (2010) studied multiple strong Benders' cuts to improve the algorithm convergence.

In order to take the advantages of parallel computing structures, scenario-based decomposition algorithms are proposed to solve the TSSP. The extensive form formulation is decomposed into scenario-based sub-problems, where each sub-problem can be solved in parallel to save computational time. There are two scenario-based decomposition algorithms in the literature that have been applied to solve the power system scheduling problems, dual decomposition algorithm, and progressive hedging decomposition algorithm. Papavasiliou *et al.* (2011) applied the dual decomposition with Lagrangian relaxation on the non-anticipativity constraints to decompose the TSSP. Due to the non-convexity of the UC problem, the dual decomposition only provides the lower bound for the UC problem (minimization problem). Papavasiliou and Oren (2013) proposed a heuristics to generate feasible solutions of the problem. Watson and Woodruff (2011) studied the progressive hedging algorithm to decompose the UC problem with uncertainty. The progressive hedging algorithm guarantees to converge to the global optimal solution for convex problems. However, cycling behavior is observed for the UC problem and the algorithm cannot converge (Ryan *et al.*, 2013). Watson and Woodruff (2011) proposed several heuristics to improve convergence of the algorithm, but the performances are not stable and the optimality cannot be guaranteed. Guo *et al.* (2015) combined dual decomposition and progressive hedging algorithms to obtain both the lower and upper bounds of the UC problem.

3.2.2 Multi-Stage Stochastic Programming

MSSP is a extension of TSSP. The stages can be seen as hierarchical decisions or temporal decisions. In contrast to TSSP, which treats the second-stage data in a scenario to reveal all at one time, MSSP attempts to capture the dynamics of unfolding uncertainty over time and adjust decisions dynamically (Zheng *et al.*, 2015).

A scenario tree is often utilized to solve the MSSP. Figure 3.1 illustrates a scenario tree with four stages, eight scenarios, and fifteen nodes.
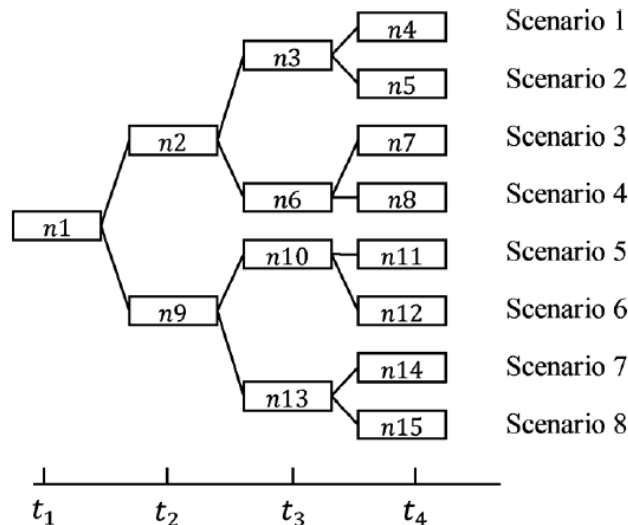
Figure 3.1: Scenario Tree Example

The decisions at any node in the decision tree should agree with each other despite how the scenario branch evolves afterwards. The MSSP is often formulated as a set of scenario-based deterministic problems with bundling constraints (Takriti *et al.*, 1996). The generic form of the MSSP is described as follows,

$$\min \quad \sum_{\forall s} \pi^s (c'x^s + (\tilde{q}^s)'y^s) \tag{3.12}$$

$$\text{s.t.} \quad Ax^s \leq b \qquad \qquad \forall s \tag{3.13}$$

$$\tilde{W}^s y^s = \tilde{h}^s - \tilde{T}^s x \qquad \qquad \forall s \tag{3.14}$$

$$x^s = x(n) \qquad \qquad \forall s \in S(n), n \tag{3.15}$$

$$x^s, y^s \geq 0 \qquad \qquad \forall s \tag{3.16}$$

where decisions x, y are corresponding to the same decisions in the TSSP. However, in the MSSP, each scenario has its own first-stage decision $x^s, \forall s$.

18

In contrast to the TSSP that all first-stage decisions are restricted to be the same, the MSSP only restricts the decisions in the same node of the decision tree to be consistent, as described in equation (3.15), where $x(n), \forall n$ are the first-stage decisions at each node of the decision tree and $S(n)$ is the subset of scenarios going through the node n.

Takriti *et al.* (1996) formulated the UC problem with uncertainty as the MSSP with bundling constraints and applied dynamic programming to solve the problem. In their model, the model is formulated without network constraints, ramping constraints, nor minimum up/down constraints. Shiina and Birge (2004) applied column generation algorithm to decompose the MSSP. The MSSP adds more computational complexity with the scenario tree structure. One of the biggest disadvantages is the cures of dimensionality that the nodes of the scenario tree grow exponentially.

3.2.3 Chance-Constrained Stochastic Programming

CCSP is another way to manage the risks by including a set of chance constraints. In the case that a generated scenario may be rare and extreme, one as an optimizer may not want to sacrifice more resources to respond to that scenario. Instead, the optimizer may want a good solution with certain confidence levels, such as 90% or 95% of the scenarios. A generic form of the chance constraints is described as follows,

$$\min \quad f(x) \tag{3.17}$$

$$\text{s.t.} \quad \mathbb{P}\{A(\xi)x \leq b(\xi)\} \geq 1 - \epsilon \tag{3.18}$$

$$x \in X \tag{3.19}$$

where $x \in \mathbb{R}^n$ are the decision variables, $A(\xi)$ and $b(\xi)$ are the technology matrix and right hand side with respect to the random variable ξ, ϵ is the risk level with small value such as 0.05 or 0.1, and X is subspace of $\mathbb{R}^n$.

19

The chance constraints have been applied in the UC problem with different risk measurements. Ozturk *et al.* (2004) included the chance constraints to satisfy the loads. Wang *et al.* (2012) enforced the chance constraints to restrict the wind power utilization in the power systems.

The chance constraints are equivalent to restricting value at risk (VaR). Conditional value at risk (CVaR) gives another way for the tradeoff. The CVaR is also referred as the expected shortfall or expected tail loss. The CVaR is a coherent and more conservative risk measurement. Suppose the loss of loads, l, are used as a risk measurement, the CVaR is described as follows,

$$\text{CVaR}_\epsilon(l(\xi)) = \mathbb{E}\left[l(\xi)|\text{VaR}_\epsilon(l(\xi)) \geq \eta\right] \tag{3.20}$$

where η is a pre-specified maximum allowed loss of loads, and

$$\text{VaR}_\epsilon(l(\xi)) = \inf\left\{l|\mathbb{P}(l \geq l(\xi)) \geq 1 - \epsilon\right\}. \tag{3.21}$$

The chance constraints are generally non-convex. Moreover, the constraints are highly dependent on the random variable distribution, which is difficult to evaluate in practice. Statistical methodologies such as Monte Carlo simulation have been applied to solve the CCSP. Ozturk *et al.* (2004) reformulated the CCSP into a set of linear constraints with statistical properties and assumptions. Wang *et al.* (2012) proposed sample average algorithms to solve the CCSP.

3.3 Robust Optimization

The robust optimization is an alternative to solve the UC problems with uncertainty. Instead of formulating scenarios, the robust optimization optimizes the problem under an uncertainty set (Bertsimas and Sim, 2003). Each point in the uncertainty set can be seen as one potential data realization during the operation. The

uncertain data (e.g., the loads and renewable resources) in the uncertainty set are restricted by some constraints such as a lower bound and an upper bound. The robust optimization for the UC problem returns the most cost-efficient solution ensuring the system reliability against the worst case (data realization).

Robust optimization (RO) has recently gained substantial popularity as a decision making tool under uncertainty, led by the work in (Ben-Tal and Nemirovski, 1998), (Ben-Tal and Nemirovski, 1999), (Bertsimas and Sim, 2004), and (Bertsimas and Thiele, 2006). The need for RO has been recognized in several power system applications: robust unit commitment (Zhao and Zeng, 2012), (Jiang *et al.*, 2012), and (Bertsimas *et al.*, 2013), transmission planning (Jabr, 2013) and (Chen *et al.*, 2014), and contingency analysis (Wang *et al.*, 2013) and (Street *et al.*, 2011), etc.

3.3.1   Uncertainty Sets

If the scenario selection is the key factor for the stochastic programming, then the uncertainty set is critical for the robust optimization. Since the robust optimization protects the worst-case scenario, then the solution is often regarded as very conservative. Therefore, it is critical to construct an effective uncertainty set that is less conservative while retaining robustness. The conservativeness of the robust optimization solution can be controlled by the formulation of the uncertainty sets (Bertsimas and Sim, 2003).

Previous studies of uncertainty sets can be divided into two groups. The first group makes mild assumptions about certain structural features of uncertainty sets, referred to as the rule-based set. The most trivial one is a box uncertainty set, where uncertain parameters are assumed to vary within an interval (Soyster, 1973). Bertsimas and Sim (2004) proposed the budget of uncertainty to adjust the conservativeness of the box uncertainty set. The uncertainty sets are modeled as polyhedral (Atamtürk

and Zhang, 2007), and ellipsoidal (Ben-Tal and Nemirovski, 1998) and (Ben-Tal and Nemirovski, 1999) structures for the sake of computational tractability.

The following lists two canonical rule-based uncertainty sets,

Cardinality-restricted uncertainty set:

$$\Omega_C = \left\{ \mathbf{d} : \sum_n \lceil |d_n - \bar{d}_n|/h_n \rceil \leq \Gamma, \ \bar{d}_n - h_n \leq d_n \leq \bar{d}_n + h_n, \forall n \right\} \tag{3.22}$$

Budget uncertainty set:

$$\Omega_B = \left\{ \mathbf{d} : \sum_n \pi_n d_n \leq \pi_0, \ \bar{d}_n - h_n \leq d_n \leq \bar{d}_n + h_n, \forall n \right\} \tag{3.23}$$

The second group utilizes data to design uncertainty sets. Bertsimas and Brown (2009) construct uncertainty sets using the theory of coherent risk measures. The confidence region of statistical hypothesis test is used to quantify the uncertainty set in (Bertsimas *et al.*, 2015). Several rules are suggested to shrink the size of uncertainty sets based on historical data in (Guan and Wang, 2014). Lorca and Sun (2015) develops dynamic uncertainty sets to capture the temporal and spatial correlations of uncertainty.

3.3.2   Two-Stage Robust Optimization

The two-stage robust optimization (TSRO) and the TSSP share many similar features. Let x be the first-stage decision variables and let y be the second-stage decision variables. The generic form of the TSRO is described as follows,

$$\min_{x \in \mathbb{R}^n} \quad c'x + \max_{\mu \in \Omega} Q(x, \mu) \tag{3.24}$$

$$\text{s.t.} \quad Ax \leq b \tag{3.25}$$

$$x \geq 0 \tag{3.26}$$

where $Q(x, \mu)$ is the optimal value of the second-stage problem with respect to first-stage variable x and data $\mu := (\tilde{q}, \tilde{h}, \tilde{T}, \tilde{W})$ in the uncertainty set Ω.

The second-stage problem is given as follows,

$$\min_{y \in \mathbb{R}^m} \quad \tilde{q}'y \tag{3.27}$$

$$\text{s.t.} \quad \tilde{W}y = \tilde{h} - \tilde{T}x \tag{3.28}$$

$$y \geq 0. \tag{3.29}$$

Instead of optimizing the expected second-stage costs, the TSRO optimizes the total costs that includes the first-stage cost and the worst-case second-stage costs, given the uncertainty set and the first-stage decisions. Therefore, the TSRO can be seen as a three-level min-max-min optimization problem. The third term "min" is to minimize the second-stage cost; the middle term "max" is to consider the worst case in the given uncertainty set Ω; and the first term "min" is to minimize the first-stage cost with the corresponding worst-case second-stage cost. The first term is referred as the outer problem; the second and the third term together are referred as the inner problem.

Jiang *et al.* (2012) applied the TSRO to the UC problem with pumped storage hydro units. Jiang *et al.* (2012) proposed an algorithm that first derived the dual of the inner problem and then generated Benders' cuts to solve the outer problem. Zhao and Zeng (2012) proposed a primal-cut algorithm to solve the TSRO. Bertsimas *et al.* (2013) proposed an outer approximation method to solve the bi-linear inner problem. Jiang *et al.* (2014) proposed an exact algorithm to solve the TSRO with polyhedral studies. Zhao and Guan (2013) unified the TSSP and TSRO with weight coefficients in the objective function to balance the computational complexity of the stochastic programming and the conservativeness of the robust optimization.

3.4 Deterministic Approximation

In existing market practices, RTO/ISOs acquire reserves to protect the power system. The reserves are the extra capacities that generators can dispatch in real-time operation to respond to the uncertainty. The reserves are necessary for maintaining system reliability. Varieties of reserves are required for different functions. However, since the power systems and markets in the U.S. leverage adequacy-based reserve policies, the security requirements do not guarantee a N-1 reliable solution on a locational basis. The procured reserves may not be deliverable in the post-contingency states due to transmission limitations. As a result, RTO/ISOs make different types of out-of-market, operator-initiated corrections in their scheduling and operation (Al-Abdullah *et al.*, 2013; LaBove *et al.*, 2014; Al-Abdullah *et al.*, 2015).

There are many different categorizations of the reserves, according to different organizations or RTO/ISOs (Ellison *et al.*, 2012). National Renewable Energy Laboratory (NREL) categorizes the reserves into regulating reserve, following reserve, contingency reserve and ramping reserve, where the first two are responsible for non-events such as variation of the loads and the last two are responsible for events which are rare and severe such as contingency and intermittent wind power (Ela *et al.*, 2011). While most RTO/ISOs have market structures to procure reserves, their reserve requirements vary significantly. California Independent System Operator (California ISO or CAISO) defines the reserves as regulation reserve, spinning reserve, non-spinning reserve and replacement reserve. The regulation reserve is utilized for Automatic Generation Control (AGC) to ensure system frequency stays at 60Hz. The spinning reserve is provided by the generator that is in-sync, connected to the power grid; while the non-spinning reserve is provided by fast-start offline generator. Both spinning and non-spinning reserve are used primarily to respond to contingen-

cies, and are required to response in approximately 10 minutes. The replacement reserve must come on-line and provide the required output within 30 minutes to replace the spinning and non-spinning reserve. CAISO provides four types of ancillary services in their market now: regulation up, regulation down, spinning reserve and non-spinning reserve (California ISO, 2015). MISO defines the reserves as regulating up/down reserve, spinning up/down reserve, and non-spinning reserve (Midcontinent ISO, 2015b).

Although modeling reserves is straightforward and easy to implement, there are still some issues with this methodology. First, the reserve requirement level (reserve margin) is determined by some rule-of-thumb methods that are based on the operators' experience. Different RTO/ISOs have different rules for their reserve requirements. For instance, a $3 + 5$ rule is proposed by NREL, where 3% of total predicted loads and 5% of total predicted wind power are required for operating reserves (Ela et al., 2011). It can be expected that, with increasing renewable power penetration in the power systems, a systematical methodology is desired to determine the reserve requirement level. Another issue for modeling reserves is that even when substantial reserves are procured, some of the reserves may not be deliverable due to transmission line congestion.

Reserve policies and reserve zone partitions to improve system security are studied by (Doherty and O'Malley, 2005), (Zheng and Litvinov, 2008), (Ortega-Vazquez and Kirschen, 2009), and (Cotilla-Sanchez et al., 2013). Lyon et al. (2014) studied intra-zonal congestion and proposed a framework to dynamically relate the minimum reserve levels to transmission stress. Lyon et al. (2015) proposed an algorithm to disqualify the reserves that cannot be delivered. In RTO/ISOs' practice, reserve zones are given to ensure the deliverability of the reserves, where certain reserve levels are required inside each of the zone. However, the reserve zones are usually determined

by geographical boundaries, which is not very efficient. Wang and Hedman (2015) proposed a K-means clustering algorithm to determine the reserve zones based on the power transfer distribution factors and transmission congestion. Wang and Hedman (2015) grouped the buses that have similar impacts on system transmission lines together as a reserve zone. Wang and Hedman (2015) proposed dynamic zones based on the power grid congestion, where different reserve zones were determined in different periods.

3.5   Conclusions

The UC problems with uncertainty are formulated as MIP problems. The stochastic programming or robust optimization introduces substantial computational complexity, which results in the computational intractability for solving the real-world large-scale power systems. Many decomposition algorithms have been proposed to solve TSSP; however, none of them are promising. The MSSP gives a more flexible UC scheduling by considering the system dynamics, but creates more computation complexity. The CCSP complicates the UC problem by including a set of non-convex constraints. As a result, though substantial literature has been focused on stochastic programming applied in the UC problems, none of them have convinced the RTO/ISOs to implement stochastic programming in practice. RTO/ISOs are still using deterministic formulations, i.e., the proxy reserve requirements, to solve the UC problems with uncertainty. However, most reserve requirement rules are base on the operators' experience and there are few systematic methods to determine the optimal reserve allocations.

The future may lie in improving the computational capability as well as developing more suitable methodologies and algorithms to solve the UC problems with uncertainty. This dissertation is built on the existing literature, combines the deter-

ministic policies with the stochastic programming and robust optimization, in order to improve the system performance, at the same time to achieve industry adoption. This dissertation is aimed to find the balance between the deterministic models and the stochastic models. The focus is on trading off the solution quality and the computational tractability.

Chapter 4

SCENARIO-BASED DECOMPOSITION ALGORITHM

4.1 Introduction

The real-world power systems involve thousands of nodes (buses) and arcs (transmission lines), which results in the stochastic programming formulation huge in size. Moreover, there is a time constraint to solve the program, usually a few hours. Therefore, directly solving a large-scale stochastic program is computationally intractable today. One of the possible ways to solve the large-scale stochastic programs is by applying scenario-based decomposition algorithms. The decomposition algorithms break the entire problem into several smaller sub-problems, where each of the sub-problems can be solved in a short time. In addition, all the sub-problems can be solved in parallel.

This chapter studies one of the scenario-based decomposition algorithms, i.e., progressive hedging (PH) algorithm, in order to take the advantages of parallel computing to solve large-scale stochastic programs.

The PH algorithm is applied to one of the most basic UC problem with uncertainty, a single-generator-failure reliable UC problem, referred to as G-1 reliable UC henceforth. G-1 reliable UC problem aims at finding a set of UC solutions that can guarantee a feasible dispatch after any single-generator-failure contingency. The problem can be formulated as a two-stage stochastic program, where the first stage is pre-contingency base case and the second stage includes post-contingency scenarios. Since the contingencies are discrete events, all scenarios can be explicitly modeled in the stochastic program.

In this chapter, several innovations are proposed for the PH algorithm. The PH algorithm is not guaranteed to converge to the global optimal solution since the UC problem involves integer variables. Slow convergence rates and cyclic behaviors have been previously observed in practice. Hedging is conventionally performed on the UC status variables. Hedging on the startup and shutdown variables is proposed and tested in this chapter. The performance of the PH algorithm is rather sensitive to the choice in the penalty factors. Thus, several strategies for choosing the penalty factors are evaluated for the cases when using the UC status variables versus using the startup and shutdown binary variables as the hedging mechanisms. A hybrid approach using both the PH and a stochastic programing formulation is implemented in order to obtain a set of feasible UC solutions and compare different hedging methods.

This chapter is organized as follows. Section 4.2 introduces the PH algorithm. Section 4.3 describes the model formulation. Section 4.4 investigates different hedging mechanisms and penalty factors. Section 4.5 carries out computational experiments on an IEEE 73-bus test case and compares the results under different proposed methods. Finally, section 4.6 concludes the chapter.

4.2   Progressive Hedging Algorithm

The PH algorithm, first proposed by Rockafellar and Wets (1991), is a decomposition algorithm based on the augmented Lagrangian relaxation. The PH solves each scenario-based sub-problem individually as a deterministic model, combines the solution of each scenario to get an average solution, and introduces a penalty to the objective for deviating away from the average solution. The PH continues with this iterative process until it reaches a certain stopping criterion. The PH "drags" all scenarios to a unified solution. The PH converges to a global optimal solution when the problem is convex (Rockafellar and Wets, 1991).

Recently, the PH algorithm has been studied to solve large-scale stochastic programming problems. The PH does not guarantee a global optimal solution for mixed integer programming (MIP) since non-convexities. Slow convergence rates and cyclic behaviors have been previously observed in practice. However, the PH can be used as a heuristic to obtain acceptable solutions for the MIP with special structures due to its computational advantages since it is trivially parallelizable. If appropriate penalty factors can be chosen to ensure convergence to a good solution, the PH is often preferred since it can be easily parallelized and then the computational performance is generally better than other decomposition techniques. Ryan *et al.* (2013) has shown that the parallel computing structure can improve the run time and make the PH possible to be implemented in practice. The PH is also not susceptible to other common drawbacks of other decomposition algorithms where a repeatedly solved master problem may grow in size to the point where it can be as challenging to solve as the original extensive form problem, which can happen for Benders' decomposition. This is referred to as bloating and such methods are known for having long tails associated to convergence. The PH may also have a long tail effect. In this chapter, a hybrid approach using the PH as a pre-solve tool for stochastic program is proposed to avoid the drawbacks. The PH also does not have issues with other techniques where there are binary variables within the second-stage subproblems. However, the primary downside of the PH is that it is a heuristic for non-convex problems. Thus, it does not directly provide a lower bound. Gade *et al.* (2014) proved the PH could provide a lower bound for the stochastic program. However, the result is still under review.

The following Algorithm 1 describes the pseudo code of the PH algorithm for G-1 reliable UC program.

Algorithm 1 Progressive Hedging Algorithm

$k = 0$
for $s \in S$ **do**
    $x^{s,(0)} = \arg\min_x(c'x + (f^s)'y^s)$
end for
$\bar{x}^{(0)} = \sum_{\forall s} \pi^s x^{s,(0)}$
for $s \in S$ **do**
    $\omega^{s,(0)} = \rho(x^{s,(0)} - \bar{x}^{(0)})$
end for
$g^{(0)} = \sum_{\forall s} \pi^s \|x^{s,(0)} - \bar{x}^{(0)}\|$
while $g^{(k)} > \epsilon$ **do**
    $k = k + 1$
    for $s \in S$ **do**
        $x^{s,(k)} = \arg\min_x(c'x + \omega^{s,(k-1)}x + \frac{\rho}{2}\|x - \bar{x}^{(k-1)}\|^2 + (f^s)'y^s)$
    end for
    $\bar{x}^{(k)} = \sum_{\forall s} \pi^s x^{s,(k)}$
    for $s \in S$ **do**
        $\omega^{s,(k)} = \omega^{s,(k-1)} + \rho(x^{s,(k)} - \bar{x}^{(k)})$
    end for
    $g^{(k)} = \sum_{\forall s} \pi^s \|x^{s,(k)} - \bar{x}^{(k)}\|$
end while

4.3   Model Formulation

The PH has been examined for the stochastic UC (SUC) problem where the uncertainty can be based on the loads uncertainty or intermittent renewable resources (wind and solar). In this chapter, the PH algorithm is studied where the uncertainty is the potential loss of a generator. There are two primary issues that make this a more difficult problem to solve: (1) RTO/ISOs are mandated to protect their system against single contingencies and, thus, G-1 is a robust policy; and (2) the loss of a generator is a dramatic event as there is a substantial loss in supply over a very short time period. While N-1 reliability mandates that the system must be able to withstand the loss of any single generator or non-radial transmission asset (line or transformer), the studies focus only on generator outages since, typically, the generator outages are more severe than transmission outages.

In this chapter, the SUC is formulated as a two-stage stochastic program (TSSP) with second-stage scenarios that explicitly represent the single-generator-failure contingencies. The power flow is modeled as a linear approximation of the actual power flow (the alternating current optimal power flow problem), which is referred as the direct current optimal power flow (DCOPF) problem based on Hedman *et al.* (2010).

The following extensive form formulation of the SUC includes the constraints for $s = 0$, i.e., the base case, and all contingency states $s \in S$. The proposed PH framework includes, for each subproblem, an extensive form of the SUC formulation with only the base case and one G-1 contingency modeled. Next, each component of the SUC model is introduced and explained.

The objective is represented as (4.1). The model assumes a linear production cost and the total cost function involves a startup cost, a no-load cost, and a variable production cost. There is no shutdown cost in this model. The objective is to minimize the cost of the base case while ensuring it can move from the base case solution to a solution that does not have involuntary load shedding without having any post-contingency constraint violations within roughly 10 minutes of the event; this is based on the typical 10-minute spinning and non-spinning reserve requirement rules that most RTO/ISOs ensure. In this model, only the spinning reserves are considered. Since the G-1 policy is a robust criterion and the goal of the day-ahead scheduling process is to minimize the pre-contingency (base case) operating costs, the objective does not consider the costs during the potential post-contingency states.

$$\min \quad \sum_{\forall t} \sum_{\forall g} \left\{ C_g^{SU} v_{gt} + C_g^{NL} u_{gt} + C_g p_{gt}^0 \right\} \tag{4.1}$$

Equation (4.2) represents the node (flow) balance constraints, which represents the Kirchhoff's current law since it imposes that all current flowing into a bus is equal to the flow exiting the bus. Equation (4.3) represents the power flow constraints,

which is a linear approximation of the Kirchhoff's law. Equation (4.4) represents the line flow limit constraints. Equation (4.5) represents the generator bounds. Note that generation p_{gt}^s is forced to zero whenever the UC status variable, u_{gt}, or the contingency indicator, $G1_g^s$, are zero. Equation (4.5) formulates the generator failure throughout all of the planning periods to satisfy the G-1 security requirement. In this stochastic extensive form formulation, a single indicator for the generator failure is used throughout the time periods. N_g^s is not indexed by t based on the modeling of the recourse state when imposing G-1 for day-ahead UC models.

$$\sum_{\forall l \in \delta^+(n)} f_{lt}^s - \sum_{\forall l \in \delta^-(n)} f_{lt}^s + \sum_{\forall g \in G(n)} p_{gt}^s = D_{nt} \quad \forall n, t, s \tag{4.2}$$

$$f_{lt}^s = B_l(\theta_{nt}^s - \theta_{mt}^s) \quad \forall l \in (n, m), t, s \tag{4.3}$$

$$-F_l \leq f_{lt}^s \leq F_l \quad \forall l, t, s \tag{4.4}$$

$$P_g^{\min} u_{gt} G1_g^s \leq p_{gt}^s \leq P_g^{\max} u_{gt} G1_g^s \quad \forall g, t, s \tag{4.5}$$

Equation (4.6) represents the relations between the commitment status, the startup, and the shutdown binary variables. Equations (4.7) and (4.8) represent the min-up and min-downtime constraints; the constraints are facet-defining inequalities for the u, v projection (Rajan and Takriti, 2005). Equations (4.9)-(4.11) impose the restrictions on the three sets of binary variables; while the startup and the shutdown variables are binary, their integrality constraints can be relaxed since (4.6)-(4.11) force the variables to always take on a binary solution, i.e., all feasible solutions for the startup and shutdown variables are guaranteed to be binary even though they are modeled as continuous variables.

$$v_{gt} - w_{gt} = u_{gt} - u_{g,t-1} \quad \forall g, t \tag{4.6}$$

$$\sum_{\forall i=t-UT_g+1}^{t} v_{gi} \leq u_{gt} \quad \forall g, t \in \{UT_g, \cdots, T\} \tag{4.7}$$

$$\sum_{\forall i=t-DT_g+1}^{t} w_{gi} \leq 1 - u_{gt} \quad \forall g, t \in \{DT_g, \cdots, T\} \tag{4.8}$$

$$0 \leq v_{gt} \leq 1 \quad \forall g, t \tag{4.9}$$

$$0 \leq w_{gt} \leq 1 \quad \forall g, t \tag{4.10}$$

$$u_{gt} \in \{0, 1\} \quad \forall g, t \tag{4.11}$$

Equations (4.12) and (4.13) impose the hourly ramp rate limits along with the startup and shutdown ramp rate limits for the generators. Each individual scenario that is solved by the PH is an extensive form SUC problem with two states: the base case state (no contingency) and one single generator outage. The reason for this approach is to not only get a unified commitment solution but to be able to find a unified base case dispatch solution. Equations (4.14) and (4.15) are included in order to ensure that each generator can move from its base case dispatch solution to a required post-contingency dispatch solution within 10 minutes. This captures the commonly adopted procedure to ensure that the system can move from the pre-contingency state to a post-contingency state without load shedding based on the 10-minute spinning and non-spinning reserve that is available within the system (California ISO, 2015).

$$p_{gt}^0 - p_{g,t-1}^0 \leq R_g^{hr} u_{g,t-1} + R_g^{SU} v_{gt} \quad \forall g, t \tag{4.12}$$

$$p_{g,t-1}^0 - p_{gt}^0 \leq R_g^{hr} u_{gt} + R_g^{SD} w_{g,t-1} \quad \forall g, t \tag{4.13}$$

$$p_{gt}^s - p_{gt}^0 \leq R_g^{10} u_{gt} \quad \forall g, t, s \tag{4.14}$$

$$p_{gt}^0 G1_g^s - p_{gt}^s \leq R_g^{10} u_{gt} \quad \forall g, t, s \tag{4.15}$$

Equations (4.16) and (4.17) state that the amount of available 10-minute spinning reserve from a committed generator is at most its 10-minute ramp rate or the difference between its capacity and its output level, whichever is lower. Equation (4.18) states that the total reserve in the system must exceed the single largest contingency (generator). These equations are the typical spinning reserve equations that are included in a deterministic UC formulation. Equations (4.16)-(4.18) are included to ensure additional reserves (system wide) are procured. These reserve constraints form a necessary condition to guarantee G-1 reliability. Also, the reserve requirement constraints help the PH achieve a unified schedule for the UC solutions across all states in less number of iterations.

$$r_{gt}^0 \leq P_g^{\max} u_{gt} - p_{gt}^0 \quad \forall g, t \tag{4.16}$$

$$r_{gt}^0 \leq R_g^{10} u_{gt} \quad \forall g, t \tag{4.17}$$

$$\sum_{\forall i} r_{it}^0 \geq r_{gt}^0 + p_{gt}^0 \quad \forall g, t \tag{4.18}$$

The above MIP can be solve by the commercial software such as CPLEX or Gurobi.

4.4   Investigation of Hedging Mechanisms

Previous literature has only considered hedging on the UC status binary variables, u. In this chapter, the PH algorithm is applied while hedging on other sets of binary variables. Specifically, the performance of hedging on the UC status variables, u, to the startup and shutdown variables, v and w, is compared under different updating rules for the penalty factor, ρ. Adjusting ρ is necessary when the chosen hedging instrument is changed since the performance of the PH is sensitive to the selection of ρ and the associated hedging mechanism (Watson and Woodruff, 2011). The primary difference between hedging on the startup and shutdown binary variables versus the

UC status variables is that there are generally far fewer startup and shutdown binary variables that take on a solution of one as compared to the UC binary variables. Furthermore, the number of discrepancies between the startup and shutdown binary variables across the different independent (deterministic) subproblems is far less than the discrepancies for the UC status variables. Since the PH algorithm, by itself, can take a long time to converge for non-convex problems, a hybrid PH approach is taken to solve the SUC problem. In order to obtain a lower bound to the SUC problem, an extensive form formulation of the SUC is solved. With the lower bound, optimality gaps can be calculated in order to provide a benchmark to evaluate performance.

4.4.1 Hedging on Startup and Shutdown Variables

The startup variables, v, and the shutdown variables, w, indicate whether the generator is turned on or off correspondingly in period t. The relation between u, v, and w is specified by (4.6). Table 4.1-4.3 show one instance of the respective solutions for the UC status, startup, and shutdown binary variables.

Table 4.1: Unit Commitment Status Variables

Period	1	2	3	4	5	6	7	8	9	10
Gen1	0	0	1	1	1	1	1	1	0	0
Gen2	0	1	1	1	1	0	1	1	1	0
Gen3	0	0	0	1	1	0	0	1	1	1
Gen4	1	1	1	1	1	1	1	1	1	1

Table 4.2: Corresponding Startup Variables

Period	1	2	3	4	5	6	7	8	9	10
Gen1	0	0	1	0	0	0	0	0	0	0
Gen2	0	1	0	0	0	0	1	0	0	0
Gen3	0	0	0	1	0	0	0	1	0	0
Gen4	0	0	0	0	0	0	0	0	0	0

Existing PH methods generally hedge on the UC status variables, u. This is intuitive since the goal is to attain a unified UC schedule. However, based on the generic description of the PH, continuous generation variables, p^0, and binary startup and

Table 4.3: Corresponding Shutdown Variables

Period	1	2	3	4	5	6	7	8	9	10
Gen1	0	0	0	0	0	0	0	0	**1**	0
Gen2	0	0	0	0	0	**1**	0	0	0	**1**
Gen3	**1**	0	0	0	0	**1**	0	0	0	0
Gen4	0	0	0	0	0	0	0	0	0	0

shutdown variables, v and w, are also candidates as hedging mechanisms. Moreover, startup variables, v, along with shutdown variables, w, also uniquely determine the commitment schedule given the initial status of a generator. From Tables 4.1-4.3, it can be easily observed that the solution matrices, with respect to v and w, have fewer instances where they are equal to one than the matrix for u. Thus, fewer discrepancies are expected while hedging on the startup and shutdown binary variables. In addition, hedging on the startup and shutdown binary variables is expected to help improve the convergence of the PH by being able to focus more intently on dragging all of these independent subproblems to a common solution due to the ability to identify the critical periods where there are discrepancies between the startup and shutdown cycles.

4.4.2 Selection of Penalty Factors

Watson and Woodruff (2011) showed the performance of the PH is rather sensitive to the choice in the penalty factors; Watson and Woodruff (2011) also showed that the penalty factors should be proportional to the cost associated to the hedged variables. Ryan *et al.* (2013) used locational marginal prices as the penalty factors for different generators and periods. A locational marginal price is obtained by fixing the optimal UC status variables, solving the DCOPF, and obtaining the dual solutions associated to the node-balance constraints. The economic translation of locational marginal prices is the additional cost of dispatching one more (or less) unit of power at node n in period t. Thus, locational marginal prices are one easy estimation to reflect

37

the cost of the hedged UC status variables, u. However, since the hedged variables in the UC problem reflect the unit's binary status as opposed to its dispatch, the corresponding locational marginal prices may not be the best hedging mechanism.

Based on the idea of using locational marginal prices as penalty factors, using shadow prices of the hedged variables as the penalty factors of the PH is proposed. The procedure to obtain the shadow prices of the hedged variables is described.

1. After solving each state model, obtain the optimal solution $(u^s)^*$;

2. Impose the constraint $u = (u^s)^*$ for each state model and re-solve the model as a linear program (LP);

3. Obtain optimal dual solution for constraint $u = (u^s)^*$ and denote it as u_{dual}^s;

4. Calculate the average dual value with $u_{dual} = \sum_{s \in S} \pi^s u_{dual}^s$.

The use of these shadow prices as penalty factors will be investigated as to whether they are better at influencing the PH algorithm to drag the UC variables to an economically efficient and unified solution. Using the same penalty factors for hedging on the UC status variables, u, and startup variables and shutdown variables, v and w, will not be proper since the penalty factor needs to be chosen while considering the hedging mechanism. Thus, the same process is applied when the hedging mechanisms are v and w, except that the shadow prices (dual solutions) associated to the optimal solutions for $v = (v^s)^*$ and $w = (w^s)^*$ are used.

The test results show that some of the shadow prices are negative. In the augmented objective function, there are two penalty terms: the first term is the linear term, $\omega^s u$, and the second term is the quadratic term, $\frac{\rho}{2}\|u - \bar{u}\|^2$. The coefficient of the quadratic term should always be nonnegative; otherwise, it would encourage the states to diverge instead of converge. Thus, the absolute values of the dual solutions defined above are used for the quadratic term.

4.4.3 Improving Convergence with Rounding

The PH algorithm for the UC problem does not guarantee convergence. Cyclic behavior and slow convergence speeds are often observed. In order to improve the convergence speed of the PH and compare the solutions of different hedging mechanisms, a heuristics within the PH is implemented to obtain the UC solution.

The extensive form model of the SUC is too computationally challenging to implement in practice with current computational capability. First, the extensive form SUC involves a huge number of continuous variables and constraints in addition to many binary variables. It generally takes way too long time to get a solution with a desired optimality gap. Moreover, when the scale of the problem is large, the extensive form becomes impossible to solve, often due to memory requirements alone. Decomposition algorithms help to ease the high memory requirements at the beginning; however, they often encounter the same problem with regards to achieving a solution with a good optimality gap within a reasonable time due to the bloating that generally occurs with the master problem. However, with the PH framework, most UC status variables converge to 1 or 0 after a moderate amount of iterations. Therefore, these converged variables can be fixed to their converged value. The extensive form model will be much easier to solve if most binary variables are fixed, which significantly reduces the problem size. In order to get more variables to be fixed, a threshold (ϵ_1, ϵ_2) can be set to separate the UC status variables into three categories,

- if $u \geq 1 - \epsilon_1$, then $u = 1$;
- if $u \leq \epsilon_2$, then $u = 0$;
- else $u \in \{0, 1\}$

Table 4.4 illustrates an instance of the average UC status solution after several iterations of the PH algorithm. There are 40 binary variables initially. With the PH,

17 variables converge to 1 and 8 variables converge to 0. Moreover, some variables are very close to the binary values; for instance, $u_{1,6} = 0.98$, $u_{1,9} = 0.02$, and $u_{2,3} = 0.01$. By selecting proper thresholds, there are roughly one-fourth of the binary variables that are left undecided.

Table 4.4: Average Unit Commitment Status Variables

Period	1	2	3	4	5	6	7	8	9	10
Gen1	0	0.21	**1**	**1**	**1**	0.98	0	0	0.02	0
Gen2	0	0.05	0.01	0	0	**1**	**1**	**1**	**1**	0.87
Gen3	0	0.22	0.38	0.44	0.54	0.73	0.67	0.67	0.67	0.08
Gen4	**1**	**1**	**1**	**1**	**1**	**1**	**1**	**1**	**1**	**1**

This heuristic can speed up the run time but it can also cause infeasibility. In addition, the performance of the heuristic largely depends on the number of fixed binary variables. In order to improve the chance to obtain a feasible solution, threshold ϵ_2 can be set to be very close to zero to allow enough flexible capacity system-wide. On the other hand, there is more flexibility with setting threshold ϵ_1 since ensuring feasibility is more likely by committing additional units. This heuristic is adopted after several iterations of the PH with different hedging schemes. The overall performance of difference strategies is compared in the next section. Since v and w variables sufficiently represent the commitment variable u, this heuristic can also be adopted when v and w are chosen to be the hedging variables, i.e., the same rounding procedure will be applied to u no matter if the hedging instrument is u or if it is a combination of v and w.

4.5   Case Study

In this chapter, the PH techniques are implemented on the modified IEEE RTS96 73-bus test case described in Hedman *et al.* (2010). The original IEEE RTS96 test case can be found from University of Washington (2015). IBM ILOG CPLEX version 12.4, with Concert Technology version 3.0, is used to implement the test cases. A

Dell Precision T7500 Workstation is used to run the C++ code. The processor of the workstation is dual six-core Intel Xeon Processor X5690 (4.46GHz, 12M L3, 6.4GT/s). The memory of the workstation is 48GB, 1333MHz, DDR3RDIMM, ECC (6DIMMS). The PH algorithm is parallelized onto 12 threads with a Linux operating system. With 99 generators, there are 99 states (1 state for each potential generator failure) and the process is repeated at most 9 times in order to solve all 99 states. Three typical sets of loads are tested, i.e., one high-load day in the winter (week 51, Tuesday); one medium-load day in the summer (week 23, Thursday); and one low-load day in fall (week 38, Sunday).

4.5.1   Stochastic Formulation

The extensive form of the SUC problem is first solved to get the lower bound for deriving the optimality gap. The optimality gap of CPLEX is set to be 1% while solving the extensive form. Table 4.5 summarizes the run times, objective values, and the optimality gaps. Not surprisingly, the extensive form formulations take very long to find a solution within the optimality gap.

Table 4.5: Extensive Form Formulation Results

	Objective Value ($)	Run Time (min)	Optimality Gap
High-load	3,072,138	397.2	0.83%
Medium-load	1,822,837	337.9	0.97%
Low-load	605,617	756.1	0.40%

Given an incumbent, feasible solution y to a minimization problem, the optimality gap would be defined as optgap%$= (y-\underline{y})/y$, where $\underline{y} =$ the greatest lower bound (the best relaxed solution). By solving the original extensive form problem with CPLEX, a lower bound is obtained. This lower bound is used to establish the optimality gaps for the corresponding PH results.

In the following tests, the heuristics described in "Improving Convergence with Rounding", is implemented. The procedure is described as follows:

1. Apply PH with the specified stopping criterion;

2. Fix the converged UC variables and then solve the extensive form model to determine the remaining variables.

Two stopping criteria are adopted for the PH algorithm. First, the number of the PH iterations is fixed to 10. The resulting UC solution (with some of the binary variables fixed) is then solved with an extensive form SUC structure. Second, the time to run the PH is fixed to be 1 hour. With a longer run time for the PH, more UC binary variables are expected to converge to a better, more unified solution. After the PH algorithm is terminated, the residual problem (i.e., only the converged binary variables are fixed while the remaining binary variables are to be determined) is formulated as an extensive form SUC with an optimality gap of 1% and the total run times are then compared. Since this extensive form SUC at this stage has some of the binary variables fixed based on the PH solution, then the true optimality gap may be larger than 1%; note that within all the subsequent tables, the reported optimality gap is based on the lower bounds obtained by solving the original extensive form the SUC.

4.5.2 Hedging on Commitment Status Variables

The PH performance is known to be sensitive to the selection of the penalty factor, ρ (Watson and Woodruff, 2011). In this subsection, several penalty factor selection strategies are tested for the PH algorithm by hedging on the UC status variable u. Table 4.6 represents three hedging mechanisms with the penalty factors set at a constant 100, a constant $1,000$, as well as set based on the locational marginal prices. In this set of experiments, the PH algorithm is set to iterate for 10 iterations and the high-load day is tested. The rounding down threshold ϵ_1 is set to be 0 and the rounding up threshold is set to be 0.98.

Table 4.6: Hedging on Commitment Status Variables

Penalty factor	Constant 100	Constant 1000	LMP
PH run time (min)	31.4	21.1	36.3
Variables fixed to 0	763	754	709
Variables fixed to 1	1,291	1,381	1,275
Variables binary	322	241	392
Extensive form run time (min)	118.3	167.8	265.8
Objective value ($)	3,072,190	3,080,500	3,075,889
Optimality gap	0.83%	1.10%	0.95%

The test results show that the PH algorithm with the proposed heuristics uses less run time and achieves comparable solutions compared to directly solving the extensive form model. Moreover, the test results show that the larger penalty factors will speed up the convergence process of the PH algorithm but return lower quality solutions. Large constant penalty factors simply force the problem to find a feasible solution since the penalty factors dominate the augmented objective function. Obviously, large penalty factors may not ensure convergence to the optimal UC solution.

When a penalty factor associated to the locational marginal prices is used, the extensive form SUC, which is solved after the PH algorithm terminates, took much longer than the other penalty factor policies, as seen in Table 4.6. Generally, the locational marginal prices are smaller in value than the other penalty factor selections, which result in the penalties having less of an influence in regards to forcing solutions to converge. Thus, this mechanism generally requires more time to solve the problem. While it may be considered that the locational marginal prices may be preferred for the penalty factors since they reflect the value of a marginal MW at each bus for each period, they are marginal signals associated to the dispatch decisions, not the UC decisions.

It is essential to note that different heuristic based rounding rules can affect the solution, i.e., solving the extensive form model after imposing a threshold based rounding rule. Setting improper rounding thresholds may cause infeasibility of the proposed

heuristics. Here, the instance of using a constant $1,000$ as the penalty factor is used to illustrate such potential infeasibility problems. Two rounding thresholds are selected for testing. First, after the PH algorithm is terminated, the binary variables with continuous solutions that are below 0.02 are rounded to 0 and the binary variables with continuous solutions greater than 0.98 are rounded to 1. The residual problem is then solved by an extensive form SUC after all of these variables are fixed. While this is a rather conservative threshold policy, the residual extensive form SUC turned out to be infeasible. Since the G-1 reliability is a robust requirement, one particular state may require a specific unit to be committed, which is what caused the residual SUC to be infeasible. Then, in order to avoid infeasible solutions, the threshold for rounding down is modified to be 0, i.e., only if the UC status variables for all states converge to 0, they will be fixed to 0 within the residual extensive form SUC. Table 4.7 illustrates the influences of these threshold policies. Therefore, in the experiments of Table 4.6, the rounding down threshold is set to be 0.

Table 4.7: Different Thresholds Comparison

Condition when variables fixed to 0	≤ 0.2	≤ 0
Variables fixed to 0	816	754
Variables fixed to 1	1,381	1,381
Variables binary	179	241
Extensive form run time (min)	28.1	167.8
Objective value ($)	Infeasible	3,080,500
Optimality gap	N/A	1.10%

4.5.3 Comparisons of Hedging on Different Variables

In this subsection, hedging on startup variables and shutdown variables is compared to hedging on UC status variables with different penalty factor selections.

Constant Numbers as the Penalty Factors

Since the density of startup variables, shutdown variables, and UC status variables are different, a constant penalty factor of $1,000$ is selected as the penalty factor for hedging on the startup variables and shutdown variables, which is then comparable to using a constant 100 as the penalty factor for hedging on the UC status variables. Table 4.8 shows the results. Here again, the PH algorithm is set to iterate for 10 iterations and the high-load day is tested.

Table 4.8: Hedging under Constant Penalty Factors

	Hedging on u	Hedging on v, w
PH run time (min)	31.4	36.2
Variables fixed to 0	763	738
Variables fixed to 1	1,291	1,242
Variables binary	322	396
Extensive form run time (min)	118.3	128.5
Objective value ($)	3,072,190	3,072,607
Optimality gap	0.83%	0.85%

The result shows the two mechanisms perform nearly the same. Thus, hedging on the startup variables and shutdown variables, v and w, is a valid method.

Coefficients in the Objective Function as the Penalty Factors

Watson and Woodruff (2011) proposed a penalty factor that is proportional to the cost of the hedging mechanism. In the objective function, the coefficient of the UC status variables, u, is the no-load cost, and the coefficient of the startup variables, v, is the startup cost. Thus, the no-load costs and the startup costs are tested as the penalty factors for hedging on UC status variables and hedging on startup variables and shutdown variables correspondingly. For this work, there is no-cost coefficient for the shutdown binary variable and, thus, the startup cost coefficient is chosen instead. Tables 4.9 and 4.10 show the performance comparisons. Three sets of load data are tested under two stopping criteria described in the "Extensive Form Formulation".

Table 4.9: Hedging under Cost Penalty Factors Fixed Iterations

Hedging on	High-load		Medium-load		Low-load	
	u	v, w	u	v, w	u	v, w
PH run time (min)	25.2	28.3	25.9	33.7	31.2	39.4
Variables fixed to 0	662	732	844	820	1,202	1,185
Variables fixed to 1	1,309	1,252	1,197	1,137	757	672
Variables binary	405	392	335	419	417	519
Extensive form run time (min)	112.9	93.2	103.9	91.2	113.2	101.3
Objective value ($)	3,066,500	3,064,020	1,816,400	1,811,990	608,008	607,391
Optimality gap	0.65%	0.56%	0.61%	0.37%	0.80%	0.69%

Table 4.10: Hedging under Cost Penalty Factors Fixed Run Time

Hedging on	High-load		Medium-load		Low-load	
	u	v, w	u	v, w	u	v, w
PH run time (min)	60	60	60	60	60	60
Variables fixed to 0	680	793	818	757	1,148	1,224
Variables fixed to 1	1,325	1,292	1,189	1,124	761	688
Variables binary	371	291	369	495	467	464
Extensive form run time (min)	100.3	80.2	97	63.2	97	91.8
Objective value ($)	3,064,780	3,064,710	1,817,790	1,810,890	607,106	605,762
Optimality gap	0.59%	0.59%	0.69%	0.31%	0.65%	0.42%

From Table 4.9 (high-load day), the use of the cost coefficients as penalty factors made more variables converge to one as compared to the results in Table 4.8 where constant penalty factors were chosen (100 for hedging on u and $1,000$ for hedging on v and w). Choosing the penalty factor based on the cost coefficients also produced a better solution with a faster run time.

In Tables 4.9 and 4.10, hedging on the startup and shutdown variables outperformed the policy of hedging on the UC variables. The optimality gaps are lower for each solution and, in some cases, much lower than the policy when hedging on the u variable. Each run time for the tests on hedging on the startup and shutdown variables is less than the run time for hedging on the UC variables. Hedging on startup and shutdown variables allows the PH algorithm to focus more intently on dragging all of the subproblems to a common solution due to the ability to identify the critical periods where there are discrepancies between the startup and shutdown cycles.

Shadow Prices as the Penalty Factors

Finally, the proposed method of using the shadow prices as the penalty factors, described in "Selection of the Penalty Factors", is tested and the results are shown in Tables 4.11 and 4.12.

Table 4.11: Hedging under Shadow Price Penalty Factors Fixed Iterations

Hedging on	High-load		Medium-load		Low-load	
	u	v, w	u	v, w	u	v, w
PH run time (min)	24.7	26.9	24.9	25.9	32.2	40.1
Variables fixed to 0	682	771	832	1,002	1,129	1,175
Variables fixed to 1	1,361	1,312	1,225	1,174	783	680
Variables binary	333	293	319	200	464	521
Extensive form run time (min)	116.7	85.5	72.7	64.6	96.9	78.2
Objective value ($)	3,071,942	3,070,792	1,812,092	1,811,620	607,132	606,828
Optimality gap	0.82%	0.79%	0.37%	0.35%	0.65%	0.60%

Table 4.12: Hedging under Shadow Price Penalty Factors Fixed Run Time

Hedging on	High-load		Medium-load		Low-load	
	u	v, w	u	v, w	u	v, w
PH run time (min)	60	60	60	60	60	60
Variables fixed to 0	701	841	962	1,057	1,085	1,183
Variables fixed to 1	1,363	1,330	1,234	1,174	778	673
Variables binary	312	205	180	145	513	520
Extensive form run time (min)	110.3	34.7	73.4	48.6	77.6	63.4
Objective value ($)	3,071,651	3,067,519	1,810,860	1,811,570	607,547	605,683
Optimality gap	0.81%	0.68%	0.31%	0.35%	0.72%	0.41%

The proposed method using shadow prices as the penalty factor gives the fastest PH run time and the fastest extensive form run time. Once again, the policy to hedge on the startup and shutdown variables dominates the solutions, both in terms of optimality gaps and run times, obtained when hedging on the UC variables, except for one solution. In Table 4.12, for the medium-load day, the solution for the hedging on v and w produces an optimality gap of 0.35% in comparison to the optimality gap of 0.31% obtained when hedging on u. Note, however, that the run time for the extensive form SUC is far better, with a time of 48.6 minutes as compared to 73.4

minutes. Since the extensive form SUC has an optimality gap stopping criterion of 1%, it is likely that if the extensive form SUC for hedging of v and w was allowed to run for at most 73.4 minutes, then the optimality gap would improve and it may very well still beat the optimality gap for the hedging on u result.

Next, the run times and optimality gaps of the three selected penalty factors, i.e., a constant number, the cost coefficients from the objective function, and shadow prices, are compared in Figure 4.1. The results are obtained with 10 PH iterations for the high-load day.
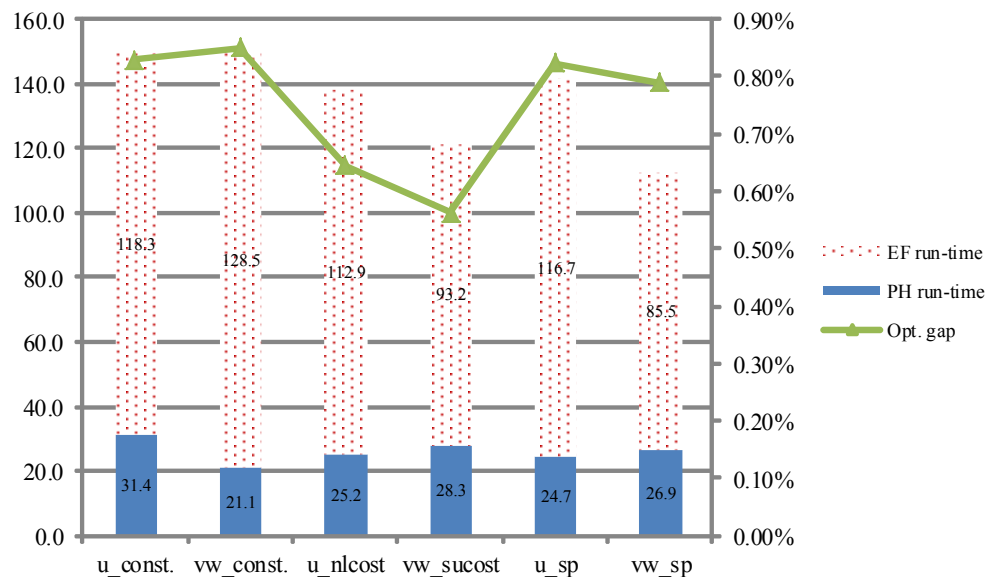
Figure 4.1: Comparison of Three Penalty Factors

The six series in Figure 4.1 represent hedging on u using a constant 100 as the penalty factor (u_const), hedging on v and w using a constant $1,000$ as the penalty factor (vw_const), hedging on u using the no-load costs as the penalty factors (u_nlcost), hedging on v and w using the startup costs as the penalty factors (vw_nlcost), hedging on u using the shadow prices as the penalty factors (u_sp), and hedging on v and

48

w using the shadow prices as the penalty factors (vw_sp). From Figure 4.1, when hedging on v and w, the total run times and the optimality gaps are generally lower, except for the case when a constant penalty factor is chosen. The two trials with constant penalty factors have the longest run time and the largest optimality gap; this is partially a result of the difficulty to choose the best constant penalty factor for both the u and the v and w hedging mechanisms and this is also due to the fact that a constant penalty factor does not differentiate between the different assets as well as between the different time periods. For the choice between using the cost coefficients from the objective in comparison to the shadow prices as penalty factors, the run times are relatively similar but the cost coefficient policy produced better optimality gaps. In these test cases, hedging on v and w, with the startup costs as penalty factors, obtains the best optimality gap and hedging on v and w, with the shadow prices as penalty factors, obtains the fastest total run time with good optimality gaps.

Next, the overall performance of hedging on v and w is compared with hedging on u using the cost coefficients as penalty factors versus using the shadow prices as penalty factors, under the three sets of loads. The results are plotted in Figures 4.2-4.4. The eight series in Figures 4.2-4.4 represent hedging on u using the no-load costs as penalty factors with 10 PH iterations (u_nlcost 10 iter), hedging on u using the no-load costs as penalty factors within 1 hour (u_nlcost 1 hr), hedging on u using the shadow prices as penalty factors with 10 PH iterations (u_sp 10 iter), hedging on u using the shadow prices as penalty factors within 1 hour (u_sp 1 hr), hedging on v and w using the startup costs as penalty factors with 10 PH iterations (vw_sucost 10 iter), hedging on v and w using the startup costs as penalty factors within 1 hour (vw_sucost 1 hr), hedging on v and w using the shadow prices as penalty factors with 10 PH iterations (vw_sp 10 iter), and hedging on v and w using the shadow prices as penalty factors within 1 hour (vw_sp 1 hr). From Figures 4.2-4.4, hedging on v and

49

w is generally better off than hedging on u, with a lower total run time and a better optimality gap. Hedging on v and w, using the shadow prices as penalty factors, gives the solution with the least total run times and the best optimality gaps. From these figures, the additional PH iterations have almost negligible impact on the computation results when hedging on u. However, when hedging on v and w, the optimality gaps are generally improved with more PH iterations. This implies that the PH algorithm is better at dragging the individual problems to good unified solutions with v and w as hedging instruments. Overall, the results suggest that hedging on v and w is at least as effective as hedging on u and, based on these specific experiments with this test case, hedging on v and w would be the preferred hedging policy.
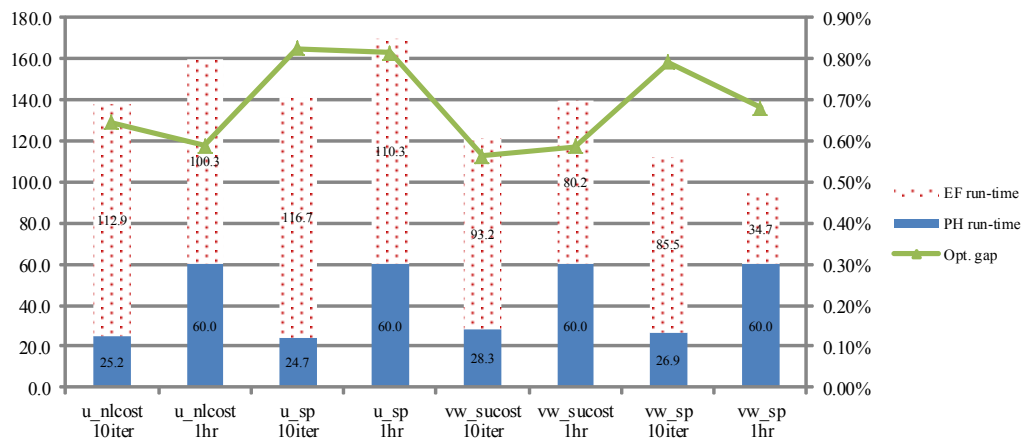
Figure 4.2: Comparison under High-Load Day Data

When the PH algorithm is allowed to run for 60 minutes, the overall run times are longer. This suggests that there may be a preferred length of time to allow the PH algorithm to run as the improvement in the solution quality may not be proportional to the number of iterations, especially since cyclic behaviors are often observed in the PH algorithm. The PH algorithm is effective at dragging a substantial portion of the
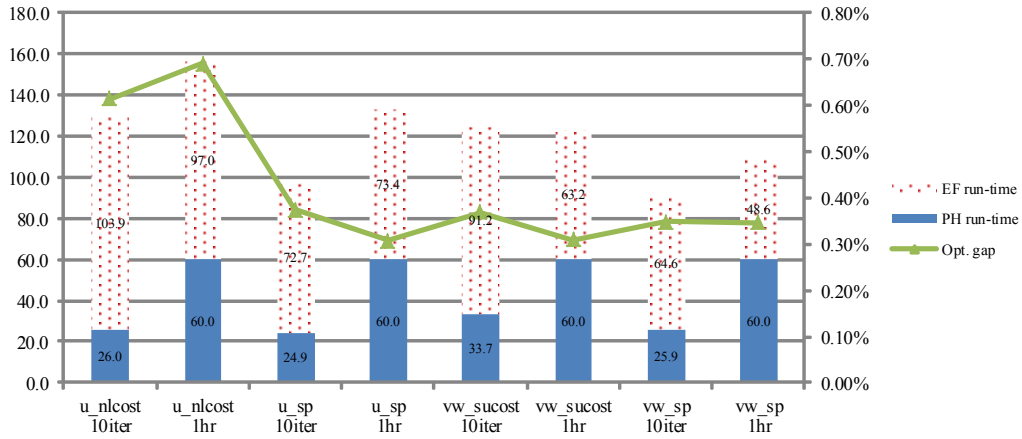
Figure 4.3: Comparison under Medium-Load Day Data
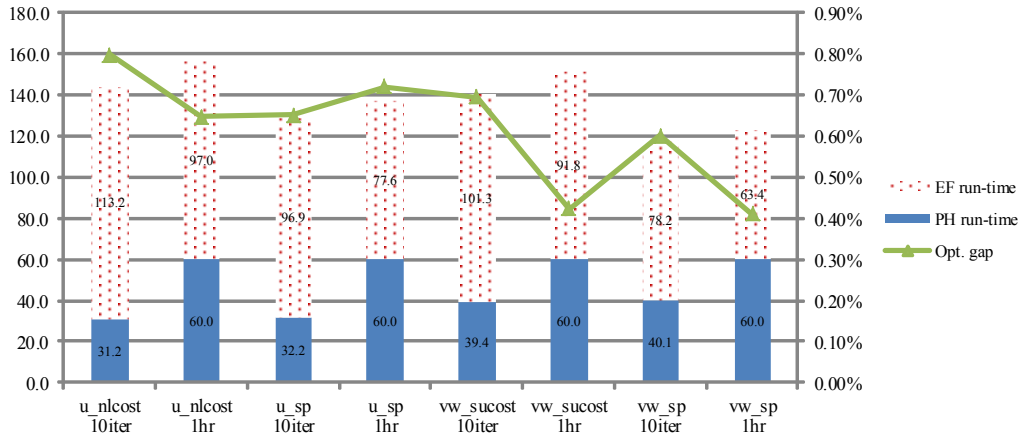
Figure 4.4: Comparison under Low-Load Day Data

binary solutions to a unified solution but not all. The results show that it is effective at substantially speeding up the time it takes to solve a stochastic program while still ensuring high-quality results (low-optimality gaps).

4.6   Conclusions

In this chapter, a hybrid algorithm using the scenario-based PH decomposition algorithms as a pre-solve heuristic is proposed to solve the UC problem while protecting against any single generator forced outage. The PH algorithm is examined by comparing its performance while using various hedging mechanisms in combination with various penalty factor selection rules. Test results show that hedging on the startup and the shutdown variables makes the PH converge faster to a good unified UC solution as compared to hedging on UC status variables for these chosen test cases; however, further analysis is needed to confirm this result. Hedging on the startup and the shutdown binary variables also suggested that a better (economically efficient) solution could be obtained; however, additional testing is needed for different test cases to see if this is a consistent result.

The PH algorithm is sensitive to the chosen penalty factor. Multiple penalty factors were tested including various constant numbers, a penalty factor based on the hedging mechanism's cost coefficient, penalty factors based on the locational marginal prices for the generator's location, and penalty factors associated to the dual solution by enforcing the binary variable (the hedging mechanisms) to take on a value obtained when solving a deterministic UC problem initially. The test results suggest that using shadow prices (dual solutions) as the penalty factors is an effective strategy to both improve the computational performance and achieve economically efficient solutions. Future work will concentrate on speeding up the convergence of the PH by selecting proper penalty factors and developing new heuristics. The proposed method will be applied to other large-scale stochastic programming problems.

Chapter 5

DATA-DRIVEN UNCERTAINTY SET

5.1   Introduction

Under the robust optimization framework, uncertainties are often characterized by a pre-defined uncertainty set, and then the system is optimized against the worst-case realizations within the set. Although solutions to robust optimization can ensure robustness, a common concern is that such an approach can be too conservative, or too costly. Therefore, it is critical to construct an effective uncertainty set that is less conservative while retaining robustness.

Except (Lorca and Sun, 2015), much of the literature of data-driven uncertainty sets focuses on analyzing data at a certain time point, overlooking the time-domain correlation. However, in many cases, uncertain data, e.g., loads or wind generation, are time-series data. In other words, the previous data realizations have strong implications on the future data realizations. Therefore, it is important to have a methodology for designing uncertainty sets that explicitly model the autocorrelation on time horizon.

In this chapter, a data-driven framework is proposed to construct uncertainty sets for both temporally and spatially correlated data. The framework is composed of two main steps. First, an autoregressive (AR) integrated (I) moving average (MA) model, which is first developed by (Box and Jenkins, 1970), is adopted to construct a time-series model by using the historical uncertain data. Next, whitening transform (Fukunaga, 2013) is performed to identify the spatial correlation of the residual uncertain data obtained from the ARIMA model. The proposed data-driven uncer-

tainty sets have similar structure as the one in (Lorca and Sun, 2015). However, the key differences are: (1) Lorca and Sun (2015) presumes that data are autoregressive correlated with certain lead time, whereas the proposed uncertainty set fully utilize data to determine the temporal correlation based on ARIMA models without making presumption on data; and (2) Lorca and Sun (2015) assumes that error terms are only spatially correlated at the same time period. In the proposed model in this chapter, besides the spatial correlation, the temporal correlation of the errors is also included if moving average process is identified from the data. Therefore, this chapter provides a more systematic and general data-driven approach as compared to Lorca and Sun (2015).

The contributions can be summarized as follows:

- A general data-driven framework is proposed for constructing uncertainty sets for temporally and spatially correlated data using time-series models.
- The data-driven uncertainty set is applied to robust unit commitment problem. Numerical experiments are conducted on the real-world power system operated by the ISO New England.
- The empirical results show that the proposed data-driven uncertainty sets outperform the rule-based uncertainty sets. By using historical data, the robust model built from the former yield less conservative UC solutions than latter while keeping system reliable.

This chapter is organized as follows. Section 5.2 reviews the ARIMA model and notations for constructing uncertainty sets. Section 5.3 describes the framework to construct the proposed data-driven uncertainty sets. Section 5.4 presents a case study of robust unit commitment with interchange flow uncertainty. Finally, section 5.5 concludes.

5.2   ARIMA Model

A brief presentation of the ARIMA model is given below. For a more detailed discussion, the reader is referred to a comprehensive time series analysis text, such as Box and Jenkins (1970), Box *et al.* (2008), and Montgomery *et al.* (2008). In power system scheduling, ARIMA model has been mainly applied to the price and wind power forecasting (Contreras *et al.*, 2003; Conejo *et al.*, 2005; Chen *et al.*, 2010).

A set of time series, y_t, can be expressed by the sum of two components: a signal, μ, and a noise, ϵ_t, i.e., $y_t = \mu + \epsilon_t, \forall t$. ARIMA model gives an efficient way to model time series. The autoregressive part AR (p) models a time series as a linear function of p previous observations in order to predict the current one. The moving average part MA(q) determines the moving average of the series with a time window size of q. Finally, the ARIMA process (p, d, q) is based on a series that has been differenced d times, with p autoregressive terms and q moving average terms. The model can be described in the following generic form:

$$\Phi(B)\nabla^d y_t = \delta + \Theta(B)\epsilon_t \tag{5.1}$$

where B is backshift operator, such that $By_y t = y_{t-1}$; $\Phi(B)$ is autoregressive function: $\Phi(B) = 1 - \sum_{i=1}^{p} \phi_i B^i$; $\Theta(B) = 1 - \sum_{i=1}^{q} \theta_i B^i$; ∇^d is differencing function: $\nabla^d = (1 - B)^d$; and δ is a scalar. The parameters, ϕ_i's, δ, and θ_i's, are chosen to best fit the data.

ARIMA model can be generalized to seasonal ARIMA if strong cyclic patterns are observed. Seasonal ARIMA $(p, d, q) \times (P, D, Q)_s$ can be described in a generic form:

$$\Phi^*(B^s)\Phi(B)\nabla^d(\nabla^s)^D y_t = \delta + \Theta^*(B^s)\Theta(B)\epsilon_t \tag{5.2}$$

where $\Phi^*(B^s) = 1 - \sum_{i=1}^{P} \phi_i^* B^{is}$, $\Theta^*(B^s) = 1 - \sum_{i=1}^{Q} \theta_i^* B^{is}$, and $(\nabla^s)^D = (1 - B^s)^D$, are seasonal autoregressive, moving average, and differencing functions, respectively.

5.3   Construct Data-Driven Uncertainty Sets

In this section, the framework for constructing the uncertainty sets for temporally and spatially correlated data is described. Denote the uncertain data at location n at time period t as $d_n t, \forall n, t$. The assumptions and a high level description of the procedure for constructing uncertainty sets are presented first. Then the detailed steps and formula are described in the rest of the section.

5.3.1   Assumptions

The following three assumptions are made to construct uncertainty sets:

1. Data are temporally autocorrelated at each location
2. The mean of the noises, ϵ_t, at each location is zero
3. Noises in different locations have static spatial correlation

Under the above assumptions, the temporally and spatially correlated data can be "whitened" in two steps:

First, ARIMA model is used to decorrelate the temporal correlation of data under assumptions 1 and 2. By properly identifying the ARIMA model, the autocorrelation of the data can be determined. The remaining noises can achieve zero mean so the second assumption is held.

Second, statistical whitening transform is applied to the noises to decorrelate spatial correlation under assumption 3.

5.3.2 Temporal Separation

At the first step, at each location n, the following ARIMA model is construct to fit historical data:

$$\Phi_n(B)d_{nt} = \delta_n + \Theta_n(B)r_{nt} \tag{5.3}$$

where $r_{nt}, \forall n, t$, are the residuals with zero mean and constant variance, and contain no temporal correlation. For each time period t, denote $\mathbf{d}^t$ and $\mathbf{r}^t (\in \mathbb{R}^N)$ as the vectors of the original time-series data and residuals across all locations, respectively, where N is the number of the locations. Then, (5.3) can be written in the matrix form as follows:

$$\boldsymbol{\Phi}(B)\mathbf{d}^t = \delta + \boldsymbol{\Theta}(B)\mathbf{r}^t \tag{5.4}$$

where $\boldsymbol{\Phi}$ and $\boldsymbol{\Theta}$ are diagonal matrices, and each diagonal element is a function of backshift operator.

5.3.3 Spatial Separation

At the second step, the spatial correlation of the residuals, $\mathbf{r}^t$, at each time period is studied since the spatial correlation of the residuals is assumed to be time-invariant under assumption 3. The spatial covariance matrix of the residuals, $\Sigma_{(NN)}$, calculated from historical data can be used to estimate the true covariance matrix. Using the eigen-decomposition theorem (Fukunaga, 2013), the covariance matrix can be decomposed as follows:

$$\Sigma = Q\Lambda Q' \tag{5.5}$$

where Λ is $N \times N$ diagonal matrix consist of eigenvalues; Q is $N \times N$ orthogonal matrix consist of eigenvectors.

Whitening is a traditional statistical method for turning the data covariance matrix into an identify matrix. Whitening is applied on the residuals to decorrelate the spatial correlation. Whitening transform is applied to $\mathbf{r}^t$ by decomposing it as follows: $\mathbf{r}^t = Q\Lambda^{-\frac{1}{2}}\epsilon^t$, where ϵ^t are uncorrelated white noises with zero mean and unit variance.

As a result, the original temporally and spatially correlated data, $d_{nt}, \forall n, t$, are "whitened" as the functions of white noises $\epsilon_{nt}, \forall n, t$ as follows:

$$\boldsymbol{\Phi}(B)\mathbf{d}^t = \delta + \boldsymbol{\Theta}(B)Q\Lambda^{-\frac{1}{2}}\epsilon^t \tag{5.6}$$

where $\mathbf{d}^t, \epsilon^t$ are historical data if $t < 0$; otherwise, the uncertain variable $\mathbf{d}^t$ can be expressed by the white noises ϵ^t.

5.3.4   White Noise Modeling

Last, the variation range of the white noises ϵ is further controlled by using the budget-constrained uncertainty sets in (Zhao and Zeng, 2012). The final data-driven uncertainty sets can be described as follows:

$$\mathbb{U} = \left\{ (\mathbf{d}, \epsilon) \left| \begin{array}{ll} \boldsymbol{\Phi}(B)\mathbf{d}^t = \delta + \boldsymbol{\Theta}(B)Q\Lambda^{-\frac{1}{2}}\epsilon^t & \forall t \\ -z_{1-\alpha} \leq \epsilon_{nt} \leq z_{1-\alpha} & \forall n, t \\ |\sum_{\forall n} \epsilon_{nt}| \leq \Gamma\sqrt{N}z_{1-\alpha} & \forall t \\ |\sum_{\forall t} \epsilon_{nt}| \leq \Gamma\sqrt{T}z_{1-\alpha} & \forall n \end{array} \right. \right\} \tag{5.7}$$

where $z_{1-\alpha}$ represents $1 - \alpha$ confidence level for standard normal distribution; Γ is a scalar to control the size of uncertainty set; T is the number of the modeled time periods.

5.4 Case Study

In this section, the case study focuses on the uncertain interchange levels in the power system operated by ISO New England (ISONE), and the proposed data-driven approach is applied to construct uncertainty sets for the robust unit commitment problem. In the robust UC, commitment status decisions are determined in the first stage (here-and-now); and dispatch decisions are determined in the second stage (wait-and-see) after the realization of uncertain data. The robust UC solves the problem with a set of UC decisions to minimize the overall costs (including both commitment and dispatch costs) under the worst plausible second-stage uncertain data realization. Since the emphasis of this chapter is the construction of uncertainty sets, the robust UC model is not described in detail here. In this case study, the column and cut generation (CCG) algorithm (Zhao and Zeng, 2012) is applied to solve the robust UC.

In the ISO system, the interchange forecast error can be more than an order of magnitude higher than the forecast errors of load and renewable. Due to its large variability, simply using a box uncertainty set for the interchange flow in robust UC will lead to overly conservative UC solution. Therefore, the proposed data-driven approach is applied to obtain an effective uncertainty set. The numerical results show that the robust UC solutions from the data-driven sets are less conservative than the rule-based uncertainty set, while remaining the robustness properties.

5.4.1 Data

There are six interchanges in the ISONE system. The hourly historical data of interchange forecast and real-time interchange flows are used in this case study. Specifically, data from 10/1/2012-12/31/2012 are used to estimate model parameters,

59

$\Omega = (\delta, \mathbf{\Phi}, \mathbf{\Theta}, \mathbf{\Lambda}, Q)$, denoted as training data; data from 1/1/2013-1/31/2013 are used to evaluate the robust UC performance with different uncertainty sets models, denoted as testing data.

5.4.2 ARIMA Model and Whitening Transform

JMP 11.0 is used to analyze training data and determine ARIMA model parameters. One of the interchange locations, Location 4, is used to demonstrate how ARIMA model is developed. Figure 5.1 shows the training data of the real-time interchange level at Location 4. By plotting the autocorrelation function (ACF) and the partial autocorrelation function (PACF) of the training data, strong autocorrelation patterns are observed. As shown in Figure 5.2, the ACF shows an exponential decay, and the PACF cuts off after the first lag. This indicates that an AR process occurs (Montgomery *et al.*, 2008). After modeling the AR process, obvious patterns are observed at lag 24, which indicates seasonal ARIMA terms are desired. Therefore a seasonal ARIMA $(1, 0, 0) \times (1, 0, 0)_2 4$ is selected to fit the data at Location 4. JMP 11.0 estimates the corresponding coefficients, $\delta, \phi, \theta, \phi^*, \theta^*$, in (5.3). Figure 5.1 plots the ACF and PACF of residuals r, which show little patterns. This suggests that the ARIMA model fits the training data well.
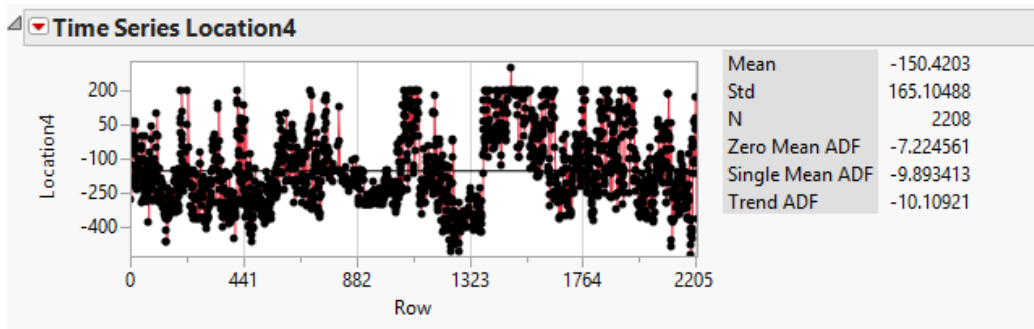
Figure 5.1: Training Data at Location 4

Resulting residuals at each location have zero mean and bell-shape distributions.

Time Series Basic Diagnostics

Lag	AutoCorr	-.8 -.6 -.4 -.2 0 .2 .4 .6 .8	Ljung-Box Q	p-Value	Lag	Partial	-.8 -.6 -.4 -.2 0 .2 .4 .6 .8
0	1.0000		.	.	0	1.0000	
1	0.9140		1847.26	<.0001*	1	0.9140	
2	0.8237		3347.96	<.0001*	2	-0.0718	
3	0.7426		4568.44	<.0001*	3	0.0081	
4	0.6692		5560.04	<.0001*	4	-0.0029	
5	0.6103		6385.01	<.0001*	5	0.0444	
6	0.5761		7120.60	<.0001*	6	0.1135	
7	0.5590		7813.37	<.0001*	7	0.0828	
8	0.5496		8483.28	<.0001*	8	0.0502	
9	0.5425		9136.39	<.0001*	9	0.0321	
10	0.5325		9765.93	<.0001*	10	0.0110	

Figure 5.2: ACF/PACF of Original Data at Location 4

Lag	AutoCorr	-.8 -.6 -.4 -.2 0 .2 .4 .6 .8	Ljung-Box Q	p-Value	Lag	Partial	-.8 -.6 -.4 -.2 0 .2 .4 .6 .8
0	1.0000		.	.	0	1.0000	
1	-0.0090		0.1808	0.6707	1	-0.0090	
2	-0.0620		8.6934	0.0129*	2	-0.0621	
3	0.0029		8.7119	0.0334*	3	0.0017	
4	-0.0195		9.5495	0.0487*	4	-0.0234	
5	-0.0652		18.9689	0.0019*	5	-0.0656	
6	-0.0226		20.1041	0.0027*	6	-0.0269	
7	0.0196		20.9568	0.0038*	7	0.0109	
8	0.0403		24.5565	0.0018*	8	0.0374	
9	0.0417		28.4083	0.0008*	9	0.0421	
10	0.0147		28.8867	0.0013*	10	0.0155	
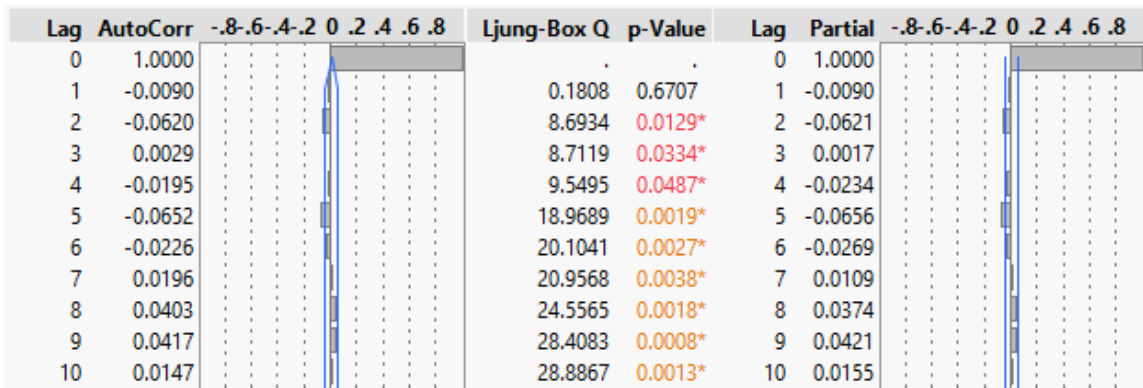
Figure 5.3: Residual ACF/PACF of ARIMA Model at Location 4

Next, whitening transform is applied to the residuals of all locations. Figure 5.4 is the scatter plot of the covariance of the residuals at six locations. It shows that the spatial correlation is not very strong. This can be further verified by the correlation matrix in Figure 5.5, where all the absolute values of non-diagonal components are smaller than 0.1. When determining (Λ, Q) in (5.6) using whitening transform, all elements with an absolute value less than 2% are considered as noises and set to zero in the covariance matrix.

5.4.3 Uncertainty Set

To construct the uncertainty set, ARIMA model is applied to four different groups of data to reduce the sizes of uncertainty sets. Table 5.1 summarizes the results.

61
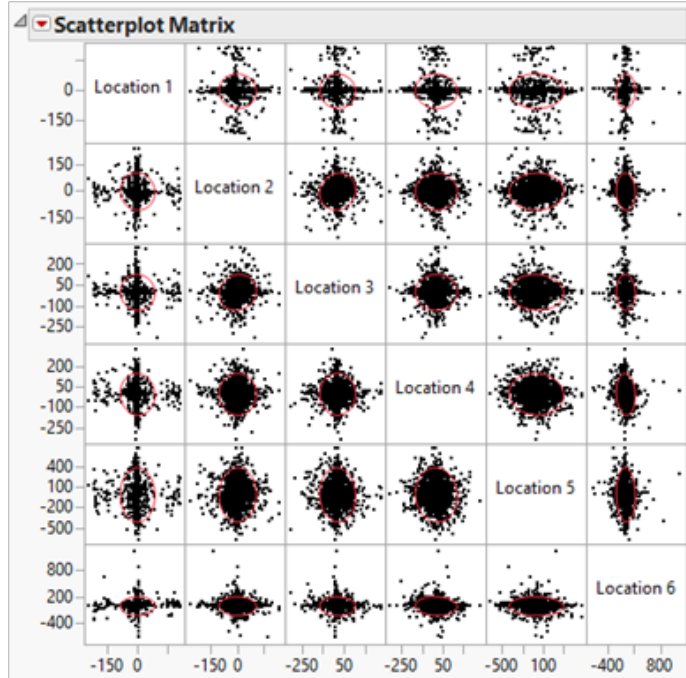
Figure 5.4: Scatter Plot of the Covariance of Residuals at 6 Locations

Figure 5.5: Correlation Matrix of the Residuals at 6 Locations

1. Real-time interchange levels at each location

2. Interchange forecast errors at each location

3. Total interchange level across all locations

4. Total interchange forecast error across all locations

Table 5.1: ARIMA Models for Different Data

	Real-time level	Errors from forecast level
Location 1	$(1,0,0) \times (1,0,0)_{24}$	$(1,0,0) \times (1,0,0)_{24}$
Location 2	$(1,0,0)$	$(1,0,0)$
Location 3	$(1,0,1) \times (1,0,0)_{24}$	$(1,0,0)$
Location 4	$(1,0,0) \times (1,0,0)_{24}$	$(1,0,0)$
Location 5	$(1,0,0) \times (1,0,1)_{24}$	$(2,0,0) \times (1,0,0)_{24}$
Location 6	$(2,0,0)$	$(1,0,0) \times (1,0,0)_{24}$
Total	$(1,0,0) \times (1,0,0)_{24}$	$(1,0,0) \times (1,0,0)_{24}$

In the budget-constrained uncertainty sets, (5.7), adopted for white noises ϵ, two budget constraints are included: one restricts the sum of the white noise across all locations in each period, and the other restricts the sum of white noise across all time periods at each location. The confidence level $\alpha = 0.01$ and $\Gamma = 0.9$.

Additionally, the upper and lower bounds obtained from historical data are imposed in uncertainty sets. The following system ramping limitation is also incorporated: the change of the total net interchange between two consecutive time periods shall not exceed 500MW.

5.4.4 Results

The performance of proposed uncertainty sets is tested. Testing data have 31 days. For each day, a deterministic security-constrained unit commitment (det SCUC) is solved using forecast interchange levels. Robust UC with different uncertainty sets are also solved to determine commitment solutions. Then, each commitment solution is passed to the real-time security-constrained economic dispatch (SCED) with actual interchange realizations to evaluate the performance of different UC solutions, including costs, system violations, and computation time. The det SCUC results are summarized in Table 5.2. Since there is a large error in the interchange forecast, violations occur in all testing days and huge penalties are applied as shown in Table 5.2.

Table 5.2: Test Results for the Deterministic SCUC

Performance measures	Deterministic SCUC
Average computation time (s)	42.47
Average UC cost ($)	3,093,846
Average dispatch cost w/o violation penalty ($)	8,926,177
Average total cost w/o violation penalty ($)	12,020,023
Average Violation Penalty Cost ($)	106,537,216
# of violated scenarios	31

Robust UC are tested with the following three different uncertainty sets:

1. The modified box uncertainty set: The uncertainty set only models data lower and upper bounds, and the ramping limitation of total interchange level change.

2. Budget-constrained uncertainty set: In addition to the constraints used in the modified box uncertainty set, this set also includes traditional budget-constrained uncertainty sets, similar to (5.7). The uncertain variables are the total interchange level across all locations in each period, and total interchange level across all periods at each location, instead of the white noises ϵ as in (5.7). The confidence level $\alpha = 0.01$ and $\Gamma = 0.9$. The autocorrelation of the data is ignored.

3. The proposed data-driven uncertainty set

The first two are rule-based uncertainty sets. As demonstrated by the results to be analyzed next, the first one is the most conservative uncertainty set, while the last set is the least conservative one. Table 5.3 summarizes the comparison results of these three sets.

Compared to the computation time of det SCUC in Table 5.2, robust UC takes more time to solve. As reported in Table 5.3, all three uncertainty sets drastically reduce the number of violation scenarios and penalty costs, indicating their operational effectiveness in reducing costly emergency actions and improving system reliability. However, the robustness comes at the expenses of increased UC, dispatch and total costs in all testing day as compared to the deterministic counterparts.

Next, the focus is on the comparison among three uncertainty sets. The proposed data-driven uncertainty set results in the least cost increase while keeping the system relatively reliable. More specifically, the modified box uncertainty set, i.e., the most conservative policy, guarantees system reliability, but it commits too many units. As a

result, its commitment cost is the highest compared to the other two uncertainty sets. The budget-constrained uncertainty set is relatively conservative compared to the proposed data-driven uncertainty set since it does not recognize the autocorrelation patterns. As shown in Table 5.3, the data-driven uncertainty set reduces commitment costs by almost 15% compared to the modified box set. All three robust solutions do not affect the dispatch cost too much. In terms of the total cost, the data-driven set results in only 8.5% cost increase over the deterministic case. By considering the temporal and spatial correlations in uncertainty sets, the proposed method can save almost half million dollars compared to the traditional modified box set.

Table 5.3: Test Results for Robust SCUC with 3 Types of Uncertainty Sets

Uncertainty sets	Modified box	Budget-constrained	Data-driven
Average computation time (s)	95	341	381
Max computation time (s)	331	1,362	1,289
Avg. UC cost ($)	4,482,361	4,317,584	4,028,774
(% increase w.r.t. det SCUC)	(44.9%)	(43.2%)	(30.2%)
Avg. dispatch cost w/o violation penalty ($)	9,013,887	9,012,315	9,009,538
(% increase w.r.t. det SCUC)	(1%)	(1%)	(0.9%)
Average total cost w/o violation penalty ($)	13,496,248	13,329,899	13,038,312
(% increase w.r.t. det SCUC)	(12.3%)	(10.9%)	(8.5%)
Average violation penalty ($)	0	311,194	29,484
# of violation scenarios	0	1	3

5.5   Conclusions

In this chapter, a framework is proposed to construct uncertainty sets based on ARIMA model and statistical whitening. The resulting uncertainty sets capture temporal and spatial correlations of data. Therefore, sizes of uncertainty sets are controlled, and the conservativeness of robust solutions is reduced. Test results on the robust unit commitment show that the proposed uncertainty sets reduce commitment costs compared to traditional rule-based uncertainty sets, which ignore autocorrelation of time series. At the same time, system reliability is improved over deterministic

policy with affordable cost increment and computational complexity. Future research will focus on building more accurate and general ARIMA model to decorrelate temporal autocorrelation.

Chapter 6

EXTREME RAY FEASIBILITY CUTS

6.1   Introduction

In this chapter, a set of feasibility cuts (constraints) for the UC problems with uncertainty are studied. It is shown that the proposed cuts, which are special cases of Benders' feasibility cuts, can be characterized by the combinatorial selection of the transmission lines and buses of the power systems. The cuts give mathematical support to ensure system reliability. Compared with the stochastic programming or the robust optimization, the extreme ray feasibility cuts can collapse the second-stage recourse into first-stage decision by taking advantages of the power system characteristics and engineering insights. Most of the computation is able to be carried out by offline simulations and study. The resulting formulation is a deterministic formulation. As a result, the computational burden is shifted from the scheduling periods to the offline study. The proposed cuts provide a more reliable solution with only little computational increment over the current reserve requirements.

The contributions of the chapter are listed as follows.

- A reformulation that considers only the available generation capacities in the recourse stage is proposed and distinguishes the traditional Benders' reformulation for two-stage stochastic programming. With the proposed reformulation, handy results are observed, which enable the corresponding extreme ray feasibility cuts to be determined by offline studies.

- Given any system operating state, a necessary and sufficient condition to ensure a feasible dispatch is explicitly presented with a polyhedral structure.

- The extreme rays of the dual cone are studied and proven to be determined by combinatorial selections of transmission lines and buses in the power system.

- The crucial extreme rays can be identified by offline simulations with engineering insights. Thus, the computational burden is shifted from scheduling periods to offline studies.

- The proposed extreme ray feasibility cuts give mathematical support rather than rule-of-thumb determination for security requirements.

- The proposed approach avoids formulating scenarios or using an iterative process to solve the UC problem with uncertainty; it solves the problem efficiently as a deterministic equivalent model with the cuts.

The rest of the chapter is organized as follows. Section 6.2 derives the feasibility cuts. Section 6.3 describes several applications of the cuts. Section 6.4 shows numerical results of test cases. Section 6.5 concludes the chapter.

6.2   Extreme Ray Feasibility Cuts

In this section, the feasibility cuts for the UC problem with uncertainty are derived. The mathematical conditions for a power system to be "reliable" is analyzed. Due to the nature of the two-stage decision process of the UC problem, a UC solution is *reliable* if in any considered real-time scenario, there is a feasible dispatch solution without load shedding. Therefore, the focus is on the second-stage feasible dispatch problem.

First, the basic linearized dispatch model is introduced in 6.2.1. Based on the dispatch model, a necessary and sufficient feasible dispatch condition is given in 6.2.2. The condition is based on a polyhedral structure (pointed cone). The extremes rays of the polyhedron are studied in 6.2.3.

6.2.1 Dispatch Model

The dispatch model is described as follows:

$$\min \quad \sum_{\forall g} C_g(p_g) \tag{6.1}$$

$$\text{s.t.} \quad L_g \leq p_g \leq H_g \qquad\qquad \forall g \tag{6.2}$$

$$i_n = \sum_{\forall g \in G(n)} p_g - D_n \qquad\qquad \forall n \tag{6.3}$$

$$-F_l \leq \sum_{\forall n} \Psi_{ln} i_n \leq F_l \qquad\qquad \forall l \tag{6.4}$$

$$\sum_{\forall n} i_n = 0 \tag{6.5}$$

This model is a linearized optimal power flow formulation, referred as direct current optimal power flow (DCOPF) model (Wood and Wollenberg, 1996). This model is widely adopted in congestion-constrained power system scheduling (Stott *et al.*, 2009). In this model, $p_g, i_n, \forall g, n$, are decision variables representing the power generation level of generator g and nodal net injection at bus n, respectively. Equation (6.1) is the objective to minimize total dispatch costs. Equation (6.2) restricts the generation lower and upper bounds. Equation (6.3) represents nodal net injection constraints. Equation (6.4) gives the network constraints. The coefficients (Ψ), referred as power transfer distribution factor (PTDF), describe the power flow distribution on each transmission line when injecting one unit of power from one certain bus to the reference bus. PTDFs are the results of the Kirchhoff's circuit laws. The PTDF-based DCOPF model provides relative independent impacts of power injection on individual transmission lines. This property enables the further exploration of the insights from mathematical conditions to the physical power system. In this chapter, it is assumed that the PTDFs are fixed, i.e., the topology does not change and a failure of a transmission line is not considered. The results can be generalized to the

changed topology by calculating new PTDFs. Equation (6.5) restricts the total nodal net injection to be zero, in other words, the total generation equals to the total loads.

6.2.2 Feasibility Necessary and Sufficient Condition

The dispatch model can be re-written as a dispatch feasibility problem as follows.

$$\max \quad 0 \tag{6.6}$$

$$\text{s.t.} \quad -p_g \qquad\qquad \leq -L_g \qquad \forall g \quad \phi_g^- \tag{6.7}$$

$$p_g \qquad\qquad \leq H_g \qquad \forall g \quad \phi_g^+ \tag{6.8}$$

$$-\sum_{\forall g \in G(n)} p_g + i_n \qquad = -D_n \qquad \forall n \quad \lambda_n \tag{6.9}$$

$$-\sum_{\forall n} \Psi_{ln} i_n \qquad \leq F_l \qquad \forall l \quad \mu_l^- \tag{6.10}$$

$$\sum_{\forall n} \Psi_{ln} i_n \qquad \leq F_l \qquad \forall l \quad \mu_l^+ \tag{6.11}$$

$$-\sum_{\forall n} i_n \qquad = 0 \qquad\qquad \tau \tag{6.12}$$

In this feasibility problem, the objective (6.6) is modified to maximize a null value. Equation (6.7)-(6.12) are the duplicate of equation (6.2)-(6.5) with listing corresponding dual variables for convenience. Next, the dual problem of this dispatch feasibility problem can be derived as follows.

$$\min \quad \sum_{\forall g} (H_g \phi_g^+ - L_g \phi_g^-) + \sum_{\forall l} F_l(\mu_l^+ + \mu_l^-) - \sum_{\forall n} D_n \lambda_n \tag{6.13}$$

$$\text{s.t.} \quad \phi_g^+ - \phi_g^- - \lambda_{n(g)} = 0 \qquad\qquad \forall g \tag{6.14}$$

$$\sum_{\forall l} \Psi_{ln}(\mu_l^+ - \mu_l^-) + \lambda_n - \tau = 0 \qquad\qquad \forall n \tag{6.15}$$

$$\phi_g^+, \phi_g^-, \mu_l^+, \mu_l^- \geq 0 \qquad\qquad \forall g, l \tag{6.16}$$

Let Q denote the feasible set of the above dual problem equation (6.14) - (6.16). Q is a pointed cone, referred as *dual cone*.

70

In order to ensure a feasible dispatch, the focus is on the current system state. The current system state is determined by the parameters in the dispatch model including $L_g, H_g, F_l, D_n, \forall g, l, n$. Specifically, $L_g, H_g, \forall g$, are available generation capacities restricted by commitment status, physical minimum and maximum generation capability (EcoMin and EcoMax), ramping capability, and generator contingency; $D_n, \forall n$, represent the real-time net load (the net load can be seen as the total load subtracts non-dispatchable wind generation) at each bus; and $F_l, \forall l$, are the transmission line capacities. A necessary and sufficient conditions that ensures a feasible dispatch with respect to the current system state is given as follows.

Proposition 1. *For any given system state parameters, $(L_g, H_g, D_n, F_l), \forall g, n, l$, the power system has a feasible dispatch if and only if, $\forall \gamma = (\phi_g^+, \phi_g^-, \mu_l^+, \mu_l^-, \lambda_n, \tau) \in Q$,*

$$\sum_{\forall g}(H_g\phi_g^+ - L_g\phi_g^-) + \sum_{\forall l} F_l(\mu_l^+ + \mu_l^-) - \sum_{\forall n} D_n\lambda_n \geq 0 \qquad (6.17)$$

Proof. This is a direct application of Farkas's Lemma (Bazaraa *et al.*, 2006).

If $\forall \gamma \in Q$, (6.17) is satisfied, then $\gamma^* = \mathbf{0}$ is the optimal solution for the dual problem since it is a feasible point in the dual cone and all other solutions have objectives that are greater than or equal to zero. Therefore, the primal problem must be feasible since there is an optimal solution for the dual problem, i.e., there exists a feasible dispatch.

If the system has a feasible dispatch, it indicates the primal problem is feasible. Then the dual problem is feasible and cannot be unbounded. From the weak duality theorem, the objective value of the dual problem must be greater than or equal to 0, i.e., (6.17) is satisfied. $\qquad \square$

Corollary 2. *If there exists a $\bar{\gamma} = (\bar{\phi}_g^+, \bar{\phi}_g^-, \bar{\mu}_l^+, \bar{\mu}_l^-, \bar{\lambda}_n, \bar{\tau}) \in Q$ such that (6.17) is not satisfied, then there is no feasible dispatch solution for the system with parameters*

$(L_g, H_g, D_n, F_l), \forall g, n, l$. *Moreover, transmission line capacity F_l, for l such that $\bar{\mu}_l^+$ or $\bar{\mu}_l^- > 0$, and generator capacity H_g (L_g) for g such that $\bar{\lambda}_{n(g)} < 0 (> 0)$ are crucial for the infeasibility.*

Proof. The conclusions follow directly from Proposition 1. The coefficients (parameters F_l, H_g, L_g) of nonzero dual values $\bar{\mu}_l^+$, $\bar{\mu}_l^-$, and $\bar{\phi}_g^+, \bar{\phi}_g^-$ are crucial for the violation of inequality (6.17), since if such parameters are changed, the system can be feasible. From (6.14), $\bar{\phi}_g^+ = \lambda_{n(g)}$ if $\lambda_{n(g)} > 0$ and $\bar{\phi}_g^- = -\lambda_{n(g)}$ if $\lambda_{n(g)} < 0$ at extreme rays, nonzero $\lambda_{n(g)}$ corresponds to the generator capacity H_g or L_g. $\qquad\square$

Corollary 2 provides an intuition to identify extreme rays that are likely to cause system infeasibility. On the other hand, the identified extreme rays along with (6.17) can be used as constraints to ensure dispatch feasibility, which are the extreme ray feasibility cuts discussed in this chapter. When $\bar{\mu}_l^+$ or $\bar{\mu}_l^- > 0$, increasing the transmission line capacity F_l increases the likelihood of feasibility of the system. Therefore, the corresponding transmission lines are likely to be congested. Similarly, if $\lambda_{n(g)} \neq 0$, the generator g is likely to be at the capacity bounds. These intuitions can be used to identify the lines and generators. The left hand of (6.17) can be seen as the summation of weighted generation capacities, weighted transmission line capacities, and weighted loads, where the weights are determined by the dual cone structure.

6.2.3   Extreme Rays of the Dual Cone

The extreme rays of the dual cone are characterized in this part. Specially, the extreme rays that cause the violation of condition (6.17) when system parameters change, i.e., uncertainty happens, are of interests, denote these rays as *crucial extreme rays*.

First, the trivial extreme rays that are unlikely to be violated are characterized.

Lemma 3. *For any extreme ray* $\gamma = (\phi_g^+, \phi_g^-, \mu_l^+, \mu_l^-, \lambda_n, \tau) \in Q$, *if* $\tau = 0$, *then* γ *is one of the following cases,*

$$\gamma_k^1 = \begin{cases} \mu_k^+ = \mu_k^- = 1 \\ \mu_l^+ = \mu_l^- = 0 \quad \forall l : l \neq k \\ \phi_g^+ = \phi_g^- = 0 \quad \forall g \\ \lambda_n = 0 \qquad \forall n \\ \tau = 0 \end{cases} \qquad \gamma_i^2 = \begin{cases} \phi_i^+ = \phi_i^- = 1 \\ \phi_g^+ = \phi_g^- = 0 \quad \forall g : g \neq i \\ \mu_l^+ = \mu_l^- = 0 \quad \forall l \\ \lambda_n = 0 \qquad \forall n \\ \tau = 0 \end{cases}$$

$$\gamma_k^3 = \begin{cases} \mu_k^+ = 1 \\ \mu_k^- = 0 \\ \mu_l^+ = \mu_l^- = 0 \qquad \forall l : l \neq k \\ \lambda_n = -\Psi_{kn} \qquad \forall n \\ \phi_g^+ = \max(\lambda_{n(g)}, 0) \quad \forall g \\ \phi_g^- = \max(-\lambda_{n(g)}, 0) \quad \forall g \\ \tau = 0 \end{cases} \qquad \gamma_k^4 = \begin{cases} \mu_k^- = 1 \\ \mu_k^+ = 0 \\ \mu_l^+ = \mu_l^- = 0 \qquad \forall l : l \neq k \\ \lambda_n = \Psi_{kn} \qquad \forall n \\ \phi_g^+ = \max(\lambda_{n(g)}, 0) \quad \forall g \\ \phi_g^- = \max(-\lambda_{n(g)}, 0) \quad \forall g \\ \tau = 0 \end{cases}$$

Proof. First, it is clear that the set of rays in the lemma are conically independent. Then, $\forall \gamma = (\phi_g^+, \phi_g^-, \mu_l^+, \mu_l^-, \lambda_n, \tau) \in Q$, if $\tau = 0$, γ can be written as the conic combination,

$$\gamma = \sum_{\forall g} \bar{\phi}_g \gamma_g^2 + \sum_{\forall l} \left[\bar{\mu}_l \gamma_l^1 + (\mu_l^+ - \bar{\mu}_l)\gamma_l^3 + (\mu_l^- - \bar{\mu}_l)\gamma_l^4 \right],$$

where $\bar{\mu}_l = \min(\mu_l^+, \mu_l^-)$ and $\bar{\phi}_g = \min(\phi_g^+, \phi_g^-)$. □

The number of extreme rays in Lemma 3 is linear to the network size. When applying these to inequality (6.17), γ_k^1 and γ_i^2 are simply corresponding to nonnegative line capacities and generator capacities. While γ_k^3 and γ_k^4 indicate that under the current system state parameters, for any single transmission line k, it has the sufficient capacity to supply the load in the optimist case. These constraints are not trivial. However, in the practical power system network, redundancy has been built and these constraints are rarely violated even when uncertainty are considered.

Next, the crucial extreme rays that are likely to be violated are characterized.

Lemma 4. *The extreme rays in Q has one-to-one correspondence to the extreme points in Q' that is obtained by fixing τ.*

Proof. From equation (6.14), $\phi_g^+, \phi_g^-, \forall g$ are determined by $\lambda_{n(g)}$. Thus the dual cone Q is described by equation (6.15).

A cone can be represented in the form, $D = \{x \in \mathbb{R} | Ax \leq 0\}$ or $D = \{z \in \mathbb{R} | Az = 0, z \geq 0\}$. Then the dual cone can be represented as,

$$
Q = \left\{ \mu^+, \mu^-, \lambda^+, \lambda^-, \tau^+, \tau^- \geq 0 \,\middle|\, \begin{bmatrix} \psi' & -\psi' & I & -I & 1 & -1 \end{bmatrix} \begin{bmatrix} \mu^+ \\ \mu^- \\ \lambda^+ \\ \lambda^- \\ \tau^+ \\ \tau^- \end{bmatrix} = 0 \right\}
$$

Denote $Q = \{\gamma \geq 0 | A\gamma = 0\}$, where $A = \begin{bmatrix} \psi' & -\psi' & I & -I & 1 & -1 \end{bmatrix}$ and $\gamma = (\mu^+, \mu^-, \lambda^+, \lambda^-, \tau^+, \tau^-)$

Consider the extreme rays that $\tau > 0$, i.e., $\tau^+ > 0, \tau^- = 0$.

W.l.o.g., let $\tau^+ = 1, \tau^- = 0$. Then polyhedron $Q' = \{x | Bx = 1, x \geq 0\}$ is obtained, where $B = \begin{bmatrix} \psi' & -\psi' & I & -I \end{bmatrix}$ and $x = (\mu^+, \mu^-, \lambda^+, \lambda^-)$

Now the Lemma becomes to prove that x is an extreme point in Q' iff $\gamma = (x, 1, 0)$ is an extreme ray in Q.

Sufficiency: prove by contradiction.

Assume γ is not an extreme ray in Q. Then $\exists$ non-identical $\gamma_1, \gamma_2 \in Q$ s.t. $\gamma = \lambda\gamma_1 + (1 - \lambda)\gamma_2, \lambda \in (0, 1)$

Since γ has $\tau^- = 0$, then $\gamma_1 = (x_1, \tau_1^+, 0)$ and $\gamma_2 = (x_2, \tau_2^+, 0)$.

74

Suppose one of τ_1^+, τ_2^+ is zero, w.l.o.g., assume $\tau_2^+ = 0$, then $x = \lambda x_1 + (1-\lambda)x_2$ and $\lambda \tau_1^+ + (1-\lambda)\tau_2^+ = \lambda \tau_1^+ = 1$.

Note $\frac{x_1}{\tau_1^+} = \lambda x_1$ is a feasible point in Q' and x_2 is a non-zero ray in recession cone of Q'.

This contradicts that x is an extreme point in Q.

Suppose none of τ_1^+, τ_2^+ is zero, i.e., $\tau_1^+, \tau_2^+ > 0$.

Then $\gamma = \lambda \gamma_1 + (1-\lambda)\gamma_2 \Rightarrow \lambda \tau_1^+ + (1-\lambda)\tau_2^+ = 1$

Note $\frac{x_1}{\tau_1^+}, \frac{x_2}{\tau_2^+}$ are two feasible points in Q', let $\beta_1 = \lambda \tau_1^+, \beta_2 = (1-\lambda)\tau_2^+$.

Then $x = \beta_1 \frac{x_1}{\tau_1^+} + \beta_2 \frac{x_2}{\tau_2^+}, \beta_1 + \beta_2 = 1, \beta_1, \beta_2 \in (0,1)$.

This contradicts that x is an extreme point in Q.

Necessity: prove by contradiction.

Assume x is not an extreme point in Q'. Then $\exists$ non-identical $x_1, x_2 \in Q'$ s.t. $x = \lambda x_1 + (1-\lambda)x_2, \lambda \in (0,1)$.

Then $\gamma = (x, 1, 0) = \lambda(x_1, 1, 0) + (1-\lambda)(x_2, 1, 0)$.

This contradicts that γ is an extreme ray of Q.

Similarly, the conclusions hold when $\tau < 0$ or $\tau = 0$. The Lemma is proved.

$\square$

Lemma 5. *For any extreme ray* $\gamma = (\phi_g^+, \phi_g^-, \mu_l^+, \mu_l^-, \lambda_n, \tau) \in Q$ *with* $\tau \neq 0$, τ *is normalized such that* $|\tau| = 1$. *Then* γ *can be represented as follows,*

$$
\gamma^5_{\tilde{L},\tilde{N}} = \begin{cases}
\mu_l^+ = \max(\tilde{\mu}_l^{\tilde{L},\tilde{N}}, 0) & l \in \tilde{L} \\
\mu_l^- = \max(-\tilde{\mu}_l^{\tilde{L},\tilde{N}}, 0) & l \in \tilde{L} \\
\mu_l^+ = \mu_l^- = 0 & \forall l \in L \setminus \tilde{L} \\
\lambda_n = 0 & \forall n \in \tilde{N} \\
\lambda_n = \tilde{\lambda}_n^{\tilde{L},\tilde{N}} & \forall n \in N \setminus \tilde{N} \\
\phi_g^+ = \max(\lambda_{n(g)}, 0) & \forall g \in G \\
\phi_g^- = \max(-\lambda_{n(g)}, 0) & \forall g \in G \\
\tau = 1
\end{cases}
\qquad
\gamma^6_{\tilde{L},\tilde{N}} = \begin{cases}
\mu_l^+ = \max(-\tilde{\mu}_l^{\tilde{L},\tilde{N}}, 0) & l \in \tilde{L} \\
\mu_l^- = \max(\tilde{\mu}_l^{\tilde{L},\tilde{N}}, 0) & l \in \tilde{L} \\
\mu_l^+ = \mu_l^- = 0 & \forall l \in L \setminus \tilde{L} \\
\lambda_n = 0 & \forall n \in \tilde{N} \\
\lambda_n = -\tilde{\lambda}_n^{\tilde{L},\tilde{N}} & \forall n \in N \setminus \tilde{N} \\
\phi_g^+ = \max(\lambda_{n(g)}, 0) & \forall g \in G \\
\phi_g^- = \max(-\lambda_{n(g)}, 0) & \forall g \in G \\
\tau = -1
\end{cases}
$$

γ^5, γ^6 are induced by the selection of two subsets: $\tilde{L} \subseteq L$, $\tilde{N} \subseteq N_G \subseteq N$, where N_G is the subset of buses with generators. Moreover, $|\tilde{L}| = |\tilde{N}|$. The selection results in a sub-square-matrix $\Psi^{\tilde{N},\tilde{L}}$, which consists of the corresponding rows $n \in \tilde{N}$ and columns $l \in \tilde{L}$. The selection is restricted such that $\Psi^{\tilde{N},\tilde{L}}$ is nonsingular. Then, $\tilde{\mu}_{\tilde{L}}^{\tilde{N},\tilde{L}} = \left(\Psi^{\tilde{N},\tilde{L}}\right)^{-1} \mathbf{1}^{\tilde{N}}$ and $\tilde{\lambda}_{N\setminus\tilde{N}}^{\tilde{N},\tilde{L}} = \mathbf{1}^{N\setminus\tilde{N}} - \Psi^{N\setminus\tilde{N},\tilde{L}}\tilde{\mu}_{\tilde{L}}^{\tilde{N},\tilde{L}}$, where $\mathbf{1}$ is the column vector with all elements as 1 with proper dimension, $\Psi^{N\setminus\tilde{N},\tilde{L}}$ is the sub-matrix consists of the corresponding rows $l \in \tilde{L}$ and columns $n \in N \setminus \tilde{N}$.

Proof. For any extreme ray with $\gamma \neq 0$, w.l.o.g., τ is normalized $|\tau| = 1$. From Lemma 4, the extreme rays in the dual cone have one-to-one correspondence with the extreme points in the polyhedron by restricting $|\tau| = 1$. The goal is equivalent to characterizing the extreme points of the following polyhedron:

$$\mathbf{\Psi}'\mu + \mathbf{I}\lambda = \mathbf{1} \text{ or } -\mathbf{1} \quad \Leftrightarrow \quad [\mathbf{\Psi}' \ \mathbf{I}] \begin{bmatrix} \mu \\ \lambda \end{bmatrix} = \mathbf{1} \text{ or } -\mathbf{1} \tag{6.18}$$

where $\mu_{|L|\times 1}$ is the line variables vector with components that $\mu_l = \mu_l^+ - \mu_l^-, \forall l$, $\lambda_{|N|\times 1}$ is the bus variables, $\mathbf{\Psi}'_{|N|\times|L|}$ is the PTDF matrix, $\mathbf{I}_{|N|\times|N|}$ is identity matrix, and $\mathbf{1}_{|N|\times 1}$ is the unit vector with all components equal to one.

After fixing τ, (6.15) is a linear system with $|N|+|L|$ variables and $|N|$ constraints. The extreme points of this polyhedron, i.e., the extreme rays of Q by fixing $\tau = 1$, can

be solved by partitioning the matrix $[\boldsymbol{\Psi}'\ \mathbf{I}]$ to a $|N| \times |N|$ basic matrix and a $|N| \times |L|$ non-basic matrix. The way to partition $[\boldsymbol{\Psi}'\ \mathbf{I}]$ is to select i, $0 \leq i \leq |N|$ line variables μ_l and $(|N| - i)$ bus variables λ_n to be the basic variables. Correspondingly, the rest $(|L| - i)$ line variables μ_l and i bus variables λ_n are selected to be non-basic variables and equal to zero. Let $\boldsymbol{\Psi}'_{\tilde{L},\tilde{N}}$ denote the resulting PTDF sub-square-matrix by selecting i columns corresponding to the basic line variables and i rows corresponding to the non-basic bus variables. Denote the extreme ray that is characterized by the selection of i lines and i, $0 \leq i \leq |N|$ buses as i-dimensional extreme ray. Then the basic line variables, denoted as μ_B, can be calculated by the following equation,

$$\mu_B = (\boldsymbol{\Psi}'_{\tilde{L},\tilde{N}})^{-1}\tilde{\mathbf{1}} \tag{6.19}$$

where $\tilde{\mathbf{1}}$ is the unit vector defined previously with suitable dimension. μ_l^+ and $\mu_l^-, \forall l$ are determined based on the sign of $\mu_l, \forall l$. Then, $\lambda_n, \forall n$ are calculated according to (6.15). Finally, ϕ_g^- and $\phi_g^+, \forall g$ are determined based on the sign of $\lambda_{n(g)}, \forall g$ according to (6.14).

These extreme rays are corresponding to $\gamma_{\tilde{L},\tilde{N}}^5$ and $\gamma_{\tilde{L},\tilde{N}}^6$. These extreme rays are characterized by the combinatorial selection of lines and buses in the system. □

With the above lemmas, all the extreme rays in Q are characterized.

Proposition 6. *The extreme rays in the dual cone include all the extreme rays* $\gamma^1, \gamma^2, ..., \gamma^6$.

Proof. The results follow directly from Lemma 3 and Lemma 5. Since all possible cases of τ are included, these are all the extreme rays. □

6.3 Applications

In this section, the derived extreme ray feasibility cuts are applied to the unit commitment problem with uncertainty. Two types of uncertainties are studied, the

single-generator-failure contingency (G-1) and load uncertainty. In the G-1 contingency modeling, a single generator could fail in any period. The system requires a feasible post-contingency dispatch in every contingency scenario. In the load uncertainty modeling, the loads at buses could vary in ranges. The loads can be seen as the residual loads by subtracting dispatched renewable resources from consumers' loads. The system requires a feasible dispatch in any realized load uncertainty scenario.

6.3.1 Offline Study to Identify Crucial Extreme Rays

Although all extreme rays have been characterized, the number of crucial extreme rays, γ^5 and γ^6 in Lemma 5, is exponential, which is at the scale of the combination number $|N| + |L|$ choose $|N|$. It is not practical to enumerate all the extreme rays. Lemma 5 shows γ^5 and γ^6 are characterized by the combinatorial selection of lines and buses in the system. From Corollary 2, the selection of lines corresponds to the congested transmission lines; and the selection of buses corresponds to the buses that have generator with extra reserves. In other works, μ_l^- or $\mu_l^+, \forall l$ is non-zero only if the corresponding transmission line l is operating at its full capacity F_l. The extreme rays induced by these selections are the crucial rays.

The selection of $\tilde{L}$ and $\tilde{N}$ can be based on historical data or experience, i.e., the congested transmission lines and the generators with reserves that are likely not fully dispatched. The selection of transmission lines and buses has the same number. It indicates whenever a transmission line is congested, there is a bus where generators have extra capacities that cannot be dispatched. Furthermore, there are strong connections between the congested lines and the buses with extra capacities. In fact, whenever a transmission line is at its full capacity, the bus with extra capacity is likely close to the congested line. The chance of higher dimensional rays, i.e., several transmission lines are at full capacities at the same time, to be crucial extreme rays

78

is much smaller than the lower dimensional extreme rays. Therefore, based on the engineering insights of the power system, the candidates of crucial extreme rays can be limited to a reasonable number.

In this chapter, an offline simulation procedure is suggested to identify the crucial extreme rays for a given power system. The procedure is described in Figure 6.1. Historical data can also be used for the selection of the crucial extreme rays.
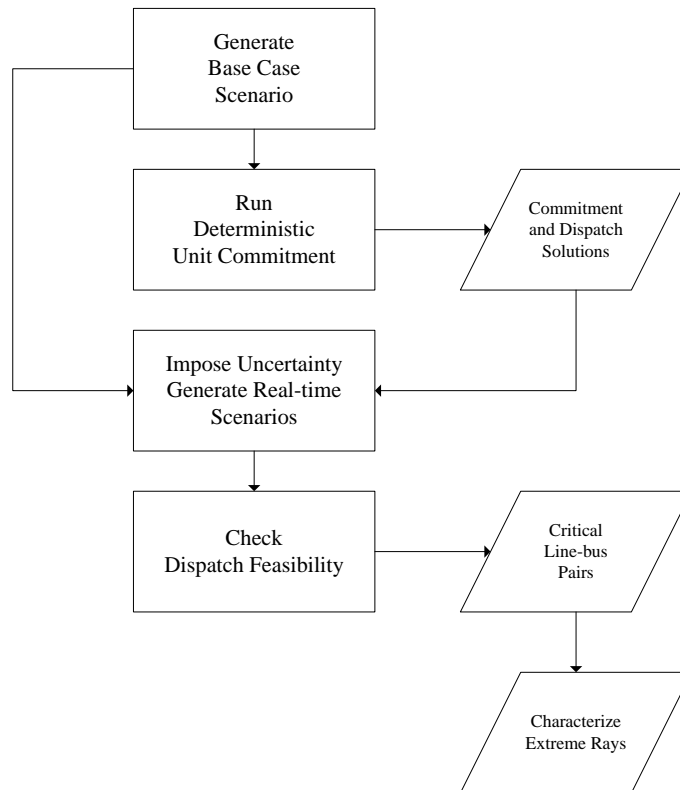
Figure 6.1: Flow Chart of Identifying Crucial Extreme Rays

First, a base case scenario is generated as the day-ahead predicted load. Then the deterministic UC model (with reserves requirements) is solved and the commitment and dispatch solutions are obtained. Next, the uncertainty is imposed. The uncertainty includes load fluctuation and system contingencies. The power flows re-dispatch after imposing the uncertainty. The re-dispatch is then examined. If there

is no feasible re-dispatch solution, then the transmission lines that reach their full capacities and the buses that have undelivered capacities are recorded to characterize the crucial extreme rays.

The crucial extreme rays, i.e., the selections of the transmission lines and buses are inherited from the power system characteristics, such as the generation and load distribution, the transferability of the network. The elections should be invariant with uncertainty in the power system. Once the crucial extreme rays have been identified, they can be utilized to respond to different types of uncertainties.

6.3.2 Sufficient Reserve Levels

Given the identified crucial extreme rays, the sufficient zonal reserve levels under uncertainty can be determined. The sufficient zonal reserve levels, represented as $\alpha\%$ of the total zonal loads, give the lower bounds of the required reserves in order to ensure the system security under uncertainty. If the $\alpha\%$ level is not achieved, then there are situations that some reserves cannot be dispatched due to system transmission limits, consequently cause security issues. For a given crucial extreme ray $\bar{\gamma}$ and the $\alpha\%$ level, denote the sufficient reserve level problem as $SRL(\bar{\gamma}, \alpha)$. The $SRL(\bar{\gamma}, \alpha)$ determines whether the $\alpha\%$ level is sufficient for the given crucial extreme ray $\bar{\gamma}$. In order to obtain the sufficient reserve levels for the entire system, all of the crucial extreme rays are considered. The algorithm to find the sufficient reserve levels is proposed and described in Algorithm 2.

This algorithm iteratively increases the $\alpha\%$ level until it is sufficient to ensure system security for all of the identified crucial extreme rays. The mixed integer programming (MIP) $SRL(\bar{\gamma}, \alpha)$ does not need to be solved to the optimality. Once a feasible solution is found and the objective value with respect to the corresponding crucial extreme ray is less than zero, it indicates the $\alpha\%$ level is not sufficient for the

Algorithm 2 Sufficient Reserve Level Algorithm

$\alpha = \alpha_0$, Insufficient = **true**
while Insufficient = **true do**
    Insufficient = **false**
    Increase α level
    for each crucial extreme ray $\bar{\gamma}_i, 1 \le i \le M$ **do**
        Solve $SRL(\bar{\gamma}, \alpha)$
        if BestIncubent < 0 **then**
            Insufficient = **true**
            Exit for Loop
        else if BestBound > 0 **then**
            Go to check the next crucial extreme ray
        end if
    end for
end while
---

given extreme ray. Then there is no need to check the remaining crucial rays, "for loop" is quit, and the $\alpha\%$ level is increased. Similarly, if the best bound of the MIP is larger than zero, it indicates that the $\alpha\%$ level is sufficient for the given crucial extreme ray. By checking the incumbent solution and the best bound of the MIP, the proposed algorithm can be solved efficiently. Once the $\alpha\%$ level has nonnegative solution of $SRL(\bar{\gamma}, \alpha)$ for all of the crucial extreme rays, the $\alpha\%$ level is claimed to be the sufficient reserve level for the system under uncertainty.

The $SRL(\bar{\gamma}, \alpha)$ is described as follows with different uncertainty modeling.

Sufficient Reserve Levels for G-1 Contingency

In this part, the uncertainty is modeled as the G-1 contingency. For each crucial extreme ray $\bar{\gamma} = (\bar{\phi}_g^+, \bar{\phi}_g^-, \bar{\mu}_l^+, \bar{\mu}_l^-, \bar{\lambda}_n, \bar{\tau}) \in Q$, denote the following generator contingency sufficient reserve level problem as $SRL^{GC}(\bar{\gamma}, \alpha)$.

$$\min \quad \sum_{\forall g} \left(P_g^{\max} \bar{\phi}_g^+ - P_g^{\min} \bar{\phi}_g^- \right) u_g (1 - x_g)$$

$$+ \sum_{\forall l} F_l (\bar{\mu}_l^+ + \bar{\mu}_l^-) - \sum_{\forall n} D_n \bar{\lambda}_n \tag{6.20}$$

s.t. $(6.3) - (6.5)$

$$p_g \geq P_g^{\min} u_g \qquad\qquad \forall g \qquad (6.21)$$

$$p_g + r_g \leq P_g^{\max} u_g \qquad\qquad \forall g \qquad (6.22)$$

$$\sum_{\forall g \in Z_k} r_g \geq \alpha\% \sum_{\forall n \in Z_k} D_n \qquad\qquad \forall k \qquad (6.23)$$

$$r_g \geq 0 \qquad\qquad \forall g \qquad (6.24)$$

$$u_g \in \{0, 1\} \qquad\qquad \forall g \qquad (6.25)$$

$$\sum_g x_g = 1 \qquad\qquad (6.26)$$

$$x_g \in \{0, 1\} \qquad\qquad \forall g \qquad (6.27)$$

The $SRL^{GC}(\bar{\gamma}, \alpha)$ aims at determining if the $\alpha\%$ level is sufficient to ensure a feasible dispatch for every post-contingency state given a set of feasible pre-contingency commitment and generation solutions that satisfy the $\alpha\%$ level reserve requirements. In this formulation, it is assumed that once the generator is committed, the resulting capacity will be $[P_g^{\min}, P_g^{\max}], \forall g$, which are the generators' minimum and maximum generation capacity. Equation (6.20) is the objective. If the objective value is less than zero, from Corollary 2, it indicates that there is no feasible dispatch in some post-contingency state; thus, the $\alpha\%$ level is not sufficient to ensure the system G-1 security; otherwise the α level is sufficient for the given crucial extreme ray. Equations (6.21) and (6.22) restrict pre-contingency generation levels with the consideration of reserves. Equation (6.23) describes the zonal reserve requirements that the total zonal reserves are more than $\alpha\%$ of the total zonal loads. Equation (6.24) restricts single

generator failure. Next, the non-linear terms $u_g(1 - x_g)$ are linearized as $y_g, \forall g$, and the $SRL^{GC}(\bar{\gamma}, \alpha)$ is represented as follows.

$$\min \quad \sum_{\forall g}(P_g^{\max}\bar{\phi}_g^+ - P_g^{\min}\bar{\phi}_g^-)y_g + \sum_{\forall l}F_l(\bar{\mu}_l^+ + \bar{\mu}_l^-) - \sum_{\forall n}D_n\bar{\lambda}_n \qquad (6.28)$$

$$\text{s.t.} \quad (6.3) - (6.5)$$

$$(6.21) - (6.27)$$

$$y_g \leq u_g \qquad\qquad\qquad\qquad\qquad\qquad\qquad \forall g \qquad (6.29)$$

$$y_g \leq (1 - x_g) \qquad\qquad\qquad\qquad\qquad\qquad \forall g \qquad (6.30)$$

$$y_g \geq u_g - x_g \qquad\qquad\qquad\qquad\qquad\qquad \forall g \qquad (6.31)$$

$$0 \leq y_g \leq 1 \qquad\qquad\qquad\qquad\qquad\qquad\qquad \forall g \qquad (6.32)$$

Sufficient Reserve Levels for Load Uncertainty

In this part, the uncertainty is modeled as the residual load uncertainty. For any given $\bar{\gamma} = (\bar{\phi}_g^+, \bar{\phi}_g^-, \bar{\mu}_l^+, \bar{\mu}_l^-, \bar{\lambda}_n, \bar{\tau}) \in Q$, denote the following load uncertainty sufficient reserve level problem as $SRL^{LU}(\bar{\gamma}, \alpha)$.

$$\min \quad \sum_{\forall g}(P_g^{\max}\bar{\phi}_g^+ - P_g^{\min}\bar{\phi}_g^-)u_g + \sum_{\forall l}F_l(\bar{\mu}_l^+ + \bar{\mu}_l^-) - \sum_{\forall n}d_n\bar{\lambda}_n \qquad (6.33)$$

$$\text{s.t.} \quad (6.3) - (6.5)$$

$$(6.21) - (6.25)$$

$$\mathbf{d} \in \mathbb{U} \qquad\qquad\qquad\qquad\qquad\qquad\qquad\qquad\qquad (6.34)$$

The differences between $SRL^{LU}(\bar{\gamma}, \alpha)$ and $SRL^{GC}(\bar{\gamma}, \alpha)$ is loads in $SRL^{LU}(\bar{\gamma}, \alpha)$ become variables and can be varied in a given load uncertainty set $\mathbb{U}$. $SRL^{LU}(\bar{\gamma}, \alpha)$ aims at determining if the $\alpha\%$ level is sufficient to ensure a feasible dispatch for any load realization within the uncertainty set given a set of feasible commitment

83

and generation solutions that satisfy the $\alpha\%$ level reserve requirements for predicted loads. The load uncertainty set is modeled as a budget uncertainty set $\mathbb{U}(\kappa_1, \kappa_2, \kappa_3)$ (Jiang *et al.*, 2014). It is represented as follows.

$$
\mathbb{U}(\kappa_1, \kappa_2, \kappa_3) = \left\{ \mathbf{d} : \begin{array}{ll} (1 - \kappa_1\%)D_{nt} \leq d_{nt} \leq (1 + \kappa_1\%)D_{nt} & \forall n, t \\ \sum_{\forall n} d_{nt} \leq (1 + \kappa_2\%) \sum_{\forall n} D_{nt} & \forall t \\ \sum_{\forall t} \sum_{\forall n} d_{nt} \leq (1 + \kappa_3\%) \sum_{\forall t} \sum_{\forall n} D_{nt} & \end{array} \right\} \qquad (6.35)
$$

The security conservativeness can be controlled by modifying the parameters $(\kappa_1, \kappa_2, \kappa_3)$.

In the algorithm, the MIP problems typically do not need to be solved to the optimality. Once a feasible solution is found and the objective value with respect to the corresponding crucial extreme ray is less than zero, it indicates the $\alpha\%$ level is not sufficient for the given extreme ray. Then there is no need to check the remaining crucial rays. The loop is terminated and the $\alpha\%$ level is increased. Similarly, if the best bound of the MIP is larger than zero, it indicates that the $\alpha\%$ level is sufficient for the given crucial extreme ray. By checking the incumbent solution and the best bound of the MIP, the proposed algorithm can be solved efficiently. Once the $\alpha\%$ level has nonnegative solution of $SRL(\bar{\gamma}, \alpha)$ for all of the crucial extreme rays, the $\alpha\%$ level is claimed to be the SRL for the system with corresponding uncertainty.

In these SRL models, the UC indicator, $u_g, \forall g$, are variables which satisfies the feasibility condition of the nominal scenario. Therefore, in the SRL formulations, it picks the worst case commitment status. The reserve level obtained by these models are conservative, but sufficient. Practically used reserve levels are much lower. However, these reserve levels provide a metric to review the effectiveness of the method.

In this part, the security constraints for the UC problem with uncertainty are developed based on Proposition 1 and the identified crucial extreme rays. The security constraints change the generators' commitment status and dispatch schedule to ensure the system security under uncertainty. The constraints cut unreliable MIP solutions from the deterministic UC feasible region. From another prospective, the constraints re-allocate the reserves in the system in order to avoid the undeliverability of the reserves due to system transmission limits. It is a mathematical way to determine the reserves in the system. The security constraints with respect to different uncertainty modelings are given as follows.

Security Constraints for G-1 Contingency

The security constraints with respect to G-1 contingency are given as follows.

$$\hat{p}_{gt}^H \leq P_g^{\max} u_{gt} \qquad \qquad \forall g, t \qquad (6.36)$$

$$\hat{p}_{gt}^H \leq p_{gt} + R_g^{10} \qquad \qquad \forall g, t \qquad (6.37)$$

$$\hat{p}_{gt}^L \geq P_g^{\min} u_{gt} \qquad \qquad \forall g, t \qquad (6.38)$$

$$\hat{p}_{gt}^L \geq p_{gt} - R_g^{10} \qquad \qquad \forall g, t \qquad (6.39)$$

$$\sum_{\forall g} G1_g^s \left(\hat{p}_{gt}^H \bar{\phi}_{ig}^+ - \hat{p}_{gt}^L \bar{\phi}_{ig}^- \right) + \sum_{\forall l} F_l (\bar{\mu}_{il}^+ + \bar{\mu}_{il}^-)$$

$$- \sum_{\forall n} D_{nt} \bar{\lambda}_{in} \geq 0 \qquad \qquad \forall s, i, t \qquad (6.40)$$

Equation (6.36)-(6.39) restrict the post-contingency available generation capacities, $\hat{p}_{gt}^L, \hat{p}_{gt}^H, \forall g, t$. The capacities are limited by the commitment status, $u_{gt}, \forall g, t$; the physical generation capability, $P_g^{\min}, P_g^{\max}, \forall g, t$; and the 10-minute fast-ramping capability, $R_g^{10}, \forall g$. Equation (6.40) are the security constraints. $G1_g^s, \forall s, g$, are the indicator parameters of generator failures. If the generator fails, $G1_g^s = 0$; otherwise

$G1_g^s = 1$. $\bar{\gamma}_i = (\bar{\phi}_{ig}^+, \bar{\phi}_{ig}^-, \bar{\mu}_{il}^+, \bar{\mu}_{il}^-, \bar{\lambda}_{in}, \bar{\tau}_i), \forall i$, are the identified crucial extreme rays, which are parameters that have been calculated from offline study.

One of the extreme rays, the zero-dimensional extreme ray, is characterized by selecting zero line variables and all bus variables to be basic variables. Then $\bar{\lambda}_n = 1, \forall n$; $\bar{\mu}_l^+ = \bar{\mu}_l^- = 0, \forall l$; $\bar{\phi}_g^- = 0, \forall g$; $\bar{\phi}_g^+ = 1, \forall g$; i.e., $\bar{\gamma}_0 = (\bar{\phi}_{0g}^+, \bar{\phi}_{0g}^-, \bar{\mu}_{0l}^+, \bar{\mu}_{0l}^-, \bar{\lambda}_{0n}, \bar{\tau}_0) = (\mathbf{1}, \mathbf{0}, \mathbf{0}, \mathbf{0}, \mathbf{1}, 1)$. The corresponding G-1 security constraints with respect to $\bar{\gamma}_0$ are simplified as follows.

$$(6.36) - (6.37)$$

$$\sum_{\forall g} G1_g^s \hat{p}_{gt}^H - \sum_{\forall n} D_{nt} \geq 0 \qquad\qquad \forall s, t \qquad\qquad (6.41)$$

The security constraints require the post-contingency available capacities must be more than the total loads, which is a necessary condition to ensure a feasible post-contingency dispatch. In fact, the above security constraints with respect to the zero-dimensional extreme ray are equivalent to the reserve requirements as follows.

$$p_{gt} \geq P_g^{\min} u_{gt} \qquad\qquad \forall g, t \qquad\qquad (6.42)$$

$$p_{gt} + r_{gt} \leq P_g^{\max} u_{gt} \qquad\qquad \forall g, t \qquad\qquad (6.43)$$

$$r_{gt} \leq R_g^{10} \qquad\qquad \forall g, t \qquad\qquad (6.44)$$

$$\sum_{\forall q \in G} r_{qt} \geq r_{gt} + p_{gt} \qquad\qquad \forall g, t \qquad\qquad (6.45)$$

The security constraints and the reserve requirements are connected. For the security constraints with respect to higher-dimensional crucial extreme rays, weighted capacities, loads, and transmission line limits are combined together to restrict the allocation of the reserves in the system. The security constraints give the mathematical supports to determine the reserves in the system.

Security Constraints for Load Uncertainty

The security constraints with respect to load uncertainty are given as follows.

$$p_{gt}^H \leq P_g^{\max} u_{gt} \qquad\qquad \forall g, t \qquad (6.46)$$

$$p_{gt}^H \leq p_{g,t-1} + R_g^{hr} u_{g,t-1} + R_g^{SU} v_{gt} \qquad\qquad \forall g, t \qquad (6.47)$$

$$p_{gt}^L \geq P_g^{\min} u_{gt} \qquad\qquad \forall g, t \qquad (6.48)$$

$$p_{gt}^L \geq p_{g,t-1} - R_g^{hr} \qquad\qquad \forall g, t \qquad (6.49)$$

$$\sum_{\forall g} \left(p_{gt}^H \bar{\phi}_{ig}^+ - p_{gt}^L \bar{\phi}_{ig}^- \right) + \sum_{\forall l} F_l (\bar{\mu}_{il}^+ + \bar{\mu}_{il}^-)$$

$$- \sum_{\forall n} d_{int}^* \bar{\lambda}_{in} \geq 0 \qquad\qquad \forall i, t \qquad (6.50)$$

Equation (6.46)-(6.49) restrict the hourly available generation capacities, i.e., $p_{gt}^L, p_{gt}^H, \forall g, t$. The capacities are limited by the commitment status, the physical generation capability, and the hourly-ramping capability. Equation (6.50) gives the security constraints for load uncertainty. $d_{int}^*, \forall i, n, t$, denote the worst-case loads given a certain extreme ray i, a time period t, and an uncertainty set $\mathbb{U}$. They can be solved by the following worst-case load problem, denoted as $WL(i, t, \mathbb{U})$, $d_{int}^* = \arg\max WL(i, t, \mathbb{U}), \forall i, n, t$.

$$\max \quad \sum_{\forall n} d_{nt} \bar{\lambda}_{in} \qquad\qquad (6.51)$$

$$\text{s.t.} \quad \mathbf{d} \in \mathbb{U} \qquad\qquad (6.52)$$

This approach is similar to the TSRO. However, the crucial extreme rays are identified by offline study. The crucial extreme rays are used as fixed parameters in solving the worst-case loads in the uncertainty set, avoiding the bi-linear terms in the TSRO. The conservativeness can be controlled by designing different uncertainty sets and tuning parameters of the uncertainty sets.

Unit Commitment Model

Finally, the security constraints are included in the SCUC problem to obtain the reliable day-ahead UC schedule under uncertainty. The formulation is based on Hedman *et al.* (2010), and given as follows, denoted as the SCUC with security constraints,

$$\min \quad \sum_{\forall t} \sum_{\forall g} \left(C_g^{SU} v_{gt} + C_g^{NL} u_{gt} + C_g p_{gt} \right) \tag{6.53}$$

$$\text{s.t.} \quad v_{gt} \geq u_{gt} - u_{g,t-1} \qquad\qquad \forall g, t \tag{6.54}$$

$$\sum_{q=t-UT_g+1}^{t} v_{gq} \leq u_{gt} \qquad\qquad \forall g, t \tag{6.55}$$

$$\sum_{q=t+1}^{t+DT_g} v_{gq} \leq 1 - u_{gt} \qquad\qquad \forall g, t \tag{6.56}$$

$$P_g^{\min} u_{gt} \leq p_{gt} \leq P_g^{\max} u_{gt} \qquad\qquad \forall g, t \tag{6.57}$$

$$p_{gt} - p_{g,t-1} \leq R_g^{hr} u_{g,t-1} + R_g^{SU} v_{gt} \qquad\qquad \forall g, t \tag{6.58}$$

$$p_{g,t-1} - p_{gt} \leq R_g^{hr} u_{gt} + R_g^{SD}(v_{gt} - u_{gt} + u_{g,t-1}) \qquad\qquad \forall g, t \tag{6.59}$$

$$i_{nt} = \sum_{\forall g \in G(n)} p_{gt} - D_{nt} \qquad\qquad \forall n, t \tag{6.60}$$

$$-F_l \leq \sum_{\forall n} \Psi_{ln} i_{nt} \leq F_l \qquad\qquad \forall l, t \tag{6.61}$$

$$\sum_{\forall n} i_{nt} = 0 \qquad\qquad \forall t \tag{6.62}$$

$$u_{gt} \in \{0, 1\} \qquad\qquad \forall g, t \tag{6.63}$$

$$0 \leq v_{gt} \leq 1 \qquad\qquad \forall g, t \tag{6.64}$$

$$\mathbf{u}, \mathbf{g} \in \mathbb{C} \tag{6.65}$$

Equation (6.53) is the objective function to minimize the total costs including the startup cost, the no-load cost, and the dispatch cost. Equations (6.54)-(6.59) are resource-level constraints. Equation (6.54) specifies the relation between the commitment variables and the startup variables. Equation (6.55)-(6.56) are the minimum

up/down requirement constraints (Rajan and Takriti, 2005). Equation (6.57) restricts the generation dispatch bounds. Equations (6.58)-(6.59) are the hourly ramping constraints. Equations (6.60)-(6.62) are system-level constraints. Equation (6.63)-(6.64) specify the unit commitment status variables and the startup variables. Equation (6.65) represents the generic form of the developed security constraints. The reserve requirements are not formulated explicitly, but are restricted by the security constraint implicitly.

The problem is still formulated as a deterministic model, thus, can be solved efficiently. Compared with the deterministic UC formulation, a set of constraints (6.65), i.e., the security constraints, are included to ensure the system reliability under uncertainty.

6.4   Cases Study

In this section, the problem is modeled as a 24-period day-ahead SCUC problem with uncertainty. Two test cases are studied in this section, a 73-bus system and a 118-bus system. The original data can be found in University of Washington (2015). Table 6.1 lists the characteristics comparison of the two systems. There are more generators (maximum capacities range from 12MW to 400MW) in the 73-bus system; while there are fewer generators (maximum capacities range from 30MW to 420MW) in the 118-system, but the network structure of the 118-bus system is more complicated.

Table 6.1: Test Cases Comparison

	# of Buses	# of Lines	# of Gen.	Total Gen. Capacities (MW)	Peak Load (MW)
RTS96 73-bus system	73	120	99	10,215	8,550
IEEE 118-bus system	118	186	54	7,220	4,519

IBM ILOG CPLEX version 12.6, with Concert Technology version 3.0, is used to implement the test cases. A Dell Precision T7500 Workstation is used to run the C++ code. The processor of the workstation is a dual six-core Intel Xeon Processor X5690 (4.46GHz, 12M L3, 6.4GT/s). The memory of the workstation is 48GB, $1,333$MHz, DDR3RDIMM, ECC (6DIMMS). The MIP gap for CPLEX is set to be 0.5%.

6.4.1 RTS96 73-Bus System

The RTS96 73-bus system naturally has three zones. Each zone has 24 buses and are almost identical with each other except that Zone3 has one more bus. Figure 6.2 shows the network of this 73-bus system.
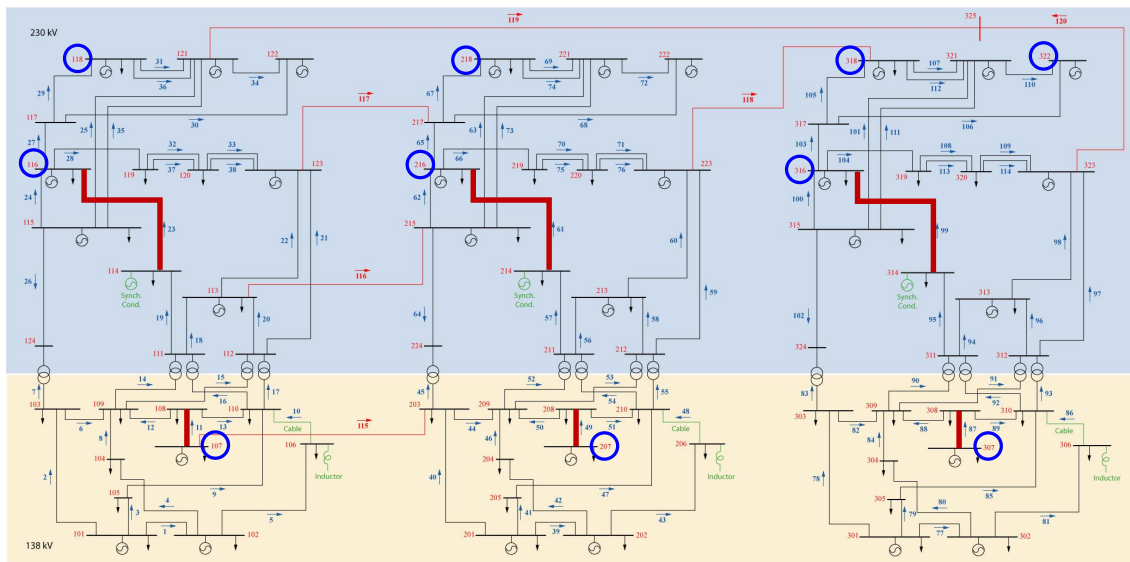
Figure 6.2: RTS96 73-Bus System

90

Crucial Extreme Rays

Different load profiles and transmission limits are tested to study the crucial extreme rays of the 73-bus system. The case profile identity "P1-P2-P3-P4" is described as follows.

- P1: Two different network configurations are tested, a 117-line system (P1=117) and a 120-line system (P1=120). Three transmission lines are switched off and on (the lines connecting bus 111-113, 211-213, 311-313 respectively) in these two networks.

- P2: Two different transmission systems are tested, a normal system (P2=N) and a congested system or (P2=C). Three transmission lines (the lines connecting bus 114-116, 214-216, 314-316 respectively) are derated from 500MW to 350MW in the congested system.

- **P3**: Two peak load distributions are tested. Figure **??** represents the peak load comparison of Load1 (P3=1) and Load2 (P3=2) in a single zone (the other two zones are duplicated). The total peak loads of both cases are 2,850MW in the single zone. However, in Load2 case, the bus 113 has a very high peak load.

- P4: Three typical load percentage profiles are tested. In the high-load day (P4=H), the loads across all periods vary from 59%-100% of the peak load; in the medium-load day (P4=M), the loads vary from 41%-66% of the peak load; in the low-load day (P4=L), the loads vary from 33%-52% of the peak load.

First, a benchmark of each system variation under G-1 contingency is studied. The problem is formulated as a TSSP, where the first stage is the pre-contingency base case and the second stage includes all the post-contingency scenarios. In the base case, all of the generators are available, i.e., there is no generator-failure in the system. In the second stage, each scenario represents an G-1 contingency, where one of the generators
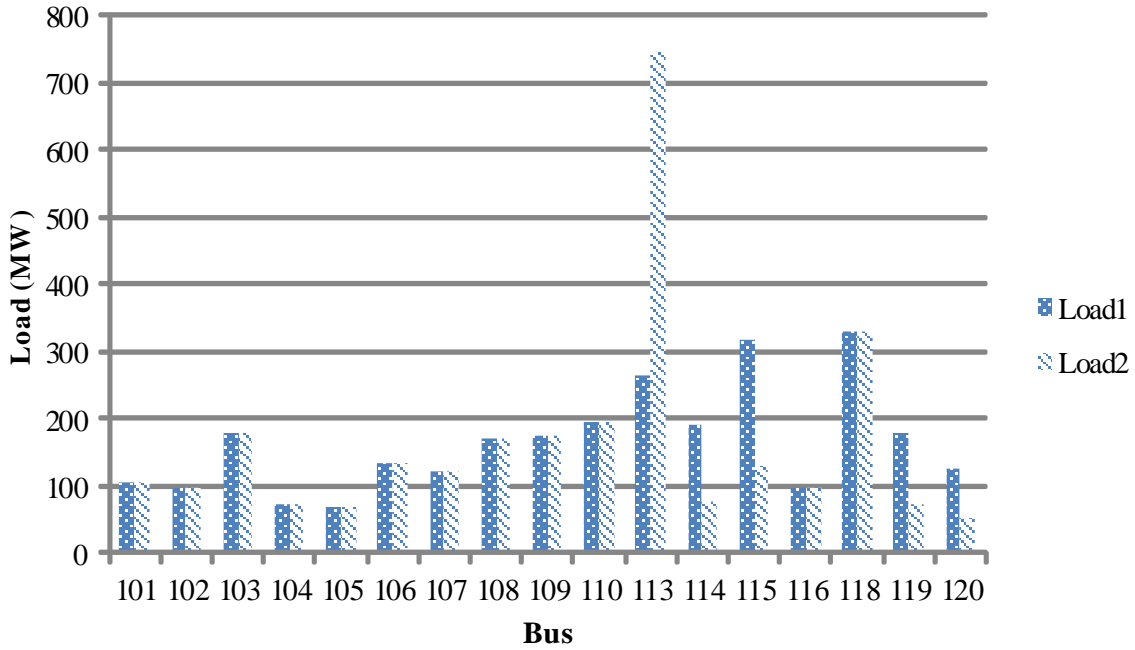
Figure 6.3: Peak Load Distribution

is failed in a certain period. The stochastic extensive form formulation (SEF) of this problem, by including all post-contingency scenarios explicitly, is very difficult to solve (Li *et al.*, 2015). The SEF introduces many second-stage (post-contingency) variables and constraints into the model, and causes the MIP to take a long time (to branch-and-bound, add cutting planes) to find the optimal solution within the desirable optimality gap. Instead of solving the SEF, a modified extensive form (MEF) algorithm is utilized as the benchmark. Figure 6.4 describes the procedure of the MEF algorithm. The master problem at first only includes the pre-contingency base case to avoid formulating all second-stage scenarios into the problem. After obtaining a set of UC and dispatch solutions, the load-shedding tests are carried out for post-contingency scenarios. If there exists non-zero load-shedding in some scenarios, then the corresponding scenario is added into the master problem with the whole set of variables and constraints of the scenario as they are formulated in the SEF. If there is

no load-shedding, the solution has met the G-1 security requirement. The MEF can solve the G-1 reliable UC problem for small test cases (73-bus system and 118-bus system) very efficiently (within few minutes). However, since each iteration of the algorithm introduces many variables and constraints into the MIP, the algorithm is expected to be unscalable.
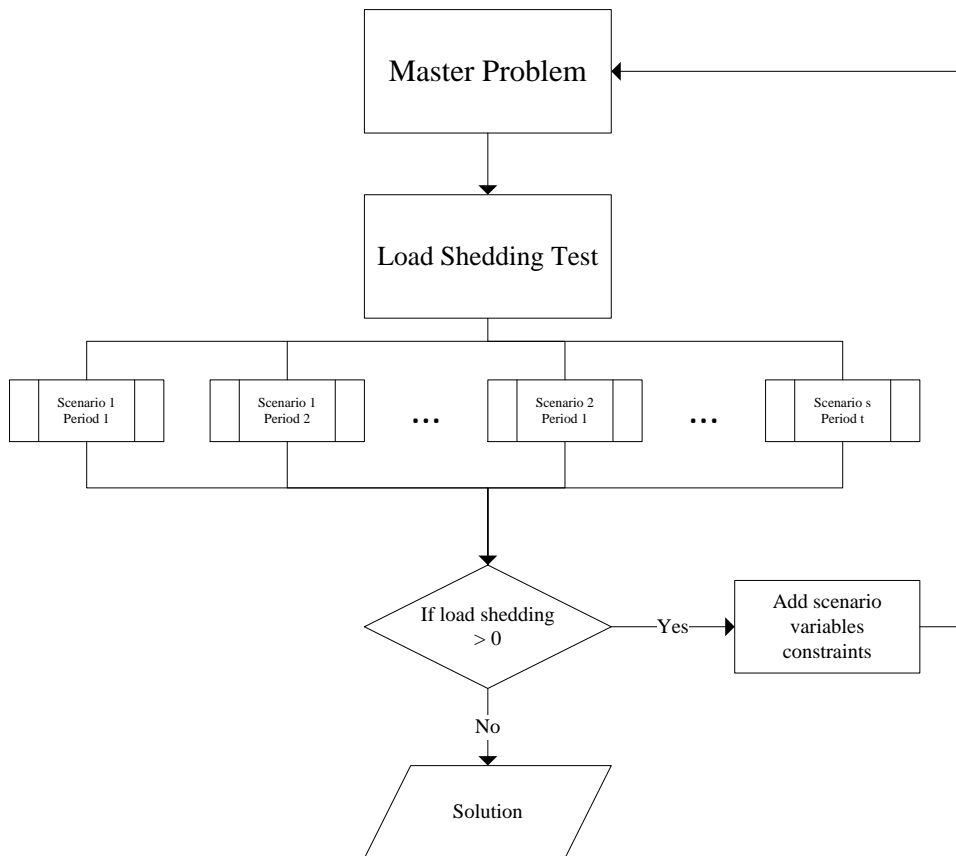
Figure 6.4: Modified Extensive Form Algorithm

Table 6.2 lists the UC solutions under different load profiles and network features. From the test results, when the thermal limits of the three selected lines are 500MW, the deterministic UC with reserves policy can ensure G-1 security for almost all cases except for the 117-line system under Load2 and high-load day. Simi-

Table 6.2: Modified Extensive Form Algorithm Results

Transmission lines #	117	117	117	120	120	120
Normal/Congested	N	N	N	N	N	N
Load distribution	1	1	1	1	1	1
Load percentage profile	L	M	H	L	M	H
Optimal solution without G-1 reliability (k$)	607	979	3,033	607	977	3,024
Load-shedding scenarios #	0	0	0	0	0	0
Total added scenarios #	0	0	0	0	0	0
Total iterations #	1	1	1	1	1	1
Optimal solution with G-1 reliability (k$)	607	979	3,033	607	977	3,024
Solution time (sec.)	12	8	12	10	10	13
Transmission lines #	117	117	117	120	120	120
Normal/Congested	N	N	N	N	N	N
Load distribution	2	2	2	2	2	2
Load percentage profile	L	M	H	L	M	H
Optimal solution without G-1 reliability (k$)	608	978	3,025	608	977	3,026
Load-shedding scenarios #	0	0	7	0	0	0
Total added scenarios #	0	0	18	0	0	0
Total iterations #	1	1	8	1	1	1
Optimal solution with G-1 reliability (k$)	608	978	3,025	608	977	3,026
Solution time (sec.)	10	10	167	10	9	12
Transmission lines #	117	117	117	120	120	120
Normal/Congested	C	C	C	C	C	C
Load distribution	1	1	1	1	1	1
Load percentage profile	L	M	H	L	M	H
Optimal solution without G-1 reliability (k$)	608	979	3,075	607	979	3,032
Load-shedding scenarios #	0	83	147	0	35	80
Total added scenarios #	0	91	154	0	44	127
Total iterations #	1	4	3	1	5	7
Optimal solution with G-1 reliability (k$)	608	982	3,098	607	979	3,035
Solution time (sec.)	11	486	276	11	158	1,014
Transmission lines #	117	117	117	120	120	120
Normal/Congested	C	C	C	C	C	C
Load distribution	2	2	2	2	2	2
Load percentage profile	L	M	H	L	M	H
Optimal solution without G-1 reliability (k$)	607	977	3,057	608	980	3,110
Load-shedding scenarios #	2	61	85	0	109	198
Total added scenarios #	2	82	146	0	109	272
Total iterations #	2	5	5	1	2	6
Optimal solution with G-1 reliability (k$)	607	981	3,063	608	986	3,130
Solution time (sec.)	34	403	918	12	242	3,092

larly, under the low-load day, the deterministic reserve policy can ensure G-1 security for almost all cases except for the 117-line system under Load2 and the de-rated transmission lines. Therefore, when the loads are low, there is little transmission congestion, the reserves can be dispatched to respond to the contingencies. Adding more

94

transmission lines may not result in decreasing the total costs, in contrast, under the medium-load or high-load day, the total cost of the 120-line system is much higher than that of the 117-line system. Switching from Load1 to Load2 generally increases the total costs. However, there are cases that the total costs under the Load2 is lower than the total costs under the Load1, such as the 117-line system under the de-rated transmission lines and the high-load day. From all 24 variations, the 120-line system under the Load2, the de-rated transmission lines, and the high-load day has the highest total costs, and it takes the longest time to solve this system variation. The solution time is positively co-related to the total costs.

Next, the lines that reach the thermal limits and the buses with extra capacities are checked in each load-shedding scenario. As mentioned previously, there are few load-shedding scenarios when the total loads are low or the transmission line capacities are high. For the systems with load-shedding under the deterministic reserve policy, the results show that the systems share the same lines that reach the thermal limits. Moreover, for each line that reaches the thermal limits, there are certain corresponding buses with extra capacities that cannot be delivered. Specifically, there are 6 transmission lines that reach the thermal limits, and three of them are the de-rated transmission lines with 350MW thermal limits (the lines connecting bus 114-116, 214-216, 314-316 respectively). The transmission lines and their corresponding buses are marked in Figure 6.2 and listed in Table 6.3. From the test results, different load profiles have little impacts on the selection of the transmission line and bus pairs to characterize the crucial extreme rays. The transmission lines that reach their thermal limits under one system variation often reach the limits in other system variations.

Table 6.3: Lines Reach Limits and Buses with Extra Capacities

Line	11	23	49	61	87	99
Bus	107	116	207	216	307	316
		118		218		318
						322

In the following tests, the 117-line system under the Load2, the de-rated transmission lines (117-C-2 system variation) is tested as the nominal test case. This variation is selected since it has moderate system congestion. The offline simulation procedure described in Figure 6.1 is performed to identify the crucial extreme rays of the system. Total nineteen crucial extreme rays are identified. The combinatorial selection of the buses and the lines are listed in Table 6.4.

Table 6.4: Crucial Extreme Rays for 73-Bus System

#	Line	Bus
1	11	107
2	23	116
3	23	118
4	49	207
5	61	216
6	61	218
7	87	307
8	99	316
9	99	318
10	99	322
11	23,49	116,207
12	23,87	116,307
13	23,49	118,207
14	23,61	118,218
15	49,87	207,307
16	49,99	207,322
17	11,49,87	107,207,307
18	23,49,87	116,207,307
19	49,87,99	209,307,322

Sufficient Reserve Levels for G-1 Contingency

Two reserve policies are adopted to study the sufficient reserve levels for G-1 contingency, a single-zonal and a 3-zonal reserve policies. The single-zonal reserve policy requires the total reserves in the power system to satisfy the $\alpha\%$ level of the total predicted loads; while the 3-zonal reserve policy adopts the zonal partition based on the system network structure (three duplicated zones), and requires the reserves in each zone to satisfy the $\alpha\%$ level of the total predicted loads within the corresponding

zone. Figure 6.5 represents the sufficient reserve levels and the corresponding total reserves required in the system under two reserve policies.
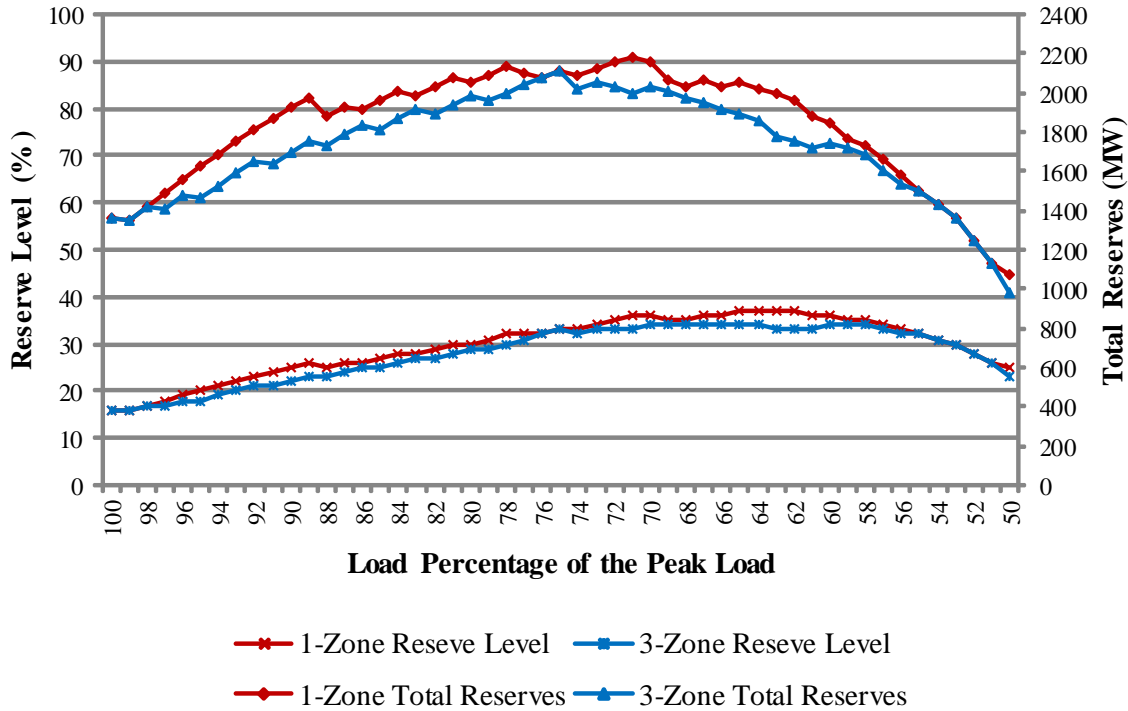
Figure 6.5: Zonal Sufficient Reserve Levels

From the results, the sufficient reserve levels are high under both single-zonal and 3-zonal reserve policies. The 3-zonal reserve policy decreases the sufficient reserve levels, but not significantly. It indicates that a better zone partition is desired. The system requires more than 1,000MW reserves to ensure G-1 security while the largest generator capacity is 400MW. When the loads are low, the system is not limited by the transmission capability very much, most of the reserves can be delivered and the sufficient reserve level is relatively low. When the loads are high, the choices of the reserve locations are limited; thus, the sufficient reserve levels are decreasing as the total loads increases. However, in some medium range of the peak-load (from 70% to 80% of the total loads), even 2,000MW reserves cannot ensure the system security. It indicates that requiring certain reserve levels in each zone may not be a very effective

policy to ensure system security, especially when the locations of the reserves can be selected from many buses. Bad reserve allocations result in the load-shedding, and it requires a large amount of reserves to avoid the bad allocations.

Next, the total reserves obtained from the MEF G-1 reliable solution and the sufficient reserves in each period of a high-load day are compared, the results are represented in Figure 6.6.
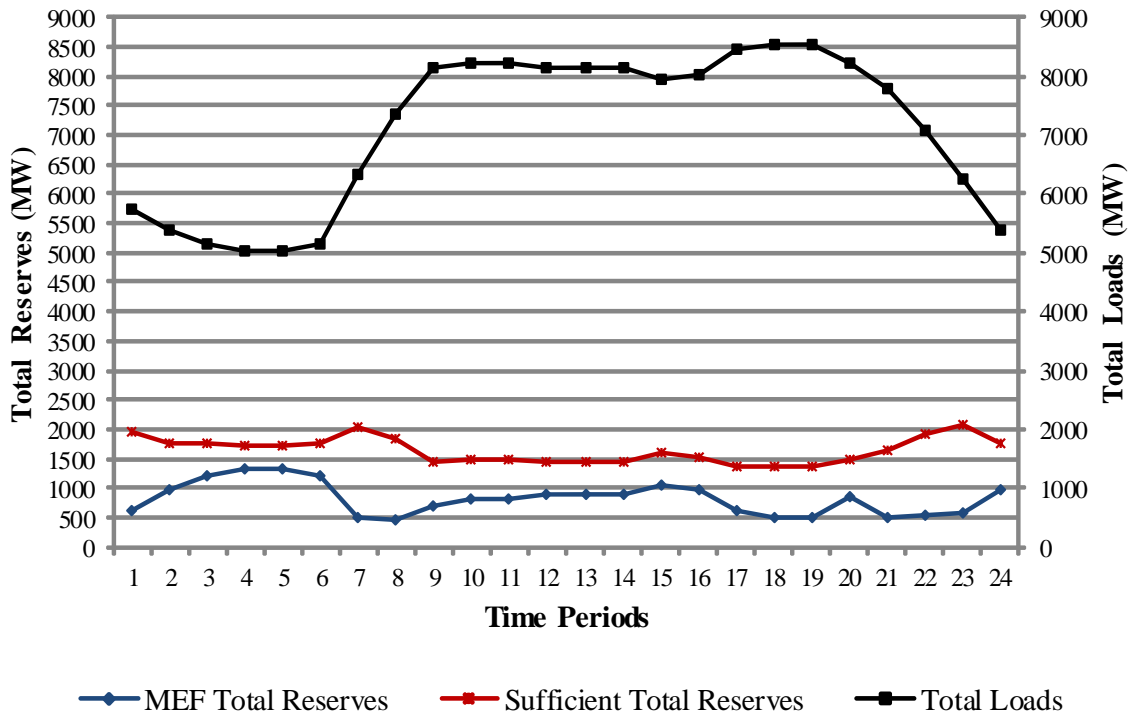
Figure 6.6: Total Sufficient Reserve Levels Comparison

From the test results, the total reserves solved from the MEF algorithm are much lower than the sufficient reserve levels for the same load percentage. It indicates that the total reserves to ensure system security can be low if the reserves are allocated properly.

Sufficient Reserve Levels for Load Uncertainty

Four uncertainty sets are adopted to study the sufficient reserve levels for load uncertainty. As defined in (6.35), parameters $(\kappa_1, \kappa_2, \kappa_3)$ characterize the uncertainty sets. The four studied uncertainty sets are selected as $(\kappa_1, \kappa_2, \kappa_3) = (5, 3, 2)$, $(8, 5, 3)$, $(10, 7, 5)$, $(15, 12, 10)$. 3-zonal reserve policy is adopted. Figure 6.7 represents the sufficient reserve levels for load uncertainty with different uncertainty set modeling.
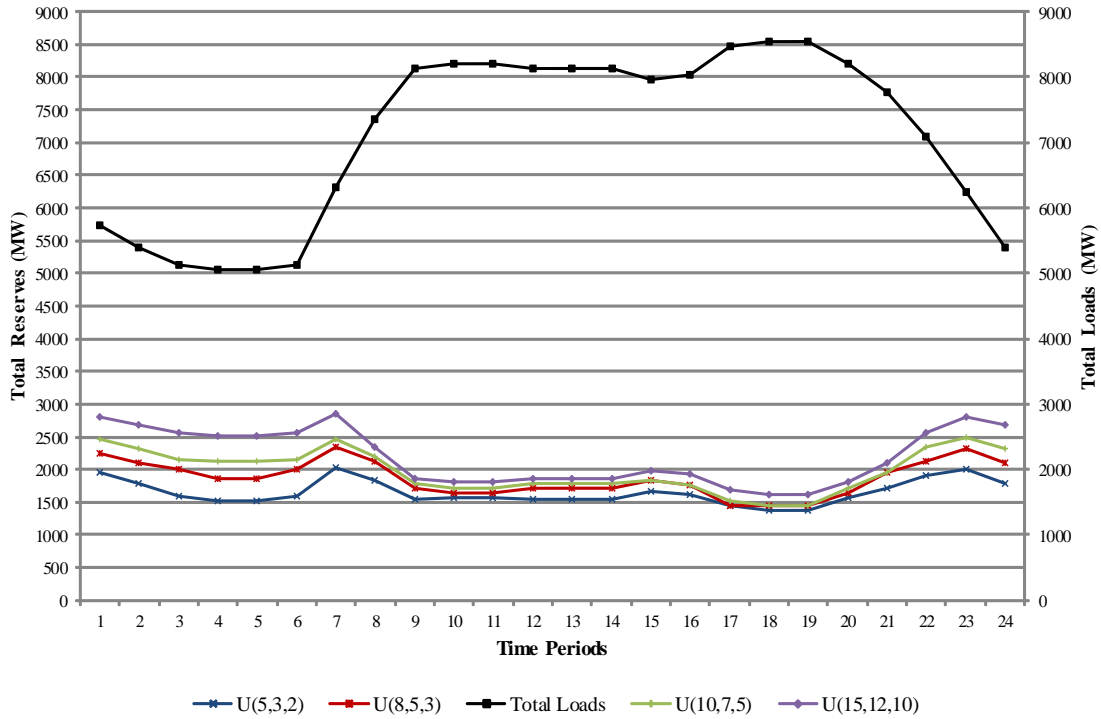
Figure 6.7: Sufficient Reserve Levels of Different Uncertainty Set Modeling

From the test results, the sufficient reserve levels increase as the load variations increase. Moreover, even under the low load variation, i.e., $(\kappa_1, \kappa_2, \kappa_3) = (5, 3, 2)$, the system requires a lot of reserves in order to ensure the system security. The results confirm that reserve level policies are not very efficient to ensure system security.

Security Constraints for G-1 Contingency

The computational performances of the proposed security constraints are studied. In this part, the problem is formulated as the UC problem with G-1 contingency. Three solution methods are compared.

The first solution method is the Benders' decomposition (BD) algorithm. The sub-problem is decomposed into each generator contingency in each time period. Multiple Benders' cuts are added to the master problem in each iteration.

The second solution method is the MEF as described previously. For both BD and MEF, the reserve requirements to cover the lost of the largest generator are modeled in the pre-contingency base case.

The last solution method, referred to as (ER), is the proposed approach that solves the problem by including the extreme rays induced security constraints. Table 6.5 show the computational performance for the UC problem with G-1 contingency. The high-load day and medium-load day profiles are tested. In the low-load day, the deterministic reserve policy can ensure the system security since there is no congestion in the power system.

Table 6.5: Computational Performance Comparison

	High-load			Medium-load		
	BD	MEF	ER	BD	MEF	ER
Objective ($)	3,063,440	3,063,490	3,064,160	980,855	981,357	980,779
Solution time (sec.)	6,481	918	40	2,895	483	46
Iteration #	288	5	-	147	5	-
Added variables	0	42,194	0	0	23,698	0
Added constraints	7,866	96,214	8,664	2,875	54,038	8,664

The cost efficiencies of the three methods are comparable. The small differences result from the MIP gap since all problems are not solved to optimal but to the solutions within 0.5% MIP gap. The proposed approach solves the problem much faster than the BD and MEF methods. There are two important factors that contribute to improve the solution time. First, the proposed approach is not an iterative al-

gorithm. It solves the problem only once as a deterministic formulation. Secondly, the proposed approach doses not introduce extra scenario-based variables into the formulation. The uncertainty is considered by including a set of constraints into the formulation. With these two features, the proposed approach has big advantages in solution time when the system is large.

In the proposed approach, the computational burdens are shifted to the offline simulations to identified the crucial extreme rays. The offline study has identified 19 extreme rays for this test case. Moreover, there are 19 out of 99 generator-failures cause security issues in the system. The security constraints are applied to all time periods. Therefore, there are total 8,664 security constraints added to the UC formulation. The number of the cuts can be further reduced by more offline studies, and it is left for future work.

Next, the average computation performance of the proposed approach is studied. One hundred high-load day scenarios are generated. In each scenario, the loads are normally distributed with a mean as the corresponding base-case load and a standard deviation as 5%, 8%, 10 % of the corresponding base-case load respectively. The solution times are summarized in Table 6.6. Table 6.6 listed the average, minimum, and maximum solution time among the 100 generated cases. Moreover, the solution time distribution for the 100 generated cases is presented. The solution time distribution is divided into 7 bins. The number of test cases in each bin is listed in the table.

Table 6.6: Solution Time Performance

Test Case	Summary (s)			Distribution (#)						
	Avg.	Min	Max	0-20	20-30	30-40	40-50	50-60	60-70	70+
5%	35.48	16	91	8	31	34	14	9	2	2
8%	38.19	16	106	4	37	29	14	6	2	8
10%	38.96	22	89	0	36	32	16	4	6	6

The test results show that the proposed security constraints approach is consistent in solution times, most test cases can be solved within a minute. Furthermore, the

load-shedding tests show that the obtained solutions are G-1 reliable for all of the generated scenarios. The identified crucial extreme rays are sufficient for the system while the loads vary.

Security Constraints for Load Uncertainty

In this part, the computational performances of the security constraints for the load uncertainty are studied. Two policies are compared. The first policy is to solve the problem as the deterministic UC model with the 3-zonal reserves; the second policy is to solve the problem by including the security constraints in the UC model. The high-load day profile is selected as the based case. Once the day-ahead UC model is solved, the commitment status are passed to the dispatch stage. In the dispatch stage, 100 test scenarios are generated. The loads in each test scenario are normally distributed with a mean of the corresponding base case load and a standard deviation as 5%, 8%, 10%, 15% of the corresponding base case load. Different uncertainty sets are adopted to respond the different level of load uncertainty. Specifically, the uncertainty sets $(\kappa_1, \kappa_2, \kappa_3) = (5, 3, 2)$, $(8, 5, 3)$, $(10, 7, 5)$, $(15, 12, 10)$ are adopted to respond to the 5%, 8%, 10%, 15% standard deviation correspondingly. In order to compare the cost efficiency, a value of lost load (VOLL) is introduced to penalize the load-shedding, the value is set to be $\$10,000$/MWh. Table 6.7 show the computational results for the load uncertainty.

From the test results, the proposed security constraints improve the system security. Compared with the deterministic zonal reserve policy, the commitment costs of the proposed approach increase, but the number of load-shedding scenarios reduce a lot. On average, the expected total costs improve consistently but not very significantly. However, on the other hand, the total costs for the worst-case scenario improve significantly. There are a few load-shedding scenarios under the proposed approach.

Table 6.7: Solutions with Load Uncertainty

	Load demand std. dev.	5%	8%	10%	15%
	Reserve level	5%	8%	10%	15%
Deter.	Commitment cost ($)	397,716	429,913	449,690	509,670
UC	Base-case total cost ($)	3,050,970	3,086,860	3,112,100	3,203,940
+	Load-shedding scenarios #	12	21	31	21
Zonal	Average dispatch cost ($)	2,662,990	2,694,640	2,737,640	2,819,940
Reserves	**Average total cost ($)**	**3,060,700**	**3,124,550**	**3,187,330**	**3,329,610**
	Worse-case total cost ($)	**3,232,940**	**3,432,670**	**3,940,620**	**4,449,770**
	Uncertainty set	(5,3,2)	(8,5,3)	(10,7,5)	(15,12,10)
Extreme	Commitment cost ($)	401,543	432,658	457,812	521,383
Ray	Base-case total cost ($)	3,049,120	3,086,040	3,121,660	3,222,610
+	Load-shedding scenarios #	1	2	5	12
Uncertainty	Average dispatch cost ($)	2,650,620	2,665,470	2,693,910	2,784,040
Set	**Average total cost ($)**	**3,052,160**	**3,098,130**	**3,151,730**	**3,305,420**
	Worse-case total cost ($)	**3,103,080**	**3,207,240**	**3,450,880**	**3,914,660**
	Average total cost (%)	0.28%	0.85%	1.13%	0.73%
	Worse-case total cost (%)	4.18%	7.03%	14.19%	13.67%

The scenarios are extreme scenarios that fall outside of the modeled uncertainty sets. By using different uncertainty set modeling, the security can be controlled. However, there is always a trade-off between the security and the cost efficiency. Generally, the proposed security constraints approach is a better way than the deterministic reserve requirements to protect the system under the load uncertainty, especially under some extreme load scenarios.

6.4.2   IEEE 118-Bus System

For this test case, the crucial extreme rays are studied and the test result for the UC problem with G-1 contingency is presented.

Crucial Extreme Rays

The offline simulations indicate that there are seven transmission lines reach the thermal limits in the load-shedding scenarios. The transmission lines reached the thermal limits and the buses with extra capacities are marked in Figure 6.8 and listed in Table 6.8.

In this system, seven crucial extreme rays are identified from offline simulations. The combinatorial selection of transmission lines and buses are listed in Table 6.9.
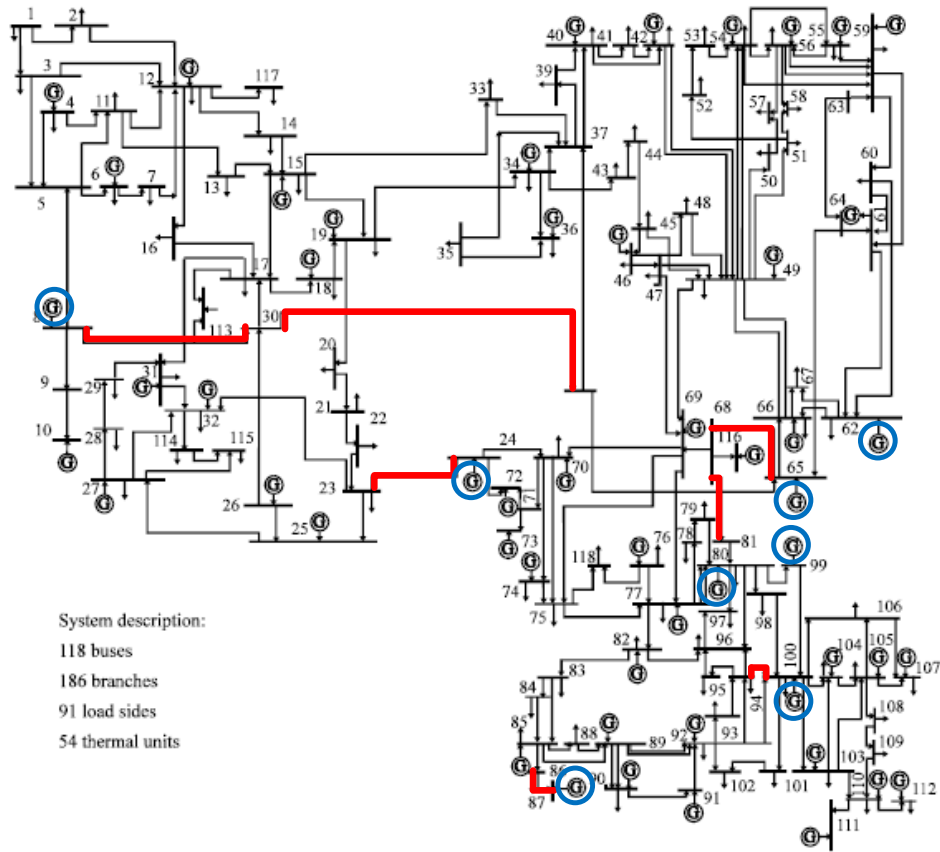
Figure 6.8: IEEE 118-Bus System

Table 6.8: Congested Lines and Responsible Buses

Line	11	37	49	110	114	148	161
Bus	8	24	8	62	80	87	103
			62	65	99		
			65	66			

Table 6.9: Crucial Extreme Rays for 118-Bus System

#	Line	Bus
1	37,148	24,87
2	49,148	65,87
3	110,148	62,87
4	110,148	65,87
5	114,148	80,87
6	37,49,148	24,65,87
7	37,148,161	24,87,100

Security Constraints for G-1 Contingency

Table 6.10 compares the computational performance under different solution methods. The previous analysis drawn from the 73-bus system are confirmed. The proposed security constraints approach solves the problem efficiently.

Table 6.10: Computational Performance Comparison

	High-load			Medium-load		
	BD	MEF	ER	BD	MEF	ER
Objective ($)	1,049,240	1,048,150	1,048,280	650,666	650,719	650,666
Solution time (sec.)	223	270	23	57	21	20
Iteration #	26	3	-	6	2	-
Added variables	0	44,217	0	0	7,514	0
Added constraints	883	100,827	9,072	41	17,134	9,072

6.5 Conclusions

With the current computational capability and limited scheduling periods to solve day-ahead UC models, stochastic UC models are not implemented in practice to solve the UC problem with uncertainty. Reserve requirement policies are wildly adopted to hedge uncertainty; however, simple zonal reserve level requirements may not be sufficient to ensure system reliability. The procured reserves may not be able to be delivered due to transmission limits.

This chapter studies a set of feasibility cuts to improve system reliability. The cuts are induced by the extreme rays of the dual cone. The extreme rays of the dual cone are explicitly characterized. This chapter shows the system reliability is related to the transmission lines that reach their limits and the buses that have extra undelivered reserves. The extreme rays of the dual cone can be characterized by the combinatorial selections of the transmission lines and buses of the power system network. As a result, the extreme ray feasibility cuts can be determined by offline simulations based on engineering insights. The proposed approach solves the UC problem with uncertainty as a deterministic model with the extreme ray feasibility

cuts, which is equivalent to the stochastic models. The proposed approach avoids the introduction of extra scenario-based variables and constraints, or the iterative process to solve the problem. Most computational burdens are able to be shifted from scheduling periods to the offline studies. The deterministic equivalent model with the extreme ray feasibility cuts can be solved efficiently and a more reliable day-ahead scheduling solution can be obtained.

Chapter 7

ENHANCING STOCHASTIC UNIT COMMITMENT WITH DATA MINING

7.1   Introduction

Stochastic unit commitment (SUC) problem is usually formulated as two-stage models where commitment decisions are determined in the first stage and dispatch decisions are determined in the second stage after the uncertain data are realized. The two-stage stochastic unit commitment is challenging to solve with current computational capability and limited scheduling time due to the inclusion of many scenario-based variables and constraints, however.

In this chapter, on top of Chapter 6, a framework is proposed to replace the two-stage stochastic UC by an enhanced deterministic model with a set of constraints, in order to avoid the inclusion of scenario-based variables and constraints. First, an offline simulation procedure is used to identify the potential crucial constraints; then, a data mining algorithm is applied to select the included crucial constraints, given a new forecast system operating condition. With the proposed framework, the difficulties of handling uncertainty are shifted from the scheduling periods to the offline simulation and data mining. The resulting enhanced deterministic model with the additional constraints can be solved efficiently and the system security is improved.

The rest of this chapter is organized as follows. Section 7.2 introduces the framework to transform the SUC to the deterministic model with a set of constraints. Section 7.3 represents a case study. Finally, section 7.4 concludes the chapter.

7.2 Methodology

A two-stage SUC can be replaced by an equivalent deterministic mixed integer program (MIP) with the inclusion of extra constraints (Benders, 1962), as shown in Figure 7.1.
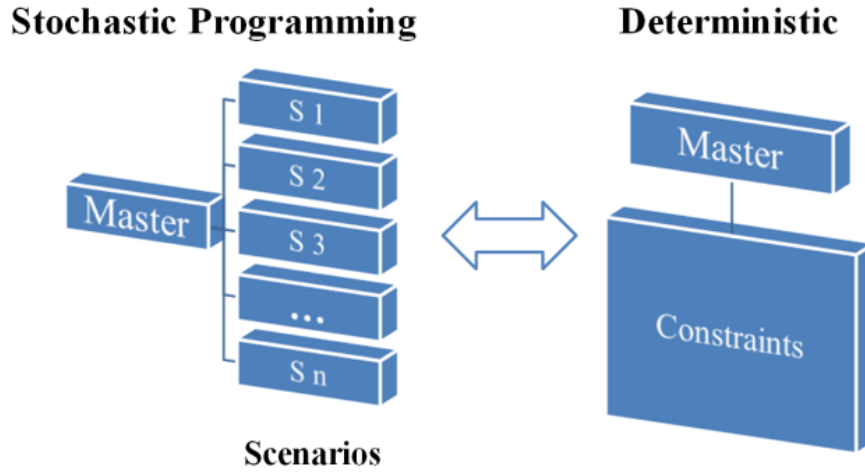
Figure 7.1: Stochastic Unit Commitment Formulations

Benders' decomposition algorithm (Benders, 1962) finds the constraints (feasibility cuts and optimality cuts) iteratively. The drawback of Benders' decomposition is that the master program is solved repeatedly and takes longer time to solve in each iteration as the algorithm proceeds, because of the inclusion of more constraints. If all necessary constraints can be identified from offline study and be included all at once, then the solution time can be reduced significantly.

In this chapter, the focus is on a SUC problem that requires the system having a feasible re-dispatch after any single-generator-failure (G-1) contingency. This problem is of interests because: 1) The North American Electric Reliability Corporation (NERC) requires the N-1 reliability criterion for system operation, which states the system must be able to withstand any single bulk element failure (generator, transmission line, or transformer) (North American Electric Reliability Corporation, 2007).

The failure of generator has more impacts on the system security. The state-of-art market models are able to handle transmission outage contingencies by imposing line outage distribution factor (LODF) based transmission security constraints, but are lack of similar deterministic constraints to hedge generator contingencies. 2) The G-1 contingencies are discrete uncertainty events which can be enumerated and listed explicitly in the SUC formulation. The proposed framework can be applied to other types of SUC problems with simple modifications.

All potential constraints to replace the two-stage G-1 secured UC formulation into the deterministic equivalent model have been characterized in Chapter 6. The constraints are indexed by (r, s, t), where r represents the extreme rays in a system dependent polyhedron, s represents the contingency scenarios (which generator is failed), t represents the time periods the contingency happen. The extreme rays in the polyhedron can be characterized by combinatorial selections of the transmission lines and buses in the system, therefore the number of the extreme rays is exponential, which further indicates that the number of potential constraints is exponential. Among the exponential number of potential constraints, only a small subset of the constraints may be violated. Define the constraints that are potentially to be violated as crucial constraints. Once all crucial constraints are identified, given a new forecast system operating condition, the included crucial constraints have to be selected. For each crucial constraint, a binary indicator parameter is assigned. If the indicator is 1, then the constraint is included for the given system operating condition; otherwise the indicator is 0. The inclusion of the crucial constraints is illustrated in Figure 7.2.

In order to complete the replacement, there are two key steps: 1) How to identify the crucial constraints? 2) Given a new forecast system operating condition, which crucial constraints to be included? In this chapter, an offline simulation procedure is proposed to identify all crucial constraints. Data mining algorithms are utilized to
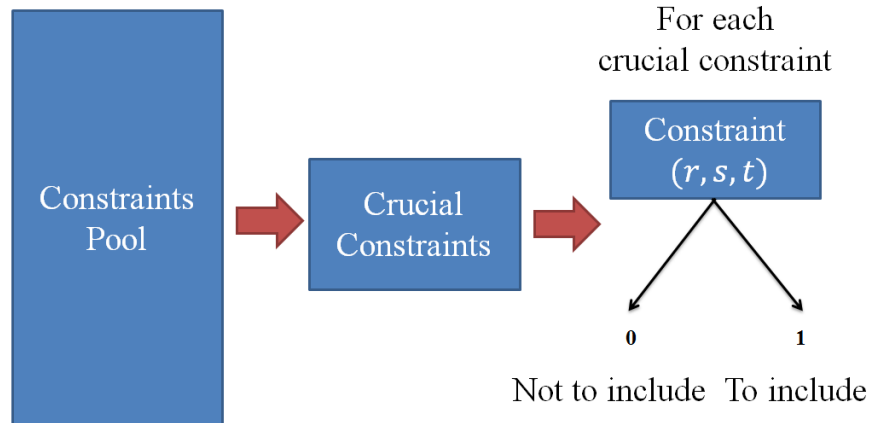
Figure 7.2: Crucial Constraints

select the included crucial constraints to be included.

7.2.1 Offline Simulation

As shown in Chapter 6, the extreme rays of the polyhedron to describe the constraints are characterized by the combinatorial selection of the transmission lines and buses in the system.The selected transmission lines are the congested lines in post-contingency states and the selected buses are the buses with extra generation capacity but cannot be delivered in post-contingency states. For a given power system (with a fixed network structure, generation mix, etc.), if the system operating condition (such as load profile) has similar characteristics, then the congested transmission lines and buses with extra capacities in the post-contingency states have similar patterns among all the cases. Therefore, the crucial constraints can be identified by solving a group of test cases with similar system operating conditions. The test cases can be obtained from historical data, or generated from simulation.

For each test case, a G-1 security-constrained UC (SCUC) is solved offline. The solution procedure is an iterative algorithm that is similar to Benders' decomposition. The UC problem is initially solved with no additional constraints but a reserve

requirement to procure the reserves more than the largest generator contingency. Then, the solution of the SCUC is tested against a contingency analysis. If there is a post-contingency scenario with load shedding, then there are some congested transmission lines and undelivered capacity in the corresponding post-contingency state. The corresponding extreme rays and security constraints can be identified and included into the master problem. Next, the problem with the identified constraints is solved again. The procedure is repeated until the UC solution is G-1 secure. As a result of the procedure, the included constraints indexed by (r, s, t) are recorded, i.e., in each specific test case, which constraint is included. As more and more test cases are solved, all crucial constraints are likely to be identified. The descried offline simulation procedure is illustrated in Figure 7.3.
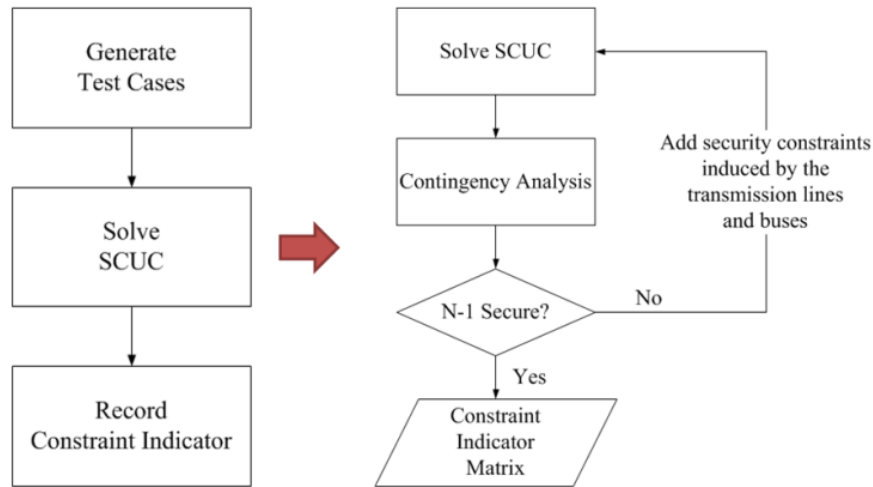
Figure 7.3: Offline Simulation Procedure

The test cases are solved offline. As opposed to the limited scheduling time window, there is enough time to solve the test case offline. Once a test case is solved, the result is used as a training data record for all future system operating conditions.

7.2.2 Data Mining

After the offline simulation, a set of crucial constraints is obtained, along with the indicator matrix describing which constraint has been included in which test cases. The number of the identified crucial constraints may still be a large number. The included crucial constraints for a given test case can be further reduced by data mining algorithms.

The test cases in the offline simulation are used as a training data set. The given new test case is treated as a testing data set. In this chapter, the forecast net load profile at each node (the load subtracts the dispatchable renewables), $D_{nt}, \forall n, t$, is used as attributes in the data mining model. A binary decision is the output, i.e., the prediction whether to include the corresponding constraint (r, s, t). The general procedure is described in Figure 7.4.
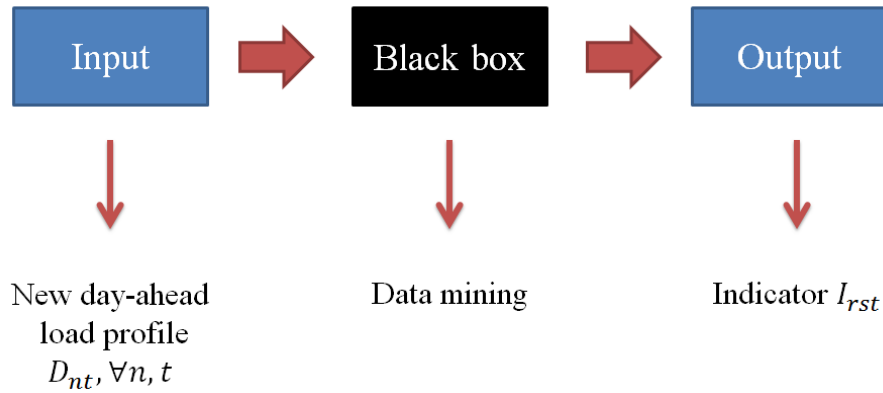
Figure 7.4: Data Mining to Identify Necessary Crucial Constraints

A decision tree algorithm (Tan *et al.*, 2006) is selected to be the data mining algorithm due to its simplicity and its ease to be interpreted. For each of the crucial constraint, a decision tree is built based on all training data to determine if the constraint needs to be included.

7.2.3 Deterministic Equivalent Model

After the previous two steps, a deterministic model with a set of selected crucial constraints is obtained to replace the two-stage SUC model.

There is no guarantee that all necessary crucial constraints can be identified. The reasons are as follows. 1) Some crucial constraints for the new case may not be identified from the offline simulation procedure. 2) The data mining algorithm ends up with a wrong prediction. However, the inclusion of the set of selected constraints can improve the system security and provides an initial market solution that requires fewer out-of-market corrections.

In this chapter, the process described in Figure 7.3 is utilized to determine an exact G-1 secured UC schedule. The goal is to solve the SCUC in one iteration. In the cases that more constraints are needed, it can be expected only a few more iterations are needed to obtain a secure solution.

Moreover, instead of a binary indicator, zero or one, the decision tree algorithm can return a probability of the prediction to be one. Then, the number of constraints to include can be traded off by a probability threshold. For instance, if the data mining algorithm predicts one constraint to be included crucial constraint with probability 0.38, then the constraint will be included if the threshold is 0.3; but not to be included if the threshold is 0.4. Since missing one constraint may have more impacts than adding one redundant constraint, a more conservative threshold should be used. In other words, the threshold should be set as a relative small number in order to include more potential crucial constraints, but not to increase the solution time of SCUC too much at the same time.

Finally, the procedure of the proposed framework embedded in the day-ahead (DA) market is illustrated in Figure 7.5.
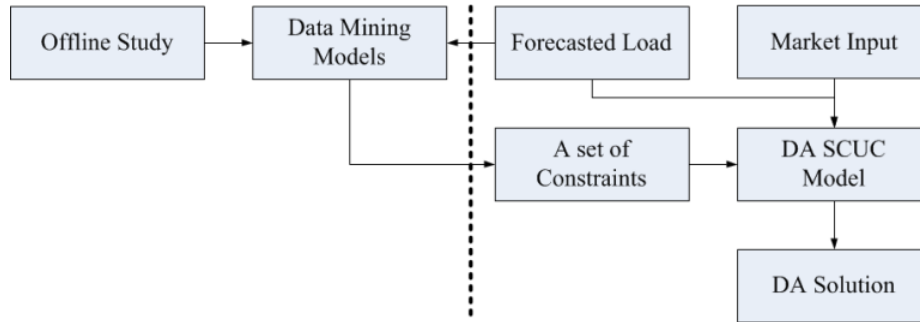
Figure 7.5: Day-Ahead Market Solution Procedure

During the offline study stage, a number of crucial constraints are identified first. For each crucial constraint, a data mining model is built to predict whether the corresponding constraint needs to be included in the DA SCUC model for a given DA forecast load. In the DA planning stage, the system operator first obtains a forecast of the net load. Then, the forecasted load profile is used with the data mining models to determine which constraints to be included. With the forecast load, the market input information, and the included crucial constraints, the DA SCUC model is solved, and a DA schedule is obtained.

7.3 Case Study

In this section, the proposed framework is tested on a modified IEEE 73-bus system (RTS 1996) (University of Washington, 2015). The test system has 73 buses, 99 generators and 117 transmission lines. The total generation capacity is 10,215MW. The peak load is 8,550MW. The G-1 SCUC is formulated as a 24-period DA model. Any generator can be failed in any time period, so there are totally 2,376 discrete scenarios.

First, the offline simulation described in Figure 7.3 is carried out. One historical load profile is selected to be the base case. In the base case, the loads in different periods vary from 59% to 100% of the peak load. One thousand test cases are generated

as the training data set and twenty test cases are generated as the testing data set. In each generated test case, the load at each bus in each period, $D_{nt}, \forall n, t$, follows a normal distribution with a mean as the corresponding base case load, and a standard deviation as 5% of the corresponding base case load.

A total of 226 crucial extreme rays are identified from the offline simulation. Figure 7.6 plots the number of identified crucial extreme rays versus the number of test cases included. From Figure 7.6, it can be seen that the total number of identified crucial extreme rays increases sharply in the first few hundred test cases; but increases more slowly after approximately 500 test cases. The results show that all crucial extreme rays are likely to be identified as a certain number of test cases have been carried out. Moreover, many of the late-discovered crucial extreme rays only appear in one single test case. These extreme rays can be seen as outliers caused by the extreme test case.
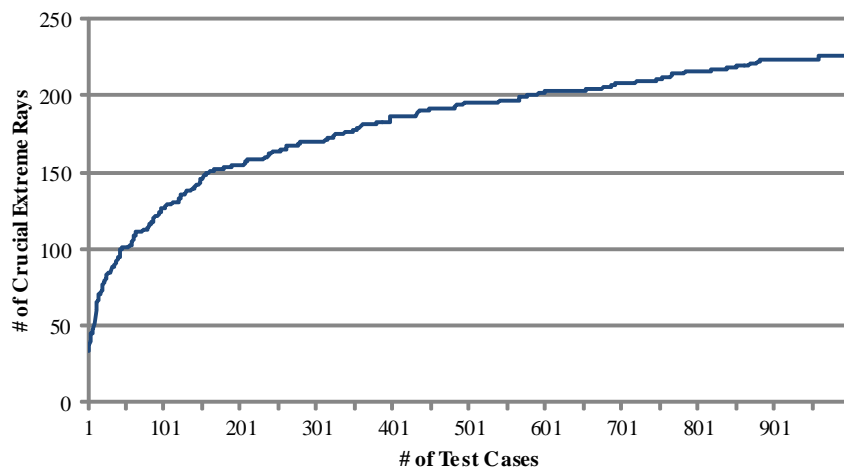
Figure 7.6: Identified Crucial Extreme Rays Increment

Table 7.1 lists the top 15 most frequent identified crucial extreme rays that are

induced by the lines (L) and buses (B) of the power system network. For instance, the most frequent crucial extreme ray #1 is induced by line L87 and bus B54, which indicates in the corresponding post-contingency states, the line L87 is congested and the bus B54 has extra capacity cannot be delivered. The situation happens 24,562 times in the offline simulation (in different test cases, contingency scenarios, and time periods).

Table 7.1: Most Frequent Crucial Extreme Rays

#	1	2	3	4	5
Frequency	24,562	17,196	16,528	12,726	11,004
Line	L87	L98	L50	L98	L23
Bus	B54	B69	B30	B65	B17
#	6	7	8	9	10
Frequency	9,367	9,050	8,655	7,982	6,972
Line	L50, L87	L23	L61	L50, L98	L50, L98
Bus	B30, B54	B15	B41	B30, B69	B30, B65
#	11	12	13	14	15
Frequency	6,328	5,924	5,104	5,080	4,726
Line	L23, L87	L98	L61	L87, L98	L23, L87
Bus	B15, B54	B63	B39	B54, B69	B17, B54

A total of 4,589 crucial constraints are identified from the offline simulation. Table 7.2 lists the top 15 most frequent identified crucial constraints with the corresponding constraint index (r, s, t). For instance, the most frequent crucial constraint #1 is corresponding to crucial extreme ray #5, scenario 57 (generator #57 is failed), and time period 23 (the generator failure happens in time period 23). Out of 1,000 test cases, 991 test cases have identified the constraint (5,57,23) as crucial constraint.

Table 7.2: Most Frequent Crucial Constraints

#	1	2	3	4	5
Frequency	991	989	968	917	916
(r, s, t)	(5,57,23)	(2,99,1)	(5,57,7)	(5,56,23)	(5,57,1)
#	6	7	8	9	10
Frequency	897	822	818	815	809
(r, s, t)	(5,56,7)	(13,89,2)	(8,89,24)	(8,89,2)	(12,24,2)
#	11	12	13	14	15
Frequency	804	794	788	788	769
(r, s, t)	(13,89,24)	(8,90,24)	(2,99,23)	(12,24,24)	(8,90,2)

Theoretically, the number of potential constraints to be included in the deterministic model is exponential. However, by the offline simulation, the number of crucial extreme rays is reduced to 226 and the number of crucial constraints is reduced to 4,589. Given a new forecast load profile, the number of the crucial constraints to be included can be further reduced with data mining.

For each identified crucial extreme ray, a decision tree is built to determine whether the constraint should be included or not given the new forecast load. The decision tree algorithm is implemented in Python code with SciKit-Learn package (SciKit-Learn, 2016). To avoid over-fitting, a maximum depth parameter is used to control the depth of the tree model. A five-fold cross-validation (Tan *et al.*, 2006) is used to determine the optimal maximum depth of the tree. Table 7.3 presents the cross-validation results. The decision trees with maximum depth equals to 4 gives the highest prediction accuracy.

Table 7.3: Cross-validation with Different Maximum Depth

Max depth	Different folds accuracy					Avg.
unlimited	0.546	0.688	0.658	0.553	0.544	0.598
3	0.453	0.755	0.728	0.671	0.631	0.648
4	0.566	0.757	0.725	0.686	0.616	0.670
5	0.487	0.764	0.725	0.631	0.632	0.648
6	0.544	0.744	0.716	0.642	0.62	0.653

Figure 7.7 presents three parts of the decision tree for crucial constraint #15. For this crucial constraint, in the offline simulation, 769 out of 1,000 test cases included the constraints. The decision tree tries to find the common features of the 769 test cases that distinguish them from the other 231 test cases. From the first part of Figure 7.7, in the root node, the splitting criterion is $X[648] \leq 493.86$. $X[648]$ corresponds to the load at bus B37, in the period T1, $D_{37,1}$. The splitting criterion gives the best separation of the cases including the constraint and the cases not including the constraint. The cases with $D_{37,1} \leq 493.83$ belong to the left descendant node and

the cases with $D_{37,1} > 493.83$ belong to the right descendant node. Then, for the two nodes at depth 1, the splitting criteria are $D_{33,1} \leq 126.23$ and $D_{37,2} \leq 439.785$ respectively. Finally, each leaf node provides a case distribution (whether the case including the constraint) for the cases falling into the node. For instance, the very left leaf node on the second part of Figure 7.7 has 4 cases not including the constraint and no case including the constraint. If a new load profile falls into this node, it is likely that the constraint is not necessary. In contrast, the very right leaf node on the third part of Figure 7.7 has 94 cases not including the constraint and 310 cases including the constraint. If a new load profile falls into this node, it is likely that the constraint is necessary, with a probability of 76.6%.
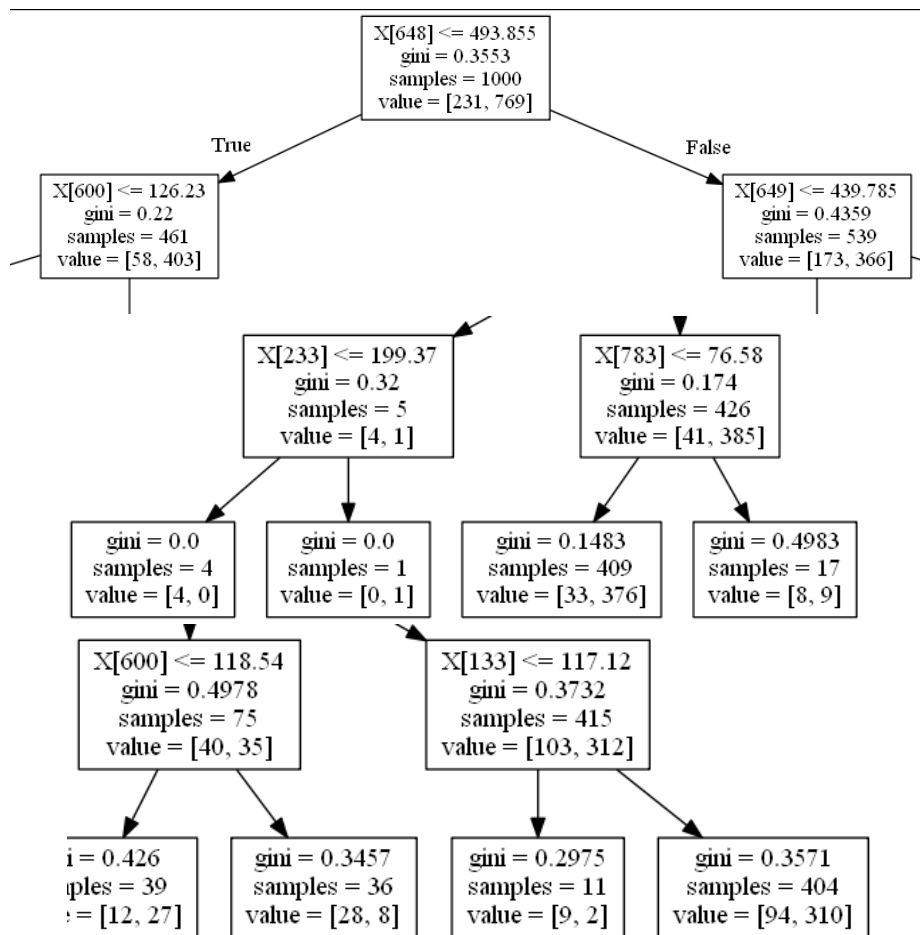
Figure 7.7: Decision Tree

In the case study, a decision trees makes a prediction of whether to include a constraint, along with a probability. Thus, a threshold can be used to select the constraints that have relative higher probabilities to be selected. In Table 7.4, the result of using different threshold values are summarized.

Table 7.4: Solution Comparison with Different Thresholds

Thresholds	# of pre-included crucial constraints	# of iterations	# of extra included crucial constraints	Average solution time for SCUC (s)
0.2	255	6.0	31.3	126.7
0.1	432	3.8	11.5	79.2
0.001	2,506	1.3	0.9	41.3

From the test results, even setting the threshold to be 0.2, many necessary crucial constraints are not pre-included. On average, five more iterations are needed and approximately 31 extra crucial constraints are included to obtain a secure solution. Further reducing the threshold to 0.1 increases the number of pre-included crucial constraints from 255 to 432 on average. However, the solution after the first iteration is still far away from the G-1 secure solution. When the threshold is set to be 0.001, the number of pre-included crucial constraints increases to 2,506 on average. However, the solutions after the first iteration are very secure. Since most test cases can be solved in one iteration, the solution time under the threshold 0.001 outperforms the others. Therefore, the threshold 0.001 is preferred.

The proposed solution method (M3) is compared with another two benchmarks: the Benders' decomposition (M1) (Benders, 1962) and the deterministic model with all identified crucial constraints (M2). The comparison is given in Table 7.5.

From Table 7.5, the iterative Benders' decomposition takes the longest computational time to solve. The Benders' decomposition can identify the necessary crucial constraint accurately. Only around 220 constraints on average are included in each

Table 7.5: Solution Comparison with Different Solution Methods

Solution Method	# of pre-included crucial constraints	# of iterations	# of extra included crucial constraints	Average solution time for SCUC (s)
M1	0	7.1	218.6	143.5
M2	4,589	1	0	48.5
M3	2,506	1.3	0.9	41.3

test case. If all identified crucial constraints are included, among the 20 generated testing test cases, it is guaranteed that the solution after the first iteration is secure. However, too many redundant constraints are included. Under the proposed solution method, the data mining algorithm reduces the number pre-included crucial constraints to 45% of the identified crucial constraints. Compared with the iterative Benders' decomposition, the average solution time of the proposed solution method is only 32% of that of Benders' decomposition. At the same time, most test cases can be solved in one iteration. Even though some test cases need to add extra crucial constraints, after the second iteration, a G-1 secure solution can be obtained. Only a few crucial constraints are not identified by the data mining algorithm. The data mining algorithm can be further improved to accurately identify the necessary crucial constraints.

Finally, the solutions of the 20 testing test cases after the first iteration are explicitly given in Table 7.6.

From the test results, with the identified crucial constraints, even if the solution method is limited to one iteration, the obtained solutions have low load shedding. The identified crucial constraints improve the system security significantly. Moreover, the solution time is stable. Most test cases can be solved within 40 seconds. The results show that including selected crucial constraints in SCUC can improve the reliability of the solution while keeping the added computational complexity at minimum.

Table 7.6: Solution for Each Testing Case

Case #	# of pre-included crucial constraints	Total cost ($)	# of load-shedding scenarios	Total load-shedding (MW)	SCUC solution time (s)
1	2,539	3,072,580	0	0	35
2	2,471	3,076,680	0	0	28
3	2,520	3,069,760	1	0.15	25
4	2,558	3,049,460	0	0	49
5	2,518	3,068,730	0	0	26
6	2,473	3,052,950	6	2.4	40
7	2,514	3,097,480	0	0	45
8	2,496	3,080,110	0	0	40
9	2,461	3,123,820	0	0	37
10	2,513	3,060,080	0	0	39
11	2,522	3,084,160	0	0	47
12	2,566	3,046,740	0	0	31
13	2,465	3,049,580	0	0	41
14	2,467	3,087,570	2	1.66	41
15	2,513	3,071,290	0	0	30
16	2,514	3,072,970	0	0	26
17	2,512	3,007,110	3	1.96	39
18	2,517	3,092,430	0	0	39
19	2,512	3,104,590	0	0	25
20	2,477	3,085,920	0	0	44

7.4 Conclusions

This chapter presents a framework to use an enhanced deterministic UC model to approximate the stochastic UC formulation. The proposed framework avoids the inclusion of scenario-based variables and constraints. The deterministic model is enhanced with a set of selected crucial security constraints that are identified from offline simulation and data mining. All crucial constraints are first identified from the offline simulation and the number of included crucial constraints is further reduced by data mining algorithm. Test results show that, even though many redundant crucial constraints are included, the proposed framework still outperforms the iterative algorithm such as Benders' decomposition (in solution time). By including the identified crucial constraints, the system security is improved significantly, and the computational complexity is increased at minimum.

Future research will focus on improving the data mining algorithm to identify the crucial constraints more accurately. In the presented decision tree models, many attributes are used as model inputs. Different algorithms can be used to reduce the dimension of the inputs. Moreover, the proposed framework will be tested for other stochastic unit commitment models.

Chapter 8

SHADOW PRICES: MARKET IMPLICATIONS OF SECURITY CONSTRAINTS

8.1 Introduction

RTO/ISOs include different types of security requirements to approximate system security issues. Power system security refers to the ability to survive potential disturbances (contingencies) without interruption to customer services (Kundur *et al.*, 2004). The North American Electric Reliability Corporation (NERC) requires the N-1 reliability criterion for system operation, which states the system must be able to withstand any single bulk element failure (generator, transmission line, or transformer) (North American Electric Reliability Corporation, 2007).

In this chapter, only a subset of N-1 events, single-generator-failure (G-1) contingencies, are considered. Transmission (or transformer) contingencies are not modeled for the following reasons. Transmission contingency modeling is handled efficiently today within existing commercial grade security-constrained unit commitment (SCUC) and security-constrained economic dispatch (SCED) tools; at the same time, the impacts of transmission line contingencies are reflected in energy prices. . Transmission contingencies are modelled by including line outage distribution factors (LODFs) to capture the change in line flows from the pre-contingency base case to the post-contingency transmission outage case. With power transfer distribution factors (PTDF) being used to capture base-case flows, LODFs then allow for the straightforward determination of post-contingency line flows. Existing SCUC and SCED tools are able to manage transmission contingencies efficiently today; however, such tools need assistance in the management of generator contingencies.

In existing market practices, RTO/ISOs acquire reserves (extra generation capacity) in order to protect the power system from generator contingencies. However, since the power systems and markets in the U.S. leverage adequacy-based reserve policies, the security requirements do not guarantee a N-1 reliable solution on a locational basis. The procured reserves may not be deliverable in the post-contingency states due to transmission limitations. As a result, RTO/ISOs make different types of out-of-market, operator-initiated corrections in their scheduling and operation (Federal Energy Regulatory Commission, 2014). These security requirements may result in committing more units or re-allocating the reserves. However, the out-of-market, operator-initiated corrections are not reflected in the market models and such discretionary changes are not transparent. The market prices are distorted and do not reflect true marginal costs. In this chapter, a set of G-1 security constraints, which play a similar role as the LODF-based transmission security constraints, are proposed to be added into SCUC and SCED in order to efficiently determine the reserve allocation with respect to post-contingency dispatch feasibility.

In the U.S. energy markets, RTO/ISOs adopt locational marginal prices (LMP) to represent energy prices (Pope, 2014). The LMP captures three components, which include the marginal energy, marginal congestion, and marginal loss components (ISO New England, 2014). In most RTO/ISOs, energy and reserves are co-optimized in a single market model (Federal Energy Regulatory Commission, 2014). Market participants submit separate bids for energy and reserve. Although the energy prices, i.e., LMPs, are coupled with reserve requirements, the existing adequacy-based reserve requirements restrict only pre-contingency base-case operating conditions and do not accurately reflect the deliverability requirements of reserves in the post-contingency states. With the proposed G-1 security constraints, the model not only captures the base-case operating conditions but also capture the post-contingency operating

conditions. The approach has a similar feature as using LODF-based transmission security constraints to consider both pre and post transmission outage contingency states. As a result of the G-1 security constraints, the reserves are re-allocated to ensure post-contingency dispatch feasibility.

In this chapter, with the market implication analysis of the proposed security constraints, a new component of LMP, marginal security component, is proposed to better represent the energy prices. The marginal security components are the weighted shadow prices corresponding to the set of G-1 security constraints. With the marginal security component, the LMPs will capture the marginal cost from a G-1 secure state to another G-1 secure state; thus, it captures the true marginal costs by restricting the dispatch feasibility in both pre-contingency base case and post-contingency states.

The main contributions of this chapter are listed as follows:

- Rather than imposing simple adequacy-based reserve requirements to hedge generator contingencies, the proposed security constraints efficiently allocate reserves in the system with the consideration of post-contingency dispatch feasibility. The proposed G-1 security constraints play the same role as the LODF-based transmission outage security constraints by considering the post-contingency state transmission limitations. The proposed G-1 security constraints can be easily combined into SCUC and SCED tools to improve the market models.

- The market implications of the proposed security constraints, i.e., the impacts of the proposed security constraints on energy prices, are analyzed in detail.

- A new component of LMP, marginal security component, is proposed in order to capture the marginal cost from a secure system state to another secure system state.

125

The rest of the chapter is organized as follows: section 8.2 analyzes the market implications of the proposed security constraint. Section 8.3 gives a 3-bus system as illustrative example. Section 8.4 represents a case study for IEEE 73-bus system. Finally, section 8.5 concludes.

8.2 Market Implications of Security Constraint

In Chapter 6, a set of G-1 security constraints have been presented to improve the system security. In this chapter, the implications of these G-1 contingency security constraints are analyzed.

The G-1 security constraint is explicitly represented as follows:

$$\sum_{\forall g} G1_g^s \left(p_{gt}^H \bar{\phi}_{ig}^+ - p_{gt}^L \bar{\phi}_{ig}^- \right) + \sum_{\forall l} F_l (\bar{\mu}_{il}^+ + \bar{\mu}_{il}^-) - \sum_{\forall n} D_{nt} \bar{\lambda}_{in} \geq 0$$

$$\forall i, s, t \qquad (8.1)$$

where, $(\bar{\phi}^+, \bar{\phi}^-, \bar{\mu}^+, \bar{\mu}^-, \bar{\lambda}), \forall i$ are given crucial extreme ray parameters of the dual cone that have been identified; index s is corresponding to G-1 contingency scenario; index t is corresponding to time period the contingency happens.

When a generator fails, the corresponding weighted capacity, $\left(p_{gt}^H \bar{\phi}_{ig}^+ - p_{gt}^L \bar{\phi}_{ig}^- \right)$, is lost, which may result in the left side of (13) to be less than zero if (8.1) is not enforced. In (8.1), $p_{gt}^L / p_{gt}^H, \forall g, t$, are the post-contingency available generation capacities, that are described in the following constraints:

$$p_{gt}^L = p_{gt} - r_{gt}^d \qquad\qquad \forall g, t \qquad\qquad (8.2)$$

$$p_{gt}^H = p_{gt} + r_{gt}^u \qquad\qquad \forall g, t \qquad\qquad (8.3)$$

$$p_{gt} - r_{gt}^d \geq P_g^{\min} u_{gt} \qquad\qquad \forall g, t \qquad\qquad (8.4)$$

$$p_{gt} + r_{gt}^u \leq P_g^{\max} u_{gt} \qquad\qquad \forall g, t \qquad\qquad (8.5)$$

$$0 \leq r_{gt}^d, r_{gt}^u \leq R_g \qquad\qquad \forall g, t \qquad\qquad (8.6)$$

In current market designs, the LMPs are used to price the energy. The LMP is interpreted as the system total dispatch costs increment/decrement by increasing/decreasing one unit of power at the corresponding location. If the security constraints (8.1) are to be included, the increment/decrement of load D_{nt} will also have impacts on these security constraints. Consider the reformulation as follows:

$$\sum_{g \in G(n)} p_{gt} - i_{nt} - d_{nt} = 0 \qquad\qquad \forall n, t \quad (\delta_{nt}) \qquad\qquad (8.7)$$

$$\sum_{\forall g} G1_g^s \left(\hat{p}_{gt}^H \bar{\phi}_{ig}^+ - \hat{p}_{gt}^L \bar{\phi}_{ig}^- \right)$$

$$+ \sum_{\forall l} F_l (\bar{\mu}_{il}^+ + \bar{\mu}_{il}^-) - \sum_{\forall n} D_{nt} \bar{\lambda}_{in} \geq 0 \qquad\qquad \forall i, s, t \quad (\xi_{it}^s) \qquad\qquad (8.8)$$

$$d_{nt} = D_{nt} \qquad\qquad \forall n, t \quad (\Delta_{nt}) \qquad\qquad (8.9)$$

The reformulation changes the original fixed loads, $D_{nt}, \forall n, t$, to variables, $d_{nt}, \forall n, t$; then enforces non-anticipativity constraints (8.9). When the load, D_{nt}, increases by one unit, it will not only affect the nodal net injection (8.7), but also affect the security constraints (8.8). Let $\delta_{nt}, \xi_{it}^s, \Delta_{nt}$ represent the shadow prices of (8.7)-(8.9) respectively; their relations are specified by the following proposition.

Proposition 7. *The shadow prices of (8.7)-(8.9) satisfy,*

$$\Delta_{nt} = \delta_{nt} + \sum_{\forall i} \sum_{\forall s} \bar{\lambda}_{in} \xi_{it}^s \qquad\qquad \forall n, t \qquad\qquad (8.10)$$

Proof. If deriving the dual of the reformulation, variables, $d_{nt}, \forall n, t$, only appear in (8.7)-(8.9), then the corresponding dual constraints are given as (8.10). □

The shadow prices, $\delta_{nt}, \forall n, t$, represent the change in the total system dispatch costs when the corresponding load, D_{nt}, increases by one unit. From (8.10), the price Δ_{nt} is separated into two parts. The first part, δ_{nt}, is the current LMP that captures the marginal energy component and marginal congestion component in the lossless model. The additional part, $\sum_{\forall i} \sum_{\forall s} \bar{\lambda}_{in} \xi_{it}^s$, is the marginal security component. The interpretation of this new component is that, if the security constraints are included in the model, when the load is increased by one unit, it may cost more in order to satisfy the security constraints. The extra costs are captured by the shadow prices of the security constraints.

8.3 Illustrative Example

In this section, an illustrative 3-bus system is used to explain the arguments in section 8.2. Figure 8.1 gives the topology of the system and Table 8.1-8.3 gives the system data.
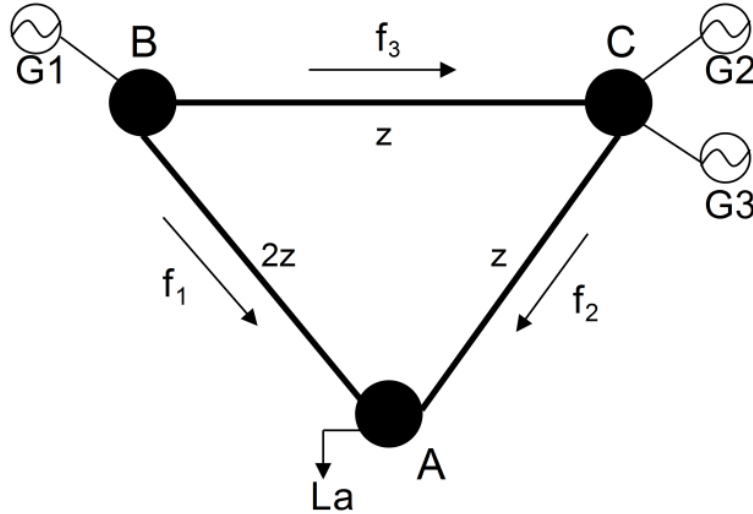
Figure 8.1: 3-Bus System

Table 8.1: Generator Data

	Gen1	Gen2	Gen3
EcoMin (MW)	5	20	5
EcoMax (MW)	45	45	40
Ramp rate (MW)	25	25	10
Variable cost ($/MW)	10	20	30
No-load cost ($)	100	100	100

Table 8.2: Shift Factors

	Line 1	Line 2	Line 3
Bus A	0	0	0
Bus B	0.5	0.5	0.5
Bus C	0.25	0.75	-0.25

Table 8.3: Load and Transmission Line Limits

Load A	40 MW
Load B	0 MW
Load C	0 MW
Thermal limit of Line 1	15 MW

The system reserve requirements, which ensure adequate reserves for G-1 contingency, are described as follows,

$$\sum_{\forall k \in G} r_k^u \geq p_g + r_g^u \qquad \forall g \qquad (8.11)$$

First, consider the base case without the proposed security constraints. The full formulation to solve this single-period problem is explicitly given as follows,

$$\min \quad 10p_1 + 20p_2 + 30p_3 + 100(u_1 + u_2 + u_3) \tag{8.12}$$

$$\text{s.t.:} \quad p_1 \geq 5u_1 \tag{8.13}$$

$$p_1 + r_1^u \leq 45u_1 \tag{8.14}$$

$$0 \leq r_1^u \leq 25 \tag{8.15}$$

$$p_2 \geq 20u_2 \tag{8.16}$$

$$p_2 + r_2^u \leq 45u_2 \tag{8.17}$$

$$0 \leq r_2^u \leq 25 \tag{8.18}$$

$$p_3 \geq 5u_3 \tag{8.19}$$

$$p_3 + r_3^u \leq 40u_3 \tag{8.20}$$

$$0 \leq r_3^u \leq 10 \tag{8.21}$$

$$p_1 + p_2 + p_3 = 40 \tag{8.22}$$

$$r_1^u + r_2^u \geq p_3 \tag{8.23}$$

$$r_1^u + r_3^u \geq p_2 \tag{8.24}$$

$$r_2^u + r_3^u \geq p_1 \tag{8.25}$$

$$0.5p_1 + 0.25(p_2 + p_3) \leq 15 \tag{8.26}$$

Equation (8.12) is objective function to minimize the summation of generation costs and commitment costs. Equations (8.14)-(8.21) are the resource-level constraints. Equation (8.21) is the system energy-balance constraint. Equations (8.23)-(8.25) specify the system reserve requirements. Equation (8.26) is the network constraint.

Since Gen1 is the cheapest generation resource, it is preferred to supply the loads. However, Gen1 generating 40MW violates the thermal limit of transmission line 1 and the reserve requirements. Therefore, the optimal solution is committing Gen1 and the second cheapest generation resource, Gen2. Table 8.4 gives the commitment and dispatch solution for the base case.

LMPs are defined as the shadow prices by increasing or decreasing one unit of power at corresponding location. In the following, the LMPs are calculated as the shadow price by increasing one unit of power.

In this base case solution, transmission line 1 is congested; thus, price separation is expected. At bus A, if the load increases to 41MW, due to the transmission limit, Gen1 cannot dispatch one more unit of power. The solution will be Gen1 decreases 1MW output and Gen2 increases 2MW. Table 8.5 gives the commitment and dispatch solution for the base case when load at bus A increases by one unit.

When the load at bus A increases by 1MW, the total cost increment is $30. Therefore, $LMP_A = 30$. Similarly, the load increment at Bus C can be only supplied by Gen2 due to transmission congestion, i.e., $LMP_C = 20$. Table 8.6 gives the LMPs for the base case.

Table 8.4: Base Case Solution

	u	p	r
Gen1	1	20	25
Gen2	1	20	25
Gen3	0	0	0
Total cost ($)		800	

Table 8.5: Base Case Solution when Load A Increases 1MW

	u	p	r
Gen1	1	19	25
Gen2	1	22	23
Gen3	0	0	0
Total cost ($)		830	

LMPs for Base Case

LMP A	$30/MWh
LMP B	$10/MWh
LMP C	$20/MWh

8.3.2 Security-Constrained Case

Although the base case solution meets the reserve requirement (8.11), it is not a secure solution with respect to G-1 contingency. Specifically, when Gen2 fails, even though Gen1 can dispatch up to 45MW, because of the network constraint, it can only dispatch 30MW instead. There is 10MW load shedding at bus A; thus, the system is not secure. Committing Gen3 is necessary.

Consider the proposed G-1 security constraints. First, characterize the extreme ray of the dual cone corresponding to the contingency. The feasible region of the dual cone for this illustrative example is given as follows ($\tau = -1$ and $\mu = \mu^+ - \mu^-$):

$$\lambda_1 = 1 \tag{8.27}$$

$$0.5\mu_1 + 0.5\mu_2 + 0.5\mu_3 + \lambda_2 = 1 \tag{8.28}$$

$$0.25\mu_1 + 0.75\mu_2 - 0.25\mu_3 + \lambda_3 = 1. \tag{8.29}$$

When Gen2 fails, transmission line 1 is congested, and bus B has extra capacities that are unable to be delivered. Based on this engineering insight, $\mu_2 = \mu_3 = 0$ and $\lambda_2 = 0$. Then all variables in the dual cone can be calculated.

$$\bar{\gamma} = \left\{ \begin{array}{lllll} \lambda_1 = 1 & \mu_1^+ = 2 & \mu_1^- = 0 & \phi_1^+ = 1 & \phi_1^- = 0 \\ \lambda_2 = 0 & \mu_2^+ = 0 & \mu_2^- = 0 & \phi_2^+ = 0 & \phi_2^- = 0 \\ \lambda_3 = 0.5 & \mu_3^+ = 0 & \mu_3^- = 0 & \phi_3^+ = 0.5 & \phi_3^- = 0 \end{array} \right\}$$

Plug in the extreme ray to the security constraint (8.1) with respect to the Gen2 failure scenario, the constraint is described as follows:

$$0.5(p_3 + r_3^u) + 30 - 40 \geq 0 \tag{8.30}$$

Combine (8.30) to (8.12)-(8.26), the security-constrained solution is given in Table 8.7. The security requirement changes the market settlement. One obvious change is to commit Gen3; thus, the total costs increase. In addition, price separation no longer exists since transmission line 1 is not congested. Table 8.8 gives the commitment and dispatch solution for the security-constrained case when load at bus A increases by one unit. Table 8.9 gives the LMPs for the security-constrained case without the marginal security component.

Table 8.7: Security-Constrained Case Solution

	u	p	r
Gen1	1	10	25
Gen2	1	20	25
Gen3	1	10	10
Total cost ($)		1,100	

Table 8.8: Security-Constrained Case Solution when Load A Increases 1MW

	u	p	r
Gen1	1	11	25
Gen2	1	20	25
Gen3	1	10	10
Total cost ($)		1,110	

Table 8.9: LMPs for Security-Constrained Case

LMP A	$10/MWh
LMP B	$10/MWh
LMP C	$10/MWh

8.3.3 Proposed Reformulation and Pricing Scheme

Consider the reformulation described in section 8.2 applied to this illustrative example, the pricing model is described as follows:

$$\min \quad 10p_1 + 20p_2 + 30p_3 \tag{8.31}$$

$$\text{s.t.:} \quad \text{resource-level constraints (8.14)-(8.21)}$$

$$\text{reserve requirement (8.23)-(8.25)}$$

$$-d_1 - i_1 = 0 \tag{8.32}$$

$$p_1 - d_2 - i_2 = 0 \tag{8.33}$$

$$p_2 + p_3 - d_3 - i_3 = 0 \tag{8.34}$$

$$i_1 + i_2 + i_3 = 0 \tag{8.35}$$

$$0.5i_1 + 0.25i_2 \le 15 \tag{8.36}$$

$$0.5(p_3 + r_3^u) + 30 - d_1 - 0.5d_3 \ge 0 \tag{8.37}$$

$$d_1 = 40 \tag{8.38}$$

$$d_2 = 0 \tag{8.39}$$

$$d_3 = 0 \tag{8.40}$$

When the load at bus A increases by 1MW, it will not only affect the nodal net injection (8.34), but also the security constraint (8.37). The security constraint (8.37) then becomes $p_3 + r_3^u \ge 22$, which implies $p_3 \ge 12$ since $r_3^u \le 10$. If the re-formulated security constraint is not enforced, the solution will have Gen1 pick up the one more unit power, as shown in Table 8.8. This solution will not cause network violation in pre-contingency state; however, this solution is not secure when Gen2 fails. When Gen2 fails, Gen3 can only ramp to 20MW, which requires Gen1 to ramp to 21MW. In the post-contingency state, transmission line 1 is congested, load shedding occurs.

Therefore, Gen3 has to increase its generation level in order to ensure the system security. The new dispatch solutions are given in Table 8.10.

The security constraint results in Gen3 increases 2MW and Gen1 decreases 1MW. The system costs increment is \$50, i.e., $LMP_A = 50$. This LMP is the summation of original LMP (\$10) and the weighted shadow prices of security constraints (\$40). When the load at bus A increases by one unit, it costs more than \$10 to supply the increment due to the security requirement. The model (8.31)-(8.40) captures the shadow prices from a secure state to a new secure state, instead of from a secure state to a feasible but not secure state.

Similarly, when the load at bus C increases by 1MW, the security constraint (8.37) requires $p_3 = 11$. Gen3 picks up the increased load. The total costs is increased by \$30, so $LMP_C = 10 + 0.5(40) = 30$. Table 8.11 gives the LMPs under the proposed pricing scheme.

The total load payment becomes \$2,000. Gen2 makes profits. Gen1 and Gen3 are marginal units. The total uplift payment is reduced to \$200. Prices separation still exists even no transmission line is congested. The prices separation is caused by the security constraints.

Table 8.10: Solution when Load A Increases 1MW with Proposed Formulation

	u	p	r
Gen1	1	9	25
Gen2	1	20	25
Gen3	1	12	10
Total cost (\$)		1,150	

Table 8.11: LMPs under Proposed Pricing Scheme

LMP A	\$50/MWh
LMP B	\$10/MWh
LMP C	\$30/MWh

8.4   Case Study

In this section, the proposed framework is tested on a modified IEEE 73-bus system (RTS 1996) (University of Washington, 2015). The test system has 73 buses, 99 generators and 117 transmission lines. The total generation capacity is 10,215MW. The peak load is 8,550MW.

The discussions in this section focus on the day-ahead energy market. The problem is formulated as 24-period day-ahead model. The loads across all periods vary from 59%-100% of the peak load. The procedure of the day-ahead energy market clearing process is described in Figure 8.2.
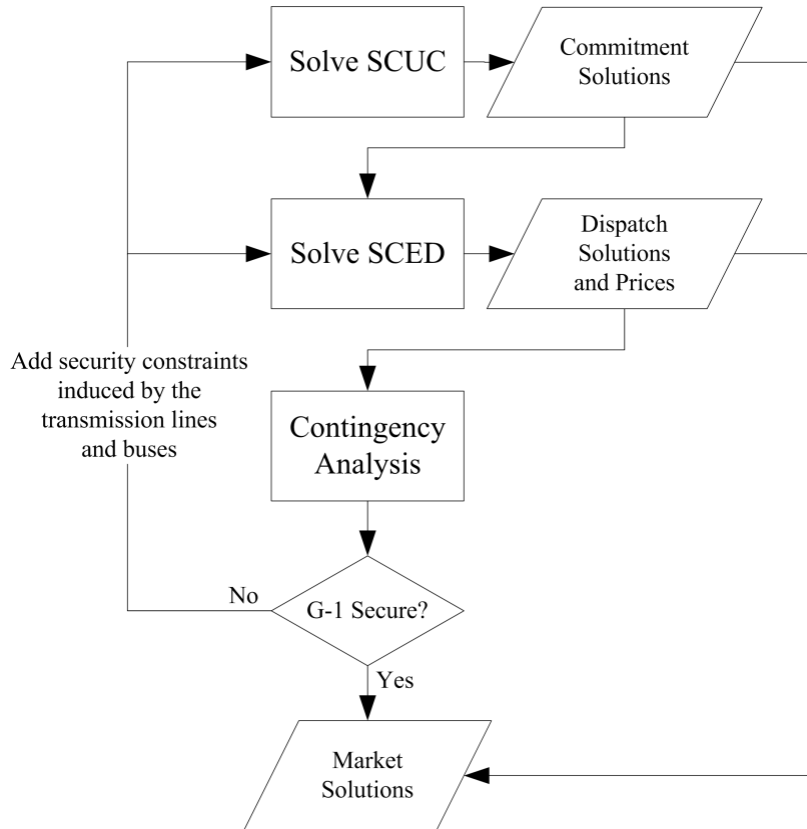
Figure 8.2: Market Clearing Process

In the clearing process, a SCUC is solved to obtain binary commitment solutions. Then, a SCED is solved. The dispatch solutions and LMPs are obtained. The dispatch

solutions are tested for G-1 contingency analysis. If the system is insecure with respect to G-1 criterion, the proposed security constraints are added with respect to the violated scenario and period. The procedure is iterated until a secure solution is obtained. The market solution is posted with the secure commitment, dispatch solutions and the prices.

The proposed extreme ray security constraints are induced by the congested transmission lines and the buses with extra capacities in the post-contingency state. In this 73-bus system, 6 lines are identified to be congested in different post-contingency states; moreover, for each of the lines, there are certain buses with extra capacities that correspond to the congested line. The candidates of the congested lines and the buses with extra capacities are marked in Figure 8.3.

Figure 8.3: 73-Bus System Diagram

Total 35 different line-bus induced extreme rays are identified. Some extreme rays appear in several G-1 scenarios and periods. Table 8.12 summarizes 15 out of 35 line-bus induced extreme rays that appear 8 times or more.

Table 8.12: Frequent Line-Bus Induced Extreme Rays

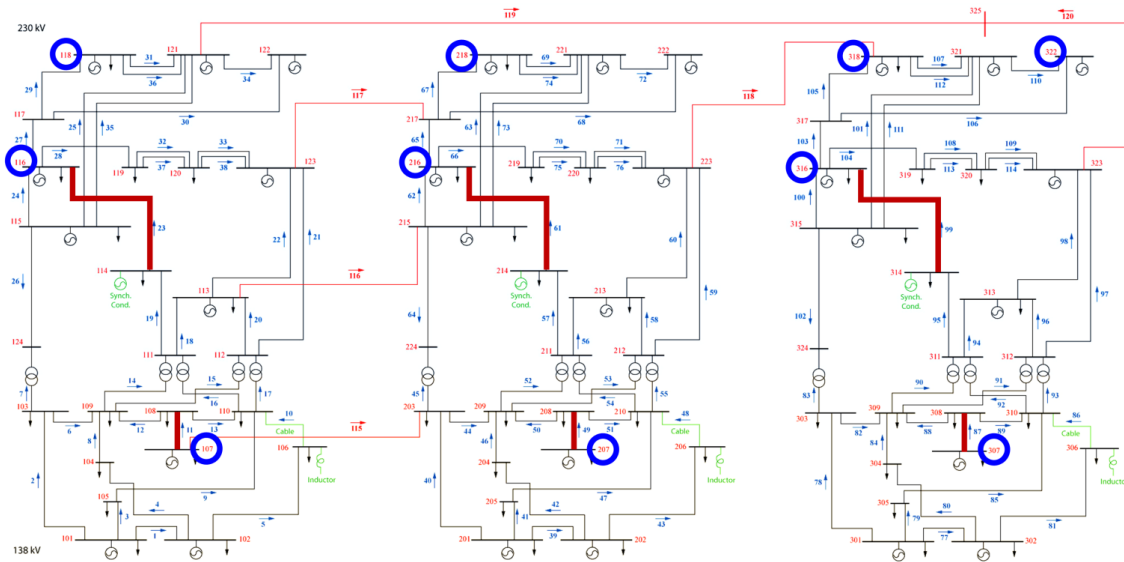| #	Frequency (times)	Lines	Buses
1	56	87	307
2	42	50,87	207,307
3	33	50	207
4	21	50,98	207,322
5	20	23,87	116,307
6	20	50,98	207,318
7	14	98	322
8	12	23,50	116,207
9	11	61	218
10	11	98	318
11	10	61	216
12	10	50,98	207,316
13	9	23	118
14	8	98	316
15	8	23,61	118,218

The added line-bus induced extreme ray security constraints in Figure 8.2 are the potential binding security constraints in SCED. If one constraint is not identified from the iterative process, then the constraint is not likely to be binding. The corresponding shadow price will be zero. Therefore, only the identified line-bus induced extreme ray security constraints are crucial to the marginal security component of LMPs. From the test results, even for the identified extreme ray security constraints, most of them are not binding in the SCED. There are eight line-bus induced extreme ray security constraints identified to be binding in SCED and contribute to the marginal security components: #1, #5, #7, #9, #11, #13, #14, and #15.

Two pricing schemes are compared: one is without the marginal security component (LMP1) and the other is with the marginal security component (LMP2). The two schemes have the same market commitment and dispatch solutions, but differ in LMPs.

First, the average price differences between the two schemes, i.e., the average marginal security components, are studied. The results are represented in Figure 8.4. The prices are increased significantly in high-load periods, as high as $47/MWh in peak-load periods. In addition, the price differences follow the pattern of total load percentage of the peak load. When the total system load increases and keeps at high level, the security constraints tend to be binding. The load increment cost more to keep the security constraints satisfied.
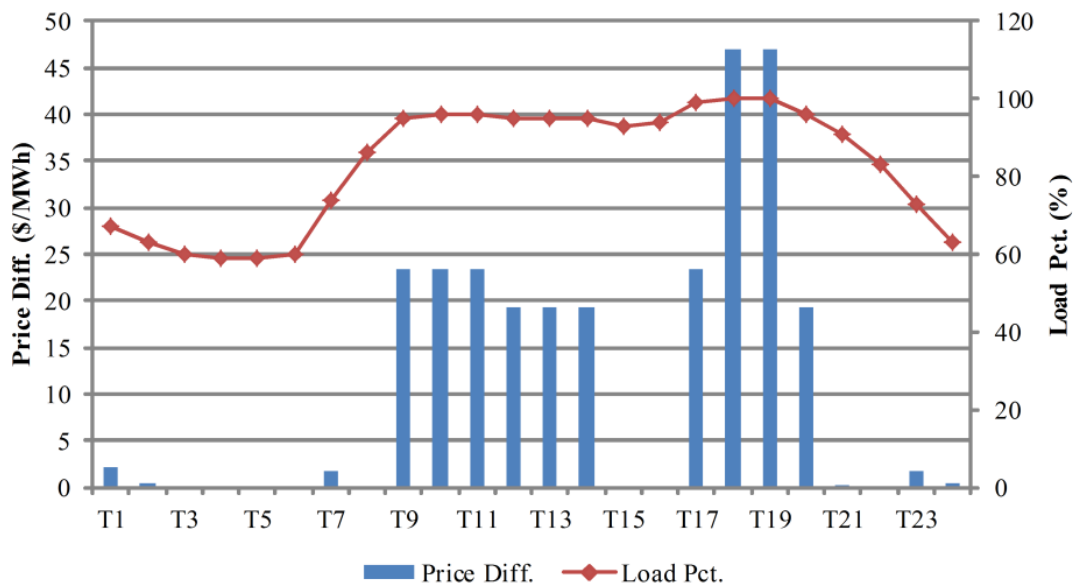
Figure 8.4: Average Price Difference Across All Periods

Figure 8.5 and Figure 8.6 select two buses to compare the two pricing schemes: bus 114, which has the largest accumulative price differences across all periods, and bus 16, which has the smallest accumulative price differences across all periods. At bus 114, the pattern is consistent with the average price difference pattern; during high-load periods, the proposed marginal security components are high. In periods 18 and 19, when at peak load, the marginal security component is as high as $213/MWh. The high price is an indication of network congestion. LMP1 represents the marginal

cost from a secure system state to a feasible system state. In periods 18 and 19, LMP1 is as high as \$156/MWh in order to move to a feasible system state. LMP2 represents the marginal cost from a secure system state to a new secure system state. It costs more to maintain a secure system state, the marginal costs in periods 18 and 19 are as high as \$369/MWh. On the other hand, at bus 116, the price differences are not significant since the original LMPs are relatively low, which indicates the network congestion does not cost more to maintain system security at the location. The marginal security components are positively correlated to the original LMPs.
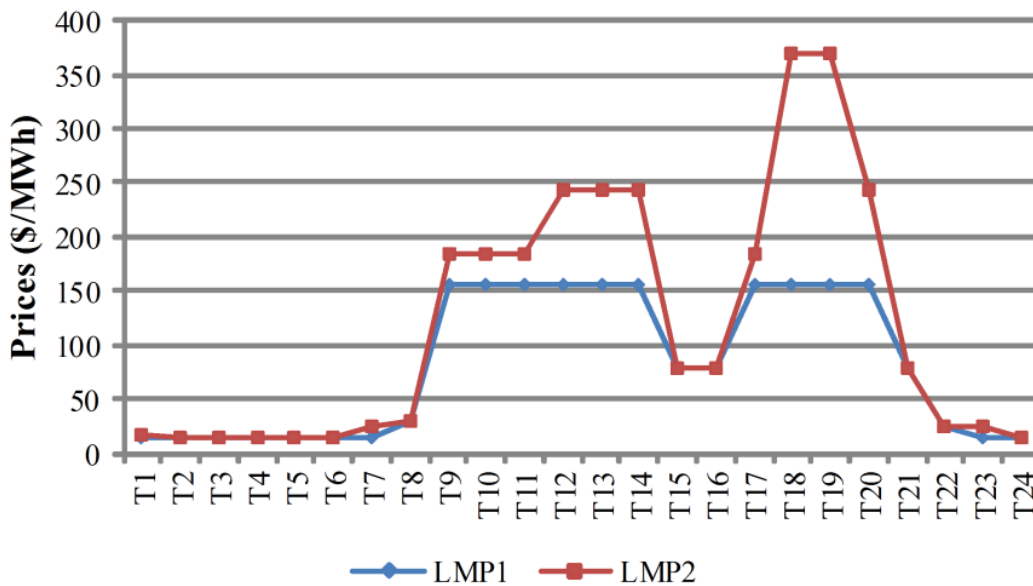
Figure 8.5: Price Comparison at Bus 114

The market surplus allocations under two pricing schemes are summarized in Table 8.13. Since energy prices are increased, the total load payment is increased 27.6% from LMP1 to LMP2. The total generation revenue is increased 43.9% from LMP1 to LMP2. The total uplift payment is reduced 49.1% from LMP1 to LMP2. Since RTO/ISOs do not prefer to implement uplift payments as they distort the market price signals, one benefit from the proposed approach is that it reduces uplift

140
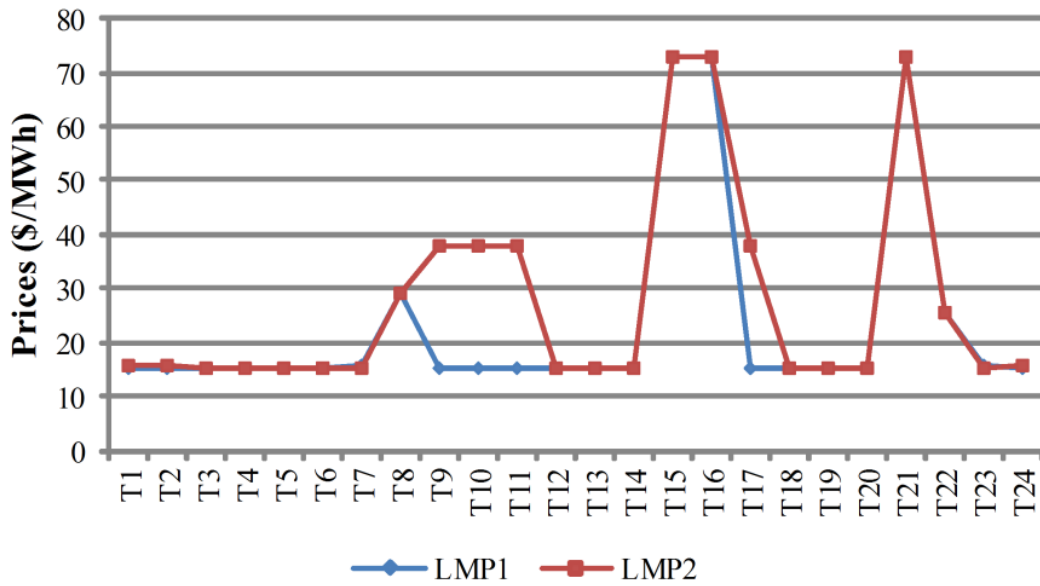
Figure 8.6: Price Comparison at Bus 116

payments. While this is not guaranteed to occur, the inclusion of security constraints further captures grid security requirements and reflects the value of service provided by generators to achieve grid security. This added value that is captured with the proposed method translates into prices that reflect that added value, which is expected to increase profits and, thus, decrease needed uplift payments.

Table 8.13: Market Surplus Allocation

	LMP1	LMP2
Total load payment ($)	8,189,920	10,446,800
Total generation revenue ($)	3,773,714	5,429,060
Total uplift payment ($)	376,826	191,779

Finally, individual generator's market surplus is analyzed. Table 8.14 lists 5 representative generators' market surplus. Gen44 and Gen47 are slow-start coal units; Gen49 is fast-start gas-turbine unit; Gen57 is nuclear unit; and Gen58 is dispatchable hydro unit. Under the proposed pricing scheme, the nuclear unit, which is with low variable cost and high capacity, has the highest profit improvement. The hydro unit also obtains significant profit increment due to the low costs. Gen44, Gen47, and

141

Gen49 are likely to be the marginal units due to the high variable generation costs. Gen44 flips from the negative profit to the positive profit. Gen47, though still has negative profit, its revenue is increased significantly. The profits of fast-start units are relatively the same.

Table 8.14: Generator Settlement

	Gen44	Gen47	Gen49	Gen57	Gen58
Capacity (MW)	100	197	12	400	50
Variable cost ($/MW)	75.6	74.8	94.7	5.5	0
Startup cost ($)	4,754	6,510	571	2,400	0
No-load cost ($)	839	1,160	73	215	0
Total generation cost ($)	121,989	165,079	1,771	57,578	0
Revenue under LMP1 ($)	104,643	115,242	482	321,022	39,827
Revenue under LMP2 ($)	132,260	159,933	776	432,359	53,627
Profit under LMP1 ($)	-17,346	-49,837	-1,289	263,444	39,827
Profit under LMP2 ($)	10,271	-5,146	-996	374,781	53,627
Profit increment ($)	27,617	44,691	293	**111,337**	13,800

8.5   Conclusions

Existing market tools, SCUC and SCED, already efficiently capture transmission contingencies but they lack an efficient approach for generator contingencies. In this chapter, a set of G-1 security constraints are proposed. The G-1 security constraints restrict system dispatch feasibility in both pre-contingency base case and post-contingency states. While existing SCUC and SCED models include reserve requirements, those requirements only require a quantity of reserve and do not impose post-contingency reserve deployment capability. With the newly proposed constraints, reserve deliverability in the post-contingency case is acknowledged.

By studying the market implications of the security constraints, a new component of LMP, a marginal security component, has been identified and added on top of the existing LMP components to better represent energy prices associated to generator contingencies. The components are composed of weighted shadow prices of the G-1 security constraints. With the proposed marginal security components, the LMPs

capture the marginal cost from a secure system state to another secure system state. The proposed advancement will not just help improve the overall system efficiency but also translates to improved price signals that better reflect available resource while considering deliverability issues associated to reserves. Future work should consider further enhancement of the security constraints along with deeper analysis on market implications of the proposed changes.

Chapter 9

CONCLUSIONS AND FUTURE WORK

9.1 Conclusions

Unit commitment (UC) problem is one of the most important power system scheduling problems. In RTO/ISOs' day-ahead markets, the UC problem is modeled and solved as a linearized network-constrained mixed integer program (MIP). The solution gives the on/off status of generators and allocates the reserves in the power system. Uncertainty in the power system complicates the scheduling process. The uncertainties in power system include the discrete event such as system element failure contingency and fluctuation of loads and renewables.

Stochastic UC models have been studied extensively in literature and are believed to give more efficient scheduling solutions amid uncertainty, in terms of both system security and cost efficiency. The stochastic UC models are usually formulated as two-stage or multi-stage models following the nature of the UC problem process, where binary commitment status and reserve allocations are determined in the first stage, and real-time dispatch is determined in the second stage.

The most straightforward stochastic UC model is to include a set of scenarios as the second-stage plausible real-time scenarios, and minimize the overall expected cost of all scenarios. However, this formulation includes many scenario-based variables and constraints, which leads to that the formulation grow in size exponentially. Although variety of decomposition algorithms have been proposed, with the current computational capability, challenges still remain for solving stochastic UC of the real-world large-scale system. One of the most promising ways to solve this type

of stochastic UC models is to develop scenario-based decomposition algorithms that take the advantage of parallel computing. Progressive hedging (PH) algorithm is a scenario-based decomposition algorithm. In the iterative PH algorithm, each scenario is solved independently, and penalized in the objective function to converge to a unified solution. The PH algorithm is proved to be converged for convex problem. Cyclic behavior is observed for MIP. Chapter 4 proposed hedging on startup and shutdown variables, and using shadow prices of commitment status non-anticipativity constraints as penalty factor. Test results show the proposed schemes help the PH algorithm converge faster. After a few PH iterations, most binary variables are able to be converged. Then, the converged variables are fixed and a reduced stochastic UC model is solved. The PH algorithm with the proposed hedging schemes is used as a pre-solve tool to converge most binary variables.

Another typical stochastic UC model is robust optimization. Robust optimization has gained increasing attention in the power system area due to its ability to model uncertainties using modest information while producing reliable solutions. Robust optimization optimizes the scheduling cost against the worst scenario in a pre-defined uncertainty set. Computationally, robust optimization is easier to solve compared with scenario-based stochastic UC. However, a common concern with the robust approach is that it can be overly-conservative. To address this issue, Chapter 5 proposed a data-driven method to construct uncertainty sets by using autoregressive integrated moving average (ARIMA) model and whitening transform on temporally and spatially correlated data. The proposed uncertainty set captures temporal and spatial correlations of data. Therefore, sizes of uncertainty sets are shrunken, and the conservativeness of robust solutions is reduced. The proposed uncertainty set is tested on a real-world power system operated by ISO New England. Numerical test results show that the proposed uncertainty set outperforms traditional uncertainty

145

sets that ignore the correlation of the data, in terms of reducing commitment costs while maintaining system security.

In this first part of this dissertation, the UC problem with uncertainty is formulated as two-stage models. Although state-of-art solution methods have been studied and improved, computational challenges remain due to the inclusion of scenario-based variables and constraints, or modeling the uncertainty sets. Alternatively, in the second part of this dissertation, the goal is to replace the two-stage stochastic model with an equivalent deterministic model with a set of constraints. In order to complete the replacement, Chapter 6 derives a necessary and sufficient condition to ensure a system feasible dispatch based on a polyhedral structure. Based on the condition, a set of security constraints to replace the stochastic model to a deterministic model is explicitly characterized. However, the number of all potential constraints is exponential. Only a subset of the constraints may be violated in real-time operation. Chapter 7 proposed an offline simulation procedure to identify the crucial constraints. The number of the constraints to be included for a new given operating condition is further reduced by data mining. With the proposed framework, the stochastic UC model is replaced by a deterministic equivalent model with the selected constraints. The equivalent deterministic model can be solved efficiently. The system security is improved significantly with the selected security constraints.

Lastly, Chapter 8 studies the market implication of the uncertainty in the power system. Due to the uncertainty in the power system, some generators are committed online for security reasons. However, the committed generators are not properly paid under the current utilized locational marginal pricing scheme. The current pricing mechanism only model pre-contingency dispatch feasibility, but does not model the post-contingency dispatch feasibility. The inclusion of the derived single-generator-failure contingency security constraints improves the existing market model. By

studying the market implication of the security constraints, the dual variables of the proposed security constraints give a security component of the energy price. Under the proposed pricing scheme, the prices capture the marginal cost from a secure system state to another secure system state and release a better pricing signal.

In summary, this dissertation thoroughly studied the UC problem with uncertainty and made several contributions to the literature and practice. Especially, a framework is proposed to replace the stochastic models by deterministic equivalent models with a set of constraints. The framework shifts the computational burden from the scheduling periods to the offline simulation and studies. The proposed framework gives an alternative way to efficiently solve the UC problem with uncertainty.

9.2   Future Work

Power system scheduling is a complex problem. Additional research is needed before the proposed methods to be implemented into practice. First of all, market models described in this dissertation are linearized models to approximate the non-linear nonconvex power system problems. Even though the market models give "perfect" solutions, additional corrections are expected to be made afterwards. For instance, because market models approximate AC power flow with linearized DC power flow model, the market solution may be AC infeasible. Corrections are needed to make the market solution from AC infeasibile to AC feasible. Most corrections are with respect to power engineering rather than optimization. Since the real-world power systems are large in scale, system operators may prefer a good but not optimal solution in a short time (heuristics) to an optimal but computational challenging solution in a long time, especially with the consideration that both solutions may need to be corrected. On the other side, a good solution can reduce the efforts in correcting phase. Therefore, the balance between the chase for optimality and the

147

solution time need to be considered when applying the algorithms to the real-world large-scale power system scheduling problems.

In current market practice, system operators prefer reserve requirement policies to hedge uncertainty in the power system. From mixed integer program (MIP) point of view, the reserve policies are cutting planes which can result in a restricted feasible region. However, the reserve policies may be too loose such that unreliabe solutions are not cut off; or, the reserve policies can be too conservative such that too many reliable solutions are cut off, resulting in a high cost of the scheduling. Much research has been done to derive proper reserve requirement policies to ensure system security (Doherty and O'Malley, 2005; Zheng and Litvinov, 2008; Ortega-Vazquez and Kirschen, 2009; Lyon *et al.*, 2014, 2015; Wang and Hedman, 2015; Hedayati-Mehdiabadi *et al.*, 2015). The questions to be answered are: 1) How to determine the reserve zones? 2) What are the adequate reserve levels in each zone? 3) How to allocate the reserves? The reserve zones in current practice are approximately determined by congestions in the power system network. However, congestions inside the zone are observed and may prevent the delivery of the reserves inside the zone. Reserve zone sharing is also under study. Most reserve requirement policies are based on operations research (optimization) oriented methodologies. There are still a lot of room to improve the current reserve policies. An alternative way to procure reserves is to generate tighter constraints to automatically restrict the reserve allocation, as the security constraints discussed in this dissertation. The constraints can disqualify undeliverable reserves and re-allocate the reserves to the proper location.

RTO/ISOs also design different market components to ensure system security amid uncertainty. For instance, capacity market has been implemented in many RTO/ISOs with a goal to have enough generation capacity to respond to the largely increased volatile and intermittent renewables. Similarly, ramping-related products

have also been proposed to reward the generators providing flexible ramping capabilities in the real-time operation. Demand response programs (Zhao *et al.*, 2013) have been implemented to make the power system more flexible against uncertainty. Do-not-exceed limits (Zhao *et al.*, 2015) for wind farms are being implementing in order to reduce the fluctuation of renewable resource output. Different market design and products can assist the power system to better hedge the risk of uncertainty. This area leave a big space to develop.

With the respect to optimization, the unit commitment scheduling problem is a special case of large-scale MIP. The discussed methodologies in this dissertation can be further improved.

Scenario-based Stochastic Unit Commitment

For scenarios-based two-stage stochastic UC models, decomposition algorithms are the promising direction to solve the UC problems for large-scale systems. The two-stage stochastic UC has "L"-shape structure, so Benders' decomposition is one of the algorithms to solve the problem. The drawback of Benders' decomposition is that the master problem need to be solved repetitively; and in each iteration, many feasibility cuts and optimality cuts are added into the mater problem, which makes the master problem take longer time to be solved. In practice, due to the large-scale system, even solving a deterministic UC (without consideration of uncertainty) may take a long time, the system operators cannot afford an iterative solution algorithm with the current computational capability and limited scheduling time. For instance, in MISO, there are 45,098 network buses, 1,401 generating units, and more than 10,000 transmission lines (Midcontinent ISO, 2015a). The day-ahead market is required to be cleared in four hours. For this large-scale system, in the UC model, if all variables and constraints are included in the MIP, the MIP won't be solved in four hours. System

operators in MISO implemented many operator-initialed heuristics to make the UC problem less computationally challenging. Scenario-based decomposition algorithm such as progressive hedging (PH) algorithm is preferred. Although the PH algorithm cannot guarantee optimality, it can take the advantages of parallel computing. The convergence of the algorithm remains as an issue. Ryan *et al.* (2013) have proposed many heuristics to improve the PH algorithm, and implement the PH algorithm to solve large-scale system UC. There are research opportunities to develop more efficient decomposition algorithms.

Another key question for scenario-based stochastic UC is how many scenarios to include and how to select the scenarios , especially with continuous uncertainty data. Adding one more scenario may increase the solution complexity exponentially. Although much literature has studied scenario selection and reduction (Dupačová *et al.*, 2003; Papavasiliou and Oren, 2013), there is still much space to explore.

In the described two-stage formulation in this dissertation, there is no integer variables in the second (recourse) stage. However, the discrete decision may exist in the recourse stage. For instance, in real-time operation, if contingency happens, system operators may turn on some fast-start generation units to respond to the contingency. The binary variables in the second stage may change the structure of the re-formulation and solution methods. Research can be carried out in for this type of problem.

Robust Unit Commitment

For robust optimization, the main difficulty lie in the bi-linear term caused by taking the dual of the inner problem. The product of uncertain data and dual variables causes the non-linearity, nonconvexity. Most literature assume special properties of the uncertainty sets in order to deal with bilinear term, such as only upper or

lower bound can be achieved or affine policy (Street *et al.*, 2011; Jiang *et al.*, 2012; Wang *et al.*, 2013; Zhao and Guan, 2013). Approximation (Bertsimas *et al.*, 2013) and exact algorithms (Jiang *et al.*, 2014) are also applied to solved the problem. A column-constraint-generation algorithm (Zhao and Zeng, 2012) is proposed and reported to solve two-stage robust optimization very efficiently; however, the algorithm is expected not be scalable to large systems due to the introduction of extra scenario-based variables and constraints.

Since the uncertainty set modeling is the key factor for robust optimization, data-driven uncertainty set is under extensive study. The question to be answered is how to model the uncertainty set such that the UC solution is robust but not be too conservative.

Moreover, as two-stage scenario-based stochastic UC, if binary decisions exist in the recourse stage, then the computational complexity increases. The problem becomes a bi-level problem with integer variables in both upper and lower level problems.

Deterministic Equivalent Model

From the test results of this dissertation, adding a set of scenario-based variables and constraints to the formulation has much more impacts on solution time than adding a set of constraints. Therefore, the framework proposed in Chapter 6 and Chapter 7 seems to be a more promising way to solve the stochastic UC problems. The framework also matches the current market practice of using a deterministic model to solve the UC problems. The constraints proposed in this dissertation have more mathematical supports rather than rule-of-thumb policies.

There are two key issues to improve the proposed framework: 1) How to characterize the constraint? 2) How to reduce the number of included constraints? In this dissertation, a set of constraints to ensure a feasible dispatch is explicitly derived

based on a dual cone. If the costs of re-dispatch is considered, then the feasible region of the dual problem is no longer a cone, but a polytope or polyhedron. How to characterize the extreme points and extreme rays for the cost-constrained dual problem is left for future study. There may be other types of constraints to improve the system security. Actually, a crucial constraint pool can be established for any kind of constraints that can improve system security. After identifying all crucial extreme rays, the next question is to reduce the number of included constraints to the deterministic model. Even though adding constraints has less impact on the solution time of MIP, the solver may take a long time to find optimal solution if too many redundant constraints are included. Data mining algorithms can help reduce the number of included crucial constraints. In this dissertation, a decision tree algorithm is adopted, other data mining algorithms such as supporting vector machine, random forest can also be tested. Moreover, in the current approach, day-ahead forecast loads at each location in each period are used as model input, which results in too many attributes for the model. Feature selection or reduction methods should be applied to reduce the dimension of input attributes. The goal is to predict the necessary crucial extreme more accurately. An alternative way to reduce the number of included constraints is to study the dominance of the constraints and represent several constraints with a single constraints. For instance, there may 10 identified crucial constraints to restrict the reserve allocation; however, if the 10 constraints can be combined together as one dominating constraint, then only one constraint needs to be added. The research to study the dominance of the constraints can give valuable contributions to both MIP theory and power system scheduling practice.

Finally, most discussed works in this dissertation are with respect to the day-ahead scheduling. The unit commitment problem also exist in short-term real-time scheduling. Future research should extend the study to real-time operations.

REFERENCES

Al-Abdullah, Y., M. A. Khorsand and K. W. Hedman, "Analyzing the impacts of out-of-market corrections", in "Bulk Power System Dynamics and Control-IX Optimization, Security and Control of the Emerging Power Grid (IREP), 2013 IREP Symposium", pp. 1–10 (IEEE, 2013).

Al-Abdullah, Y. M., M. Abdi-Khorsand and K. W. Hedman, "The role of out-of-market corrections in day-ahead scheduling", Power Systems, IEEE Transactions on **30**, 4, 1937–1946 (2015).

Atamtürk, A. and M. Zhang, "Two-stage robust network flow and design under demand uncertainty", Operations Research **55**, 4, 662–673 (2007).

Bazaraa, M. S., H. D. Sherali and C. M. Shetty, *Nonlinear Programming: Theory and algorithm* (John Wiley and Sons, Inc., 2006), 3rd edn.

Ben-Tal, A. and A. Nemirovski, "Robust convex optimization", Mathematics of Operations Research **23**, 4, 769–805 (1998).

Ben-Tal, A. and A. Nemirovski, "Robust solutions of uncertain linear programs", Operations Research Letters **25**, 1, 1–13 (1999).

Benders, J. F., "Partitioning procedures for solving mixed-variables programming problems", Numerische mathematik **4**, 1, 238–252 (1962).

Bertsimas, D. and D. B. Brown, "Constructing uncertainty sets for robust linear optimization", Operations Research **57**, 6, 1483–1495 (2009).

Bertsimas, D., V. Gupta and N. Kallus, "Data-driven robust optimization", Operations Research (2015).

Bertsimas, D., E. Litvinov, X. A. Sun, J. Zhao and T. Zheng, "Adaptive robust optimization for the security constrained unit commitment problem", IEEE Transactions on Power Systems **28**, 1, 52–63 (2013).

Bertsimas, D. and M. Sim, "Robust discrete optimization and network flows", Mathematical Programming **98**, 1-3, 49–71 (2003).

Bertsimas, D. and M. Sim, "The price of robustness", Operations Research **52**, 1, 35–53 (2004).

Bertsimas, D. and A. Thiele, "Robust and data-driven optimization: Modern decision-making under uncertainty", INFORMS tutorials in operations research: models, methods, and applications for innovative decision making p. 137 (2006).

Birge, J. R. and F. Louveaux, *Introduction to Stochastic Programming* (Springer-Verlag New York, Inc., 1997).

Bo, R., C. Wu, J. Yan, L. Hecker and Z. Zhou, "Lodf-based transmission solution screening method in economic transmission planning", in "2015 IEEE Power & Energy Society General Meeting", pp. 1–5 (IEEE, 2015).

Bouffard, F., F. D. Galiana and A. J. Conejo, "Market-clearing with stochastic security-part i: formulation", Power Systems, IEEE Transactions on **20**, 4, 1818–1826 (2005).

Box, G. E. and G. M. Jenkins, "Time series analysis: Forecasting and control", (1970).

Box, G. E., G. M. Jenkins and G. C. Reinsel, *Time Series Analysis: Forecasting and Control* (John Wiley and Sons, Inc., 2008), 4th edn.

California ISO, "Company information and facts", `http://www.caiso.com/Documents/CompanyInformation_Facts.pdf` (2011).

California ISO, "Market products and services help meet demand", `http://www.caiso.com/market/Pages/ProductsServices/Default.aspx` (2015).

California Public Utilities Commission, "California Renewables Portfolio Standard (RPS)", `http://www.cpuc.ca.gov/PUC/energy/Renewables/` (2015).

Carøe, C. C. and R. Schultz, "Dual decomposition in stochastic integer programming", Operations Research Letters **24**, 1, 37–45 (1999).

Chen, B., J. Wang, L. Wang, Y. He and Z. Wang, "Robust optimization for transmission expansion planning: Minimax cost vs. minimax regret", Power Systems, IEEE Transactions on **29**, 6, 3069–3077 (2014).

Chen, P., T. Pedersen, B. Bak-Jensen and Z. Chen, "Arima-based time series model of stochastic wind power generation", Power Systems, IEEE Transactions on **25**, 2, 667–676 (2010).

Conejo, A. J., M. A. Plazas, R. Espinola and A. B. Molina, "Day-ahead electricity price forecasting using the wavelet transform and arima models", Power Systems, IEEE Transactions on **20**, 2, 1035–1042 (2005).

Contreras, J., R. Espinola, F. J. Nogales and A. J. Conejo, "Arima models to predict next-day electricity prices", IEEE Transactions on Power Systems **18**, 3, 1014–1020 (2003).

Cotilla-Sanchez, E., P. D. Hines, C. Barrows, S. Blumsack and M. Patel, "Multi-attribute partitioning of power networks based on electrical distance", Power Systems, IEEE Transactions on **28**, 4, 4979–4987 (2013).

Davis, C. and T. Overbye, "Linear analysis of multiple outage interaction", in "System Sciences, 2009. HICSS'09. 42nd Hawaii International Conference on", pp. 1–8 (IEEE, 2009).

Doherty, R. and M. O'Malley, "A new approach to quantify reserve demand in systems with significant installed wind capacity", Power Systems, IEEE Transactions on **20**, 2, 587–595 (2005).

Dourbois, G. A., P. N. Biskas, D. I. Chatzigiannis, A. G. Vlachos and A. G. Bakirtzis, "A nodal-based day-ahead market clearing with multi-period products and transmission security constraints", in "Electrotechnical Conference (MELECON), 2016 18th Mediterranean", pp. 1–6 (IEEE, 2016).

Dupačová, J., N. Gröwe-Kuska and W. Römisch, "Scenario reduction in stochastic programming", Mathematical Programming **95**, 3, 493–511 (2003).

Edison Electric Institute, "Key facts about the electric power industry", `http://www.eei.org/about/key-facts/Documents/KeyFacts.pdf` (2013).

Ela, E., M. Milligan and B. Kirby, "Operating reserves and variable generation", Technical report NREL/TP-5500-51978, National Renewable Energy Laboratory (2011).

Ellison, J. F., L. S. Tesfatsion, V. W. Loose and R. H. Byrne, "A survey of operating reserve markets in U.S. ISO/RTO-managed electric energy regions", Project report SAND2012-1000, Sandia National Laboratory (2012).

Energy Information Administration, "Annual energy outlook 2014", `http://www.eia.gov/forecasts/aeo/er/pdf/0383er(2014).pdf` (2014).

Energy Information Administration, "Revenue and expense statistics for major U.S. investor-owned electric utilities", `http://www.eia.gov/electricity/annual/html` (2015).

Federal Energy Regulatory Commission, "Recent ISO software enhancements and future software and modeling plans", Staff report, Federal Energy Regulatory Commission (2011).

Federal Energy Regulatory Commission, "Price formation in organized wholesale electricity markets", Staff report AD14-14-000, Federal Energy Regulatory Commission (2014).

Fukunaga, K., *Introduction to statistical pattern recognition* (Academic press, 2013).

Gade, D., G. Hackebeil, S. Ryan, J. Watson, R. Wets and D. Woodruff, "Obtaining lower bounds from the progressive hedging algorithm for stochastic mixed-integer programs", Under review (2014).

Guan, Y. and J. Wang, "Uncertainty sets for robust unit commitment", IEEE Transactions on Power Systems **29**, 3, 1439–1440 (2014).

Guo, G., G. Hackebeil, S. M. Ryan, J.-P. Watson and D. L. Woodruff, "Integration of progressive hedging and dual decomposition in stochastic integer programs", Operations Research Letters (2015).

Guo, J., Y. Fu, Z. Li and M. Shahidehpour, "Direct calculation of line outage distribution factors", IEEE Transactions on Power Systems **24**, 3, 1633–1634 (2009).

Hedayati-Mehdiabadi, M., J. Zhang and K. W. Hedman, "Wind power dispatch margin for flexible energy and reserve scheduling with increased wind generation", Sustainable Energy, IEEE Transactions on **6**, 4, 1543–1552 (2015).

Hedman, K. W., M. C. Ferris, R. P. O'Neill, E. B. Fisher and S. S. Oren, "Co-optimization of generation unit commitment and transmission switching with N-1 reliability", IEEE Transactions on Power Systems **25**, 2, 1052–1063 (2010).

Hillier, F. S. and G. J. Liberman, *Introduction to Operations Research* (McGraw-Hill Companies, Inc., 2005), 8th edn.

ISO New England, "Real-time price formation", `http://www.iso-ne.com/static-assets/documents/2014/08/price_information_technical_session1.pdf` (2014).

Jabr, R. A., "Robust transmission network expansion planning with uncertain renewable generation and loads", Power Systems, IEEE Transactions on **28**, 4, 4558–4567 (2013).

Jiang, R., J. Wang and Y. Guan, "Robust unit commitment with wind power and pumped storage hydro", IEEE Transactions on Power Systems **27**, 2, 800–810 (2012).

Jiang, R., M. Zhang, G. Li and Y. Guan, "Two-stage network constrained robust unit commitment problem", European Journal of Operational Research **234**, 3, 751–762 (2014).

Kundur, P., J. Paserba, V. Ajjarapu, G. Andersson, A. Bose, C. Canizares, N. Hatziargyriou, D. Hill, A. Stankovic, C. Taylor *et al.*, "Definition and classification of power system stability ieee/cigre joint task force on stability terms and definitions", Power Systems, IEEE Transactions on **19**, 3, 1387–1401 (2004).

LaBove, G. L., R. B. Hytowitz and K. W. Hedman, "Market implications of reliability unit commitment formulations for day-ahead scheduling", in "PES General Meeting— Conference & Exposition, 2014 IEEE", pp. 1–5 (IEEE, 2014).

Li, C., M. Zhang and K. W. Hedman, "N-1 reliable unit commitment via progressive hedging", Journal of Energy Engineering **141**, 1, B4014004 (2015).

Lorca, A. and X. A. Sun, "Multistage adaptive robust optimization for the unit commitment problem", IEEE Transactions on Power Systems **30**, 4, 1702–1713 (2015).

Lubin, M., K. Martin, C. G. Petra and B. Sandıkçı, "On parallelizing dual decomposition in stochastic integer programming", Operations Research Letters **41**, 3, 252–258 (2013).

Lyon, J. D., K. W. Hedman and M. Zhang, "Reserve requirements to efficiently manage intra-zonal congestion", IEEE Transactions on Power Systems **29**, 1, 251–258 (2014).

Lyon, J. D., M. Zhang and K. W. Hedman, "Locational reserve disqualification for distinct scenarios", IEEE Transactions on Power Systems **30**, 1, 357–364 (2015).

Midcontinent ISO, "Overview of MISO day-ahead markets", `http://www.atcllc.com/oasis/Customer_Notices/NCM_MISO_DayAhead111507.pdf` (2007).

Midcontinent ISO, "Day-ahead market clearing software performance improvement", `http://www.ferc.gov/CalendarFiles/20150619141000-M1%20-%202%20-%20CHEN%20-%20M1-Ychen.pdf` (2015a).

Midcontinent ISO, "Miso business practices manuals", `https://www.misoenergy.org/LIBRARY/BUSINESSPRACTICESMANUALS/Pages/BusinessPracticesManuals.aspx` (2015b).

Montgomery, D. C., C. L. Jennings and M. Kulahci, *Introduction to Time Series Analysis and Forecasting* (John Wiley and Sons, Inc., 2008).

National Academy of Engineering, "Greatest engineering achievements of the 20th century", `http://www.greatachievements.org/` (2015).

Nemhauser, G. L. and L. A. Wolsey, *Integer and Combinatorial Optimization* (John Wiley and Sons, Inc., 1999).

North American Electric Reliability Corporation, "Reliability concepts", Report, North American Electric Reliability Corporation (2007).

Ortega-Vazquez, M. A. and D. S. Kirschen, "Estimating the spinning reserve requirements in systems with significant wind power generation penetration", Power Systems, IEEE Transactions on **24**, 1, 114–124 (2009).

Ozturk, U. A., M. Mazumdar and B. A. Norman, "A solution to the stochastic unit commitment problem using chance constrained programming", IEEE Transactions on Power Systems **19**, 3, 1589–1598 (2004).

Papavasiliou, A. and S. S. Oren, "Multiarea stochastic unit commitment for high wind penetration in a transmission constrained network", Operations Research **61**, 3, 578–592 (2013).

Papavasiliou, A., S. S. Oren and R. P. O'Neill, "Reserve requirements for wind power integration: A scenario-based stochastic programming framework", IEEE Transactions on Power Systems **26**, 4, 2197–2206 (2011).

Pope, S. L., "Price formation in ISOs and RTOs - Principles and improvements", Report, FTI Consulting (2014).

Rajan, D. and S. Takriti, "Minimum up down polytopes of the unit commitment problem with start-up costs", Research report RC23628(W0506-050), IBM Research Division (2005).

Rockafellar, R. T. and R. J.-B. Wets, "Scenarios and policy aggregation in optimization under uncertainty", Mathematics of Operations Research **16**, 1, 119–147 (1991).

Ruiz, P. A., A. Rudkevich, M. C. Caramanis, E. Goldis, E. Ntakou and C. R. Philbrick, "Reduced MIP formulation for transmission topology control", in "Communication, Control, and Computing (Allerton), 2012 50th Annual Allerton Conference on", pp. 1073–1079 (IEEE, 2012).

Ryan, S. M., R. J.-B. Wets, D. L. Woodruff, C. Silva-Monroy and J.-P. Watson, "Toward scalable, parallel progressive hedging for stochastic unit commitment", in "Power and Energy Society General Meeting", (IEEE, 2013).

SciKit-Learn, "Scikit-learn user guide", `http://scikit-learn.org/stable/user_guide.html` (2016).

Shahidehpour, M., W. F. Tinney and Y. Fu, "Impact of security on power systems operation", Proceedings of the IEEE **93**, 11, 2013–2025 (2005).

Shapiro, A., D. Dentcheva and A. Ruszczynski, *Lectures on Stochastic Programming: Modeling and theory* (Society for Industrial and Applied Mathematics and the Mathematical Programmign Society, 2009).

Shiina, T. and J. R. Birge, "Stochastic unit commitment problem", International Transactions in Operational Research **11**, 1, 19–32 (2004).

Sood, P., D. Tylavsky and Y. Qi, "Improved dc network model for contingency analysis", in "North American Power Symposium (NAPS), 2014", pp. 1–6 (IEEE, 2014).

Souag, S., F. Benhamida, Y. Salhi, A. Bendaoud and F. Z. Gherbi, "Sensitivity factor for power system security analysis using labview", in "Renewable and Sustainable Energy Conference (IRSEC), 2013 International", pp. 385–390 (IEEE, 2013).

Soyster, A. L., "Technical noteconvex programming with set-inclusive constraints and applications to inexact linear programming", Operations Research **21**, 5, 1154–1157 (1973).

Stott, B., J. Jardim and O. Alsac, "DC power flow revisited", IEEE Transactions on Power Systems **24**, 3, 1290–1300 (2009).

Street, A., F. Oliveira and J. M. Arroyo, "Contingency-constrained unit commitment with security criterion: A robust optimization approach", Power Systems, IEEE Transactions on **26**, 3, 1581–1590 (2011).

Tahanan, M., W. van Ackooij, A. Frangioni and F. Lacalandra, "Large-scale unit commitment under uncertainty: a literature survey", Technical report TR-14-01, Università di Pisa (2014).

Takriti, S., J. R. Birge and E. Long, "A stochastic model for the unit commitment problem", IEEE Transactions on Power Systems **11**, 3, 1497–1508 (1996).

Tan, P.-N., M. Steinbach and V. Kumar, *Introduction to data mining* (2006).

University of Washington, "Power systems test case archive", `https://www.ee.washington.edu/research/pstca/` (2015).

U.S.-Canada Power System, "Final report on the August 14, 2003 blackout in the United States and Canada: Causes and recommendations", Report, U.S.-Canada Power System Outage Task Force (2004).

Wang, F. and K. W. Hedman, "Dynamic reserve zones for day-ahead unit commitment with renewable resources", IEEE Transactions on Power Systems **30**, 2, 612–620 (2015).

Wang, J., M. Shahidehpour and Z. Li, "Security-constrained unit commitment with volatile wind power generation", IEEE Transactions on Power Systems **23**, 3, 1319–1327 (2008).

Wang, Q., Y. Guan and J. Wang, "A chance-constrained two-stage stochastic program for unit commitment with uncertain wind power output", IEEE Transactions on Power Systems **27**, 1, 206–215 (2012).

Wang, Q., J.-P. Watson and Y. Guan, "Two-stage robust optimization for nk contingency-constrained unit commitment", Power Systems, IEEE Transactions on **28**, 3, 2366–2375 (2013).

Watson, J.-P. and D. L. Woodruff, "Progressive hedging innovations for a class of stochastic mixed-integer resource allocation problems", Computational Management Science **8**, 4, 355–370 (2011).

Winston, W. L., *Operations Research: Applications and algorithms* (Wadsworth, Inc., 1993), 3rd edn.

Wood, A. J. and B. F. Wollenberg, *Power Generation, Operation and Control* (John Wiley and Sons, Inc., 1996), 2nd edn.

Wu, L. and M. Shahidehpour, "Accelerating the benders decomposition for network-constrained unit commitment problems", Energy Systems **1**, 3, 339–376 (2010).

Wu, L., M. Shahidehpour and T. Li, "Cost of reliability analysis based on stochastic unit commitment", IEEE Transactions on Power Systems **23**, 3, 1364–1374 (2008).

Zhao, C. and Y. Guan, "Unified stochastic and robust unit commitment", IEEE Transactions on Power Systems **28**, 3, 3353–3361 (2013).

Zhao, C., J. Wang, J.-P. Watson and Y. Guan, "Multi-stage robust unit commitment considering wind and demand response uncertainties", IEEE Transactions on Power Systems **28**, 3, 2708–2717 (2013).

Zhao, J., T. Zheng and E. Litvinov, "Variable resource dispatch through do-not-exceed limit", IEEE Transactions on Power Systems **30**, 2, 820–828 (2015).

Zhao, L. and B. Zeng, "Robust unit commitment problem with demand response and wind energy", in "Power and Energy Society General Meeting", (IEEE, 2012).

Zheng, Q., J. Wang and A. L. Liu, "Stochastic optimization for unit commitment - a review", IEEE Transactions on Power Systems **30**, 4, 1913–1924 (2015).

Zheng, Q., J. Wang, P. M. Pardalos and Y. Guan, "A decomposition approach to the two-stage stochastic unit commitment problem", Annals of Operations Research **210**, 1, 387–410 (2013).

Zheng, T. and E. Litvinov, "Contingency-based zonal reserve modeling and pricing in a co-optimized energy and reserve market", Power Systems, IEEE Transactions on **23**, 2, 277–286 (2008).

APPENDIX A

ACRONYMS

AC	Alternating Current
ACOPF	Alternating Current Optimal Power Flow
AGC	Automatic Generation Control
ARIMA	Autoregressive Integrated Moving Average
BD	Benders Decomposition
CAISO	California Independent System Operator
CCSP	Chance-constrained Stochastic Programming
CVaR	Conditional Value at Risk
DAM	Day-ahead Market
DCOPF	Direct Current Optimal Power Flow
ED	Economic Dispatch
ER	Extreme Ray
FERC	Federal Energy Regulatory Commission
G-1	Single Generator Failure
ISF	Injection Shift Factor
ISO	Independent System Operator
ISONE	Independent System Operator New England
LP	Linear Programming
LODF	Line Outage Distribution Factor
LR	Lagrangian Relaxation
LSE	Load Serving Entity
LMP	Locational Marginal Price
MEF	Modified Extensive Form
MILP	Mixed Integer Linear Programming
MIP	Mixed Integer Programming
MISO	Midcontinent Independent System Operator
MSSP	Multi-stage Stochastic Programming
NERC	North American Electric Reliability Corporation
NREL	National Renewable Energy Laboratory
OMC	Out-of-Market Correction
OPF	Optimal Power Flow
OR	Operations Research
PH	Progressive Hedging
PJM	Pennsylvania-New Jersey-Maryland Interconnection
PTDF	Power Transfer Distribution Factor
RTO	Regional Transmission Organization
RTM	Real-time Market
RUC	Residual or Robust Unit Commitment
SCUC	Security Constrained Unit Commitment
SCED	Security Constrained Economic Dispatch
SEF	Stochastic Extensive Form
SO	System Operator
SPP	Southwest Power Pool
SUC	Stochastic Unit Commitment
TSSP	Two-stage Stochastic Programming
TSRO	Two-stage Robust Optimization
UC	Unit Commitment
VaR	Value at Risk

APPENDIX B

NOMENCLATURE

Sets and Indices:

$g \in G$	generators
$g \in G^f$	fast-start generators
$g \in G(n)$	generators at bus n
$i \in I$	extreme rays
$j \in J$	wind farms
$k \in K$	zones
$l \in L$	transmission lines
$l \in \delta^-(n)$	transmission lines from bus n
$l \in \delta^+(n)$	transmission lines to bus n
$n \in N$	buses
$n \in Z_k$	buses in zone k
$t \in T$	time periods
$s \in S$	scenarios

Parameters:

B_l	transmission line susceptance
C_g	linearized dispatch cost
C_g^{NL}/C_g^{SU}	no-load/startup cost
D_{nt}	predicted loads
DT_g/UT_g	minimum down/up time
F_l	transmission line rating
$G1_g^s$	G-1 indicator
H_g/L_g	available capacity bounds
P_g^{max}/P_g^{min}	generation capabilities
R_g^5/R_g^{10}	5-minute/10-minute contingency ramping capability
$R_g^{hr}/R_g^{SD}/R_g^{SU}$	hourly/shutdown/startup/ ramping capability
Q_k^{min}	zonal reserve requirement
π^s	scenario probability
Ψ_{ln}	PTDF

Unit Commitment Variables

u_{gt}	commitment status
v_{gt}	startup status
w_{gt}	shutdown status

Dispatch Variables

d_{nt}	loads
f_{lt}	transmission line flow
i_{nt}	bus injection
p_{gt}	generation
p_{gt}^H/p_{gt}^L	available generation bounds
$\hat{p}_{gt}^H/\hat{p}_{gt}^L$	post-contingency available generation bounds
r_{gt}	reserves
θ_{nt}	bus angle

Dual Cone Variables

λ_n	dual variables of node-balance constraint
μ_l^+/μ_l^-	dual variables of transmission bounds
ϕ_g^+/ϕ_g^-	dual variables of generation bounds
τ	dual variables of total injection constraint

APPENDIX C

SUPPLEMENTAL MATERIALS

C.1   Linear Programming

Linear programming (LP) is one special subset of constrained optimization (or mathematical programming) where the objective function and all constraints are in linear relation (Winston, 1993). The canonical form of LP is represented as follows,

$$\min \quad c'x \tag{C.1}$$
$$\text{s.t.} \quad Ax \leq b \tag{C.2}$$
$$x \in \mathbb{R}^n \tag{C.3}$$

where $x_{n \times 1}$ is decision variable and $(A_{m \times n}, b_{m \times 1}, c_{n \times 1})$ are parameters. Equation (C.1) is the objective function of the LP and (C.2) is a set of m linear constraints.

Any of the LP can be transformed into a standard form as follows,

$$\min \quad c'x \tag{C.4}$$
$$\text{s.t.} \quad Ax + s = b \tag{C.5}$$
$$x \geq 0 \tag{C.6}$$

where $s_{n \times 1}$ is slack variable vector.

Many algorithms have been developed to solve the LP. Theoretical result shows that there exist a polynomial algorithm to solve the LP (Hillier and Liberman, 2005). However, in practice, the most efficient algorithm to solve the LP is simplex method, which is not a polynomial algorithm. Commercial software solvers such as CPLEX, Gurobi combine many techniques together (simplex, dual simplex, interior point method) to solve the LP.

C.2   Convex Sets and Polyhedron

Definition 8. *Let $v^1, v^2, \cdots, v^k$ be vectors in $\mathbb{R}^n$, a convex combination of the vectors is defined as $w = \sum_{i=1}^{k} \lambda_i v^i$ such that $\lambda_i \in \mathbb{R}_+, \forall i$, and $\sum_{i=1}^{k} \lambda_i = 1$.*

Definition 9. *A set $S \in \mathbb{R}^n$ is said to be convex if the convex combination of any two points in S also belongs to the set, i.e., $\forall x^1, x^2 \in S \Rightarrow \lambda x^1 + (1-\lambda)x^2 \in S, \forall \lambda \in [0, 1]$.*

Definition 10. *A convex hull of a given set S, denoted by $conv(S)$, is defined as the minimum convex set that contains all points in S.*

Definition 11. *$S = \{x \in \mathbb{R}^n | p'x = \alpha\}$ is called a hyperplane. $S = \{x \in \mathbb{R}^n | p'x \geq \alpha\}$ is called a half-space. A polyhedron P is any set in $\mathbb{R}^n$ that can be represented as the intersection of a finite number of half-spaces.*

Definition 12. *A set $C \subseteq \mathbb{R}^n$ is said to be a cone if $\forall x \in C$ and $\forall \theta > 0$, $\theta x \in C$. A set $C \subseteq \mathbb{R}^n$ is said to be a pointed cone if $\forall x \in C$ and $\forall \theta \geq 0$, $\theta x \in C$.*

Proposition 13. *The feasible region of a LP is a polyhedron and it is a convex set (Bazaraa et al., 2006).*

Proof. By definition, the feasible region of a LP, $P = \{x \in \mathbb{R}^n | Ax \leq b\}$ is the intersection of m half-spaces, i.e., $\sum_{j=1}^{n} a_{ij}x_j \leq b_i, \forall i = 1, 2, \cdots, m$. $\forall x^1, x^2 \in P, Ax^1 \leq b, Ax^2 \leq b$. Let $y = \lambda x^1 + (1 - \lambda)x^2, \forall \lambda \in [0, 1]$, then $Ay = \lambda Ax^1 + (1 - \lambda)Ax^2 \leq \lambda b + (1 - \lambda)b = b, \Rightarrow y \in P$, thus P is a convex set. $\square$

C.3 Duality

For every LP, there is an associated LP with it called its dual. The relationship between the original problem (called the primal) and the dual problem is extremely useful in many ways (Hillier and Liberman, 2005).

Primal:

$$\min \quad c'x \tag{C.7}$$
$$\text{s.t.} \quad Ax \leq b \tag{C.8}$$
$$x \geq 0 \tag{C.9}$$

Dual:

$$\max \quad b'y \tag{C.10}$$
$$\text{s.t.} \quad A'y \leq c \tag{C.11}$$
$$y \leq 0 \tag{C.12}$$

Table C.1 summarizes primal-dual formulation corresponding relation and Table C.2 summarizes primal-dual feasibility corresponding relation.

Table C.1: Primal-dual Formulation Corresponding Relation

	Primal	Dual
	Minimize Z	Maximize W
	constraint i:	variable y_i:
Sensible	$\geq$ form	$y_i \geq 0$
Odd	= form	unconstrained
Bizarre	$\leq$ form	$y_i \leq 0$
	variable x_j:	constraint j:
Sensible	$x_j \geq 0$	$\leq$ form
Odd	unconstrained	= form
Bizarre	$x_j \leq 0$	$\geq$ form

Table C.2: Primal-dual Feasibility Corresponding Relation

	Optimal	Unbounded	Infeasible
Optimal	$\checkmark$	$\times$	$\times$
Unbounded	$\times$	$\times$	$\checkmark$
Infeasible	$\times$	$\checkmark$	$\checkmark$

Theorem 14 (Weak Duality Theorem). *For any primal (minimization problem) feasible solution and dual feasible solution, the corresponding primal objective is greater than or equal to the dual corresponding objective, i.e., $Z \geq W$.*

Theorem 15 (Strong Duality Theorem). *If there exists an optimal solution for primal problem, then there also exists an optimal solution for dual problem, and the corresponding objective of primal problem equals to the corresponding objective of dual problem, i.e., $Z^* = W^*$, where the star indicates the optimal solution.*

Proposition 16 (Complementary Slackness)**.** *If both primal and dual have optimal solution* x^*, y^* *respectively, then the following conditions hold,*

$$(b_i - \sum_{j=1}^{n} a_{ij}x_j)y_i^* = 0, \forall i = 1, 2, \cdots, m \tag{C.13}$$

$$(c_j - \sum_{i=1}^{m} a_{ij}y_i)x_j^* = 0, \forall j = 1, 2, \cdots, n \tag{C.14}$$

C.4   Mixed Integer Programming

Mixed integer programming (MIP) is another subset of constrained optimization problems where some decision variables are restricted to take integer values. Without specification, the MIP refers to mixed integer linear programming (MILP) here and forth. The generic form of the MIP is represented as follows Nemhauser and Wolsey (1999),

$$\min \quad c'x + h'y \tag{C.15}$$
$$\text{s.t.} \quad Ax + Gy \leq b \tag{C.16}$$
$$x \in \mathbb{Z}^{n_1}, y \in \mathbb{R}^{n_2} \tag{C.17}$$

where $y_{1 \times n_2}$ are continuous variables, however $x_{1 \times n_1}$ can be only integer values. Parameters c, h, A, G, b are with corresponding dimensions.

Since the discrete nature of integer variables, the MIP results in the feasible regions that are not convex sets. Non-convex problems are difficult to solve. In computational complexity theory, the corresponding decision problem of the MIP is NP-complete and the MIP is said to be a NP-hard problem, which means there does not exist any known polynomial solution algorithm to solve the problem efficiently.

Commercial softwares combine branch-and-bound algorithms and cutting-plane algorithms to solve the MIP. The former first solves the LP relaxation problem of the MIP, branches the fractional integer variable and prunes nodes with certain criterion. The latter generates cutting planes to cut the LP optimal but not MIP feasible solution iteratively, aims at obtaining the tightest formulation of the MIP, as known as the facet-defining constraints.

C.5   Benders Decomposition

Benders' decomposition Benders (1962) is a decomposition method which can solve the MIP with special structure efficiently (Nemhauser and Wolsey, 1999). Benders' decomposition breaks the MIP into a master problem and subproblems. Considering the following MIP,

$$\min \quad c'x + h'y \tag{C.18}$$
$$\text{s.t.} \quad Ax + Gy \leq b \tag{C.19}$$
$$x \in \mathbb{Z}_+^{n_1}, y \in \mathbb{R}_+^{n_2} \tag{C.20}$$

Suppose that there is a solution for all integer variables, then by fixing the integer variables, the problem denoted as $LP(\bar{x})$ becomes,

$$\min \quad h'y \tag{C.21}$$
$$\text{s.t.} \quad Gy \leq b - A\bar{x} \tag{C.22}$$
$$y \in \mathbb{R}_+^{n_2} \tag{C.23}$$

By taking its dual denoted as $D(\bar{x})$,

$$\max \quad u'(b - A\bar{x}) \tag{C.24}$$
$$\text{s.t.} \quad u'G \leq h \tag{C.25}$$
$$u \leq 0 \tag{C.26}$$

Let $Q = \{u : u'G \leq h, u \leq 0\}$, and $u^k, k = 1, 2, \cdots, K$ be a set of extreme points of Q, $\gamma^j, j = 1, 2, \cdots, J$ be a set of extreme rays of Q, the Benders' reformulation is represented as follows.

$$\min \quad c'x + \eta \tag{C.27}$$
$$\text{s.t.} \quad \eta \geq (u^k)'(b - Ax) \quad \forall k \tag{C.28}$$
$$(\gamma^j)'(b - Ax) \leq 0 \quad \forall j \tag{C.29}$$
$$x \in \mathbb{Z}_+^{n_1}, \eta \in \mathbb{R}_+ \tag{C.30}$$

Equation (C.28) is referred as optimality cuts since if there exists an extreme point u^k such that $(u^k)'(b - Ax) > \eta$ then the optimality is not achieved. Equation (C.29) is referred as feasibility cuts since if there exists an extreme ray γ^j such that $(\gamma^j)'(b - Ax) > 0$ then the feasibility is not achieved.

Then the master problem of Benders' decomposition is described as follows,

$$\min_{x,\eta} \quad c'x + \eta \tag{C.31}$$
$$\text{s.t.} \quad \eta \geq (\bar{u}^k)'(b - Ax) \quad \forall k \in C^O \tag{C.32}$$
$$(\bar{\gamma}^j)'(b - Ax) \leq 0 \quad \forall j \in C^F \tag{C.33}$$
$$x \in \mathbb{Z}_+^{n_1}, \eta \in \mathbb{R}_+ \tag{C.34}$$

where C^O and C^F are the subsets of optimality cuts and feasibility cuts respectively.

The subproblem of Benders' decomposition is,

$$\max_u \quad u'(b - A\bar{x}) \tag{C.35}$$
$$\text{s.t.} \quad u'G \leq h \tag{C.36}$$
$$u \leq 0 \tag{C.37}$$

The following Algorithm 3 describes the structure of the algorithm,

---

Algorithm 3 Benders' Decomposition Algorithm

---

loop
    solve master problem **return** $(\bar{x}, \bar{\eta})$
    solve subproblem
    if unbounded **then**
        return $\bar{\gamma}$, **add** feasibility cut to the master problem
    else
        return $\bar{u}, \bar{u}'(b - A\bar{x})$
        if $\bar{u}'(b - A\bar{x}) > \bar{\eta}$ **then**
            add optimality cut to the master problem
        else
            exit loop
        end if
    end if
end loop

C.6   Lagrange Relaxation

Definition 17. *A problem R where $z^R = \min\{g(x)|x \in Y\}$ is the relaxation of problem P where $z^P = \min\{f(x)|x \in X\}$, if $f(x) \geq g(x)$, $\forall x \in X$ and $X \subseteq Y$. (Nemhauser and Wolsey, 1999; Bazaraa et al., 2006)*

Proposition 18. *The following statements hold for the relaxation problem R and the original problem P.*

- *If R is infeasible, then P is infeasible*
- *If P and R have optimal solutions, then $z^P \geq z^R$*
- *If x^R is an optimal solution to R such that $x^R \in X$ and $g(x^R) = f(x^R)$, then x^R is an optimal solution to P*

Consider the following problem,

$$\min \quad c'x \tag{C.38}$$
$$\text{s.t.} \quad Ax \leq b \tag{C.39}$$
$$Dx \leq d \tag{C.40}$$
$$x \in X \tag{C.41}$$

By dropping the complicating constraints $Dx \leq d$ and putting it to the objective function with penalty $\lambda \geq 0$, the Lagrangian relaxation (LR) of the problem is obtained as follows,

$$\min \quad c'x - \lambda'(d - Dx) \tag{C.42}$$
$$\text{s.t.} \quad Ax \leq b \tag{C.43}$$
$$x \in X \tag{C.44}$$

Let $LR(\lambda)$ denote the above problem and $z^{LR}(\lambda)$ denote the objective value of the above problem, the Lagrangian dual problem is defined as,

$$z^{LD} = \max_{\lambda \geq 0} z^{LR}(\lambda) \tag{C.45}$$

Theorem 19. *Let $P = \{x : Dx \leq d\}$ and $Q = \{x \in X : Ax \leq b\}$, then*

$$z^{LD} = \min\{c'x : x \in P \cap conv(Q)\} \tag{C.46}$$

Proof. Let $x^k, k = 1, 2, \cdots, K$ be a set of extreme points of $conv(Q)$ and $\gamma^j, j = 1, 2, \cdots, J$ be a set of extreme rays of $conv(Q)$, then by Minkowski's theorem, $\forall x \in conv(Q), x = \sum_k \alpha_k x^k + \sum_j \beta_j \gamma^j, \sum_k \alpha_k = 1, \forall \alpha_k, \beta_j \geq 0$. For any given $\lambda \geq 0$, $z^{LR}(\lambda) = \min_{k=1,2,\cdots,K}\{c'x^k - \lambda'(d - Dx^k) : (c' + \lambda'D)\gamma^j \geq 0, \forall j\}$ since the optimal solution has to be one of the extreme points if the optimal solution exists. Then the Lagrangian dual problem can be reformulated as

$$
\begin{aligned}
\max \quad & \eta \\
\text{s.t.} \quad & \eta \leq c'x^k - \lambda'(d - Dx^k) \quad \forall k \\
& (c' + \lambda'D)\gamma^j \geq 0 \quad \forall j \\
& \lambda \geq 0
\end{aligned}
$$

reordering the terms,

$$
\begin{aligned}
\max \quad & \eta \\
\text{s.t.} \quad & \eta + \lambda'(d - Dx^k) \leq c'x^k \quad \forall k \qquad (\alpha_k) \\
& -\lambda'D\gamma^j \leq c'\gamma^j \quad \forall j \qquad (\beta_j) \\
& \lambda \geq 0
\end{aligned}
$$

take the dual,

$$
\begin{aligned}
\min \quad & \sum_k c'x^k \alpha_k + \sum_j c'\gamma^j \beta_j \\
\text{s.t.} \quad & \sum_k (d - Dx^k)\alpha_k - \sum_j D\gamma^j \beta^j \geq 0 \\
& \sum_k \alpha_k = 1 \\
& \alpha_k, \beta_j \geq 0 \quad \forall k, j
\end{aligned}
$$

equivalent to,

$$\min \quad c' \left(\sum_k \alpha_k x^k + \sum_j \beta_j \gamma^j \right)$$

$$\text{s.t.} \quad D \left(\sum_k \alpha_k x^k + \sum_j \beta^j \gamma^j \right) \leq d$$

$$\sum_k \alpha_k = 1$$

$$\alpha_k, \beta_j \geq 0 \quad \forall k, j$$

equivalent to,

$$\min \quad c' x$$

$$\text{s.t.} \quad Dx \leq d$$

$$x \in conv(Q)$$

Therefore, $z^{LD} = \min\{c'x : x \in P \cap conv(Q)\}$, the theorem is proved. $\quad\square$

Theorem 20. $z^{LR}(\lambda)$ *is a piece-wise linear concave function with respect to λ.*

Proof. Suppose $\forall \lambda \geq 0$, there exists an optimal solution for $z^{LR}(\lambda)$, i.e., it is not unbounded, then the optimal solution has to be an extreme point of $conv(Q)$ as defined before. Let $f^k(\lambda) = c'x^k - \lambda'(d - Dx^k)$ where $x^k, k = 1, 2, \cdots, K$ is one of the extreme points of $conv(Q)$, then $z^{LR}(\lambda) = \min_{k=1,2,\cdots,K}\{f^k(\lambda)\}$. For any two points λ^1, λ^2, let $\lambda^3 = \alpha\lambda^1 + (1-\alpha)\lambda^2, \alpha \in (0,1)$. Suppose $z^{LR}(\lambda^3) = f^i(\lambda^3)$, then $z^{LR}(\lambda^3) = f^i(\alpha\lambda^1 + (1-\alpha)\lambda^2) = \alpha f^i(\lambda^1) + (1-\alpha)f^i(\lambda^2)$ since $f^i(\lambda)$ is a linear function with respect to λ. Since $f^i(\lambda^1) \geq \min_{k=1,2,\cdots,K}\{f^k(\lambda^1)\}$ and $f^i(\lambda^2) \geq \min_{k=1,2,\cdots,K}\{f^k(\lambda^2)\}$, we have $z^{LR}(\lambda^3) \geq \alpha z^{LR}(\lambda^1) + (1-\alpha)z^{LR}(\lambda^2)$, thus $z^{LR}(\lambda)$ is a concave function with respect to λ by definition. Moreover, $z^{LR}(\lambda)$ is the minimum of a finite set of linear functions, thus $z^{LR}(\lambda)$ is piecewise linear function with finite many break points. $\quad\square$

Since $z^{LR}(\lambda)$ is a piece-wise linear function, sub-gradient algorithm is often adopted to solve the Lagrangian dual problem. In addition, after dropping the complicating constraints, the problem can be decomposed into several smaller problems which are easier to solve.

C.7   Dual Decomposition

Dual decomposition (DD) algorithm, first proposed by Carøe and Schultz (1999), is decomposition algorithm based on the Lagrangian relaxation. The TSSP can be re-formulated as follows,

$$\min \quad \sum_{\forall s} \pi^k (c'x^s + (\tilde{q}^s)'y^s) \tag{C.47}$$

$$\text{s.t.} \quad Ax^s \leq b \qquad\qquad \forall s \tag{C.48}$$

$$\tilde{W}^s y^s = \tilde{h}^s - \tilde{T}^s x \qquad\qquad \forall s \tag{C.49}$$

$$x^s = x^0 \qquad\qquad \forall s \tag{C.50}$$

$$x^s, y^s \geq 0 \qquad\qquad \forall s \tag{C.51}$$

The reformulation (Carøe and Schultz, 1999; Lubin *et al.*, 2013) introduces the scenario-based first-stage decision variables $x^s, \forall s$, and the non-anticipativity constraint equation (C.50). Let $F^s = \{(x^s, y^s)|Ax^s \leq b, \tilde{T}^s x + \tilde{W}^s y^s = \tilde{h}^s, x^s, y^s \geq 0\}$, then the problem is equivalent to,

$$z = \min \left\{ \sum_{\forall s} \pi^s (c'x^s + (\tilde{q}^s)'y^s) : (x^s, y^s) \in F^s, x^s = x^0, \forall s \right\} \tag{C.52}$$

The only binding constraint is the non-anticipativity constraint, using the Lagrangian relaxation to relax this constraint, the Lagrangian relaxation for a set of given $\bar{\lambda} = (\bar{\lambda}^1, \bar{\lambda}^2, \cdots, \bar{\lambda}^s)$ is described as follows.

$$D(\bar{\lambda}) = \min \left\{ \sum_{\forall s} \left[L^s(x^s, y^s, \bar{\lambda}^s) - (\bar{\lambda}^s)'x^0 \right] : (x^s, y^s) \in F^s, \forall s \right\} \tag{C.53}$$

where $L^s(x^s, y^s, \bar{\lambda}^s) = \pi^s (c'x^s + (\tilde{q}^s)'y^s) + (\bar{\lambda}^s)'x^s$. Let $\sum_{\forall s} \bar{\lambda}^s = 0$, then the problem can be decomposed into s scenario-based sub-problems,

$$D^s(\bar{\lambda}^s) = \min \left\{ L^s(x^s, y^s, \bar{\lambda}^s) : (x^s, y^s) \in F^s, \forall s \right\} \tag{C.54}$$

Since the Lagrangian relaxation provides the lower bound for the original problem, then Lagrangian dual is defined as,

$$z^{LD} = \max_{\lambda} \left\{ \sum_{\forall s} D^s(\lambda^s) : \sum_{\forall s} \lambda^s = 0 \right\} \tag{C.55}$$

The Lagrangian dual is a concave function with respect to λ. For each of the sub-problem $D^s(\lambda^s)$, the solution $\bar{x}^s$ given $\bar{\lambda}^s$ is a sub-gradient of the problem (Nemhauser and Wolsey, 1999).

$$D^s(\lambda^s) \leq D^s(\bar{\lambda}^s) + (\bar{x}^s)'(\lambda^s - \bar{\lambda}^s) \tag{C.56}$$

The Lagrangian dual problem can be solved by a cutting plane algorithm (Lubin *et al.*, 2013). The master problem is described as follows,

$$\max \quad \sum_{\forall s} \theta_s \tag{C.57}$$

$$\text{s.t.} \quad \sum_{\forall s} \lambda^s = 0 \qquad\qquad \forall s \tag{C.58}$$

$$\theta_s \le D^s(\bar{\lambda}^{s,k}) + (\bar{x}^{s,k})'(\lambda^s - \bar{\lambda}^{s,k}) \qquad\qquad \forall s, k \tag{C.59}$$

The following Algorithm 4 (Lubin *et al.*, 2013) describes the pseudo code of the the DD algorithm for SUC.

Algorithm 4 Dual Decomposition Algorithm

$k = 0$
$\bar{\lambda}^{s,0} = 0, \forall s$
while $g^{(k)} > \epsilon$ **do**
   for $s \in S$ **do**
      Solve $D^s(\bar{\lambda}^{s,k})$, obtain $(x^s)^*$
      $\bar{x}^{s,k} \leftarrow (x^s)^*$
   end for
   Solve the mater problem, obtain $(\theta_s)^*, (\lambda^s)^*, \forall s$
   $k = k + 1$
   $\bar{\lambda}^{s,k} \leftarrow (\lambda^s)^*, \forall s$
   $g^{(k)} = \dfrac{\sum_{\forall s}\left[(\theta_s)^* - D^s(\bar{\lambda}^{s,k-1})\right]}{1 + |\sum_{\forall s} D^s(\bar{\lambda}^{s,k-1})|}$
end while

The DD algorithm provides a lower bound of the original problem. Heuristics have been proposed to generate a feasible solution of the original problem to obtain an upper bound (Papavasiliou and Oren, 2013).

C.8 Direct Current Optimal Power Flow

The electric power flow is an alternating current (AC) based flow and follows the Kirchhoff's circuit laws when transferring in the power grid. On top of economic dispatch, system operators also need to take optimal power flow (OPF), also referred as network constraints, into consideration when making the scheduling decisions. Alternating current optimal power flow (ACOPF) formulates a non-linear mathematical programming problem and is extremely difficult to solve when the system is large. Instead of solving ACOPF, the system operators solve a direct current optimal power flow (DCOPF) model, which is a simplified linear model from the ACOPF model based on some assumptions (Wood and Wollenberg, 1996). After obtaining the DCOPF solution, system operators make a set of justifications to ensure the solution is AC feasible. The following is the derivation of DCOPF model.

Z: impedance R: resistance X: reactance
Y: admittance G: conductance B: susceptance
V: voltage I: current E: electric potential
S: complex power P: real power Q: reactive power

$$Z = R + jX, \ Y = G + jB$$

$$Y = \frac{1}{Z}, \ G = \frac{R}{R^2 + X^2}, \ B = -\frac{X}{R^2 + X^2}$$

$$I = YV$$

$$\begin{bmatrix} I_1 \\ I_2 \\ \vdots \end{bmatrix} = \begin{bmatrix} Y_{11} & Y_{12} & \cdots \\ Y_{21} & Y_{22} & \cdots \\ \vdots & \vdots & \ddots \end{bmatrix} \begin{bmatrix} V_1 \\ V_2 \\ \vdots \end{bmatrix}$$

For bus i, if there is a line from bus i to bus j, $Y_{ij} = -y_{ij}$, while $Y_{ii} = \sum_j y_{ij} + y_{ig}$ for all lines from bus j connected to bus i. The following Figure C.1 shows one example (Wood and Wollenberg, 1996).
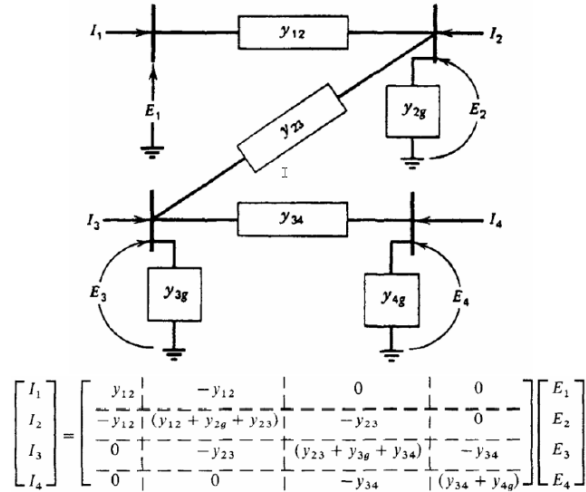

$$\begin{bmatrix} I_1 \\ I_2 \\ I_3 \\ I_4 \end{bmatrix} = \begin{bmatrix} y_{12} & -y_{12} & 0 & 0 \\ -y_{12} & (y_{12} + y_{2g} + y_{23}) & -y_{23} & 0 \\ 0 & -y_{23} & (y_{23} + y_{3g} + y_{34}) & -y_{34} \\ 0 & 0 & -y_{34} & (y_{34} + y_{4g}) \end{bmatrix} \begin{bmatrix} E_1 \\ E_2 \\ E_3 \\ E_4 \end{bmatrix}$$

Figure C.1: Admittance Example
(Wood and Wollenberg, 1996)

Net power injection into bus i,

$$S_i = P_i + jQ_i = V_i I_i^*$$

characterize I_i^*,

$$I_i = \sum_{k=1}^{N} Y_{ik} V_k$$

$$I_i^* = \left(\sum_{k=1}^{N} Y_{ik} V_k \right)^* = \sum_{k=1}^{N} Y_{ik}^* V_k^*$$

$$\Rightarrow P_i + jQ_i = V_i \sum_{k=1}^{N} Y_{ik}^* V_k^* = \sum_{k=1}^{N} V_i Y_{ik}^* V_k^*$$

Denote $Y_{ik} = \bar{G}_{ik} + j\bar{B}_{ik}$,

$$P_i + jQ_i = \sum_{k=1}^{N} V_i Y_{ik}^* V_k^*$$

$$= \sum_{k=1}^{N} (|V_i|e^{j\theta_i})(\bar{G}_{ik} + j\bar{B}_{ik})^*(|V_k|e^{j\theta_k})^*$$

$$= \sum_{k=1}^{N} |V_i||V_k|(\bar{G}_{ik} - j\bar{B}_{ik})e^{j(\theta_i - \theta_k)}$$

$$= \sum_{k=1}^{N} |V_i||V_k|(\bar{G}_{ik} - j\bar{B}_{ik})[\cos(\theta_i - \theta_k) + j\sin(\theta_i - \theta_k)]$$

Reorder the equation,

$$P_i + jQ_i = \sum_{k=1}^{N} |V_i||V_k|(\bar{G}_{ik} - j\bar{B}_{ik})[\cos(\theta_i - \theta_k) + j\sin(\theta_i - \theta_k)]$$

$$= \sum_{k=1}^{N} |V_i||V_k|[\bar{G}_{ik}\cos(\theta_i - \theta_k) + \bar{B}_{ik}\sin(\theta_i - \theta_k)]$$

$$+ j\sum_{k=1}^{N} |V_i||V_k|[\bar{G}_{ik}\sin(\theta_i - \theta_k) - \bar{B}_{ik}\cos(\theta_i - \theta_k)]$$

$$\Rightarrow P_i = \sum_{k=1}^{N} |V_i||V_k|[\bar{G}_{ik}\cos(\theta_i - \theta_k) + \bar{B}_{ik}\sin(\theta_i - \theta_k)]$$

$$Q_i = \sum_{k=1}^{N} |V_i||V_k|[\bar{G}_{ik}\sin(\theta_i - \theta_k) - \bar{B}_{ik}\cos(\theta_i - \theta_k)]$$

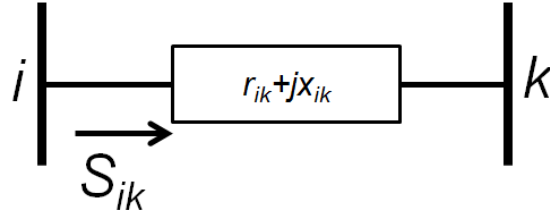Now consider the power flow for a single line as shown in Figure C.2,

Figure C.2: Power Flow for a Single Line

$$\bar{G}_{ii} = G_{ik}, \bar{G}_{ik} = -G_{ik}, \bar{B}_{ii} = B_{ik}, \bar{B}_{ik} = -B_{ik}$$

$$P_{ik} = |V_i|^2 G_{ik} - |V_i||V_k|[G_{ik}\cos(\theta_i - \theta_k) + B_{ik}\sin(\theta_i - \theta_k)]$$
$$Q_{ik} = -|V_i|^2 B_{ik} - |V_i||V_k|[G_{ik}\sin(\theta_i - \theta_k) - B_{ik}\cos(\theta_i - \theta_k)]$$

where $z_{ik} = z_{ki} = r_{ik} + jx_{ik}$, $y_{ik} = y_{ki} = \frac{1}{z_{ik}} = \frac{r_{ik}}{r_{ik}^2 + x_{ik}^2} - j\frac{x_{ik}}{r_{ik}^2 + x_{ik}^2}$

DCOPF model makes the following assumptions,

- Ignore reactive power
  - $Q_{ik} \approx 0$
- All voltages are 1 p.u.
  - $|V_i| = |V_k| \approx 1$
- Voltage angle differences across a line are small
  - $\theta_i - \theta_k \approx 0$
  - $\sin(\theta_i - \theta_k) \approx \theta_i - \theta_k$
  - $\cos(\theta_i - \theta_k) \approx 1$
- The resistance of a line is far less than the reactance of the line
  - $r_{ik} \ll x_{ik}$
  - $B_{ik} = -\frac{x_{ik}}{r_{ik}^2 + x_{ik}^2} \approx -\frac{1}{x_{ik}}$

$$
\begin{aligned}
S_{ik} &= P_{ik} + jQ_{ik} \\
&\approx P_{ik} \\
&= |V_i|^2 G_{ik} - |V_i||V_k|[G_{ik}\cos(\theta_i - \theta_k) + B_{ik}\sin(\theta_i - \theta_k)] \\
&\approx G_{ik} - [G_{ik}\cos(\theta_i - \theta_k) + B_{ik}\sin(\theta_i - \theta_k)] \\
&\approx G_{ik} - G_{ik} - B_{ik}(\theta_i - \theta_k) \\
&\approx \frac{1}{x_{ik}}(\theta_i - \theta_k)
\end{aligned}
$$

$$P_{ik} = B_{ik}(\theta_k - \theta_i) = \frac{1}{x_{ik}}(\theta_i - \theta_k)$$

The following gives the DCOPF formulation,

$$\min \quad \sum_{\forall g} C_g(p_g) \tag{C.60}$$

$$\text{s.t.} \quad L_g \leq p_g \leq H_g \qquad \qquad \forall g \tag{C.61}$$

$$\sum_{l \in \delta^+(n)} f_l - \sum_{l \in \delta^-(n)} f_l + \sum_{g \in G(n)} p_g = D_n \qquad \forall n \tag{C.62}$$

$$f_l = B_l(\theta_n - \theta_m) \qquad \qquad \forall l = (m, n) \tag{C.63}$$

$$-F_l \leq f_l \leq F_l \qquad \qquad \forall l \tag{C.64}$$

This resulting formulation is referred as B-θ formulation. By canceling bus angle variables θ, another formulation is obtained and is referred as power transfer distribution factor (PTDF) or shift factor formulation.

Let $\mathbf{B}_{L \times L}$ be a $L \times L$ diagonal matrix where each component represents the corresponding susceptance of the transmission line. Let $\mathbf{A}_{N \times L}$ be the $N \times L$ node-arc incidence matrix of the transmission network, where for each column l there is one 1 (m^{th} component) indicating that transmission line l is from bus m, one -1 (n^{th} component) indicating that transmission line l is to bus n and all other components are 0. Let $\mathbf{f}_{L \times 1}$ be the vector of line flow. Let $\theta_{N \times 1}, \mathbf{p}_{N \times 1}, \mathbf{d}_{N \times 1}$ be the vector of bus angle, power generation and load demands at the bus respectively. Then (C.62) and (C.63) can be written in the matrix form (Ruiz *et al.*, 2012),

$$-\mathbf{A}\mathbf{f} = \mathbf{d} - \mathbf{p} \tag{C.65}$$

$$\mathbf{f} = -\mathbf{B}\mathbf{A}'\theta \tag{C.66}$$

$$\Rightarrow \quad \mathbf{A}\mathbf{B}\mathbf{A}'\theta = \mathbf{d} - \mathbf{p} \tag{C.67}$$

Let $\mathbf{M}_{N \times N} = \mathbf{A}\mathbf{B}\mathbf{A}'$ be the nodal-susceptance matrix of the network. In order to cancel θ, the invertible matrix of $\mathbf{M}$ is desired. However, $\mathbf{M}$ is not invertible since $\mathbf{A}$ is not full rank matrix. Generally, rank($\mathbf{A}$) $= N - 1$, then $\mathbf{M}$ becomes invertible by eliminating one row of $\mathbf{A}$. Now introducing a reference bus, suppose the first bus is the reference bus, then the corresponding reduced matrix and vector $\mathbf{A}^-_{(N-1) \times L}, \theta^-_{(N-1) \times 1}, \mathbf{p}^-_{(N-1) \times 1}, \mathbf{d}^-_{(N-1) \times 1}$ by eliminating the first bus are obtained. $\mathbf{M}^-_{(N-1) \times (N-1)} = \mathbf{A}^-\mathbf{B}(\mathbf{A}^-)'$. Set the bus angle of the reference bus to be 0.

$$\mathbf{M}^-\theta^- = \mathbf{d}^- - \mathbf{p}^- \tag{C.68}$$

$$\mathbf{f} = -\mathbf{B}(\mathbf{A}^-)'\theta^- \tag{C.69}$$

$$\Rightarrow \quad \theta^- = (\mathbf{M}^-)^{-1}(\mathbf{d}^- - \mathbf{p}^-) \tag{C.70}$$

$$\Rightarrow \quad \mathbf{f} = -\mathbf{B}(\mathbf{A}^-)'(\mathbf{M}^-)^{-1}(\mathbf{d}^- - \mathbf{p}^-) \tag{C.71}$$

$$\Rightarrow \quad \mathbf{f} = \mathbf{B}\left[\mathbf{0}, (\mathbf{A}^-)'(\mathbf{M}^-)^{-1}\right](\mathbf{p} - \mathbf{d}) \tag{C.72}$$

$$\Rightarrow \quad \mathbf{f} = \mathbf{\Psi}(\mathbf{p} - \mathbf{d}) \tag{C.73}$$

Here the $\mathbf{\Psi}_{L \times N} = \mathbf{B}\left[\mathbf{0}, (\mathbf{A}^-)'(\mathbf{M}^-)^{-1}\right]$ is the PTDF matrix, sometimes referred as the injection shift factors (ISF) matrix, describes the power flow distribution on each transmission line when injecting one unit power from one certain bus to the reference bus. The PTDF is the result of the Kirchhoff's circuit laws. The PTDF-based DCOPF model has been adopted by many RTO/ISOs. The advantage of this model is that system operator can only include a subset of transmission lines which are the possible congested lines into the formulation and relax the ones that will not be congested. Then the number of constraints is reduced, which may improve the solution time. However, one limitation for PTDF-based model is that when the topology of the power grid changes, the PTDF will change.

The following gives the economic dispatch with network constraints (PTDF-based DCOPF formulation) (Wood and Wollenberg, 1996).

$$\min \quad \sum_{\forall g} C_g(p_g) \tag{C.74}$$

$$\text{s.t.} \quad L_g \leq p_g \leq H_g \qquad \forall g \tag{C.75}$$

$$\sum_{\forall g} p_g = \sum_{\forall n} D_n \tag{C.76}$$

$$-F_l \leq \sum_{\forall n} \Psi_{nl} \left(\sum_{g \in G(n)} p_g - D_n \right) \leq F_l \qquad \forall l \tag{C.77}$$

While this model makes many simplification assumptions such as only real power is considered, it is still one of the most important market models to start with.

C.9   Unit Commitment

The following gives a full SCUC model based on (Hedman *et al.*, 2010).

$$\min \quad \sum_{\forall t} \sum_{\forall g} C_g^{SU} v_{gt} + C_g^{NL} u_{gt} + C_g p_{gt} \tag{C.78}$$

$$\text{s.t.} \quad v_{gt} \geq u_{gt} - u_{g,t-1} \qquad \forall g, t \tag{C.79}$$

$$\sum_{i=t-UT_g+1}^{t} v_{gi} \leq u_{gt} \qquad \forall g, t \tag{C.80}$$

$$\sum_{i=t+1}^{t+DT_g} v_{gi} \leq 1 - u_{gt} \qquad \forall g, t \tag{C.81}$$

$$p_{gt} \geq P_g^{\min} u_{gt} \qquad \forall g, t \tag{C.82}$$

$$p_{gt} + r_{gt} \geq P_g^{\max} u_{gt} \qquad \forall g, t \tag{C.83}$$

$$p_{gt} - p_{g,t-1} \leq R_g^{hr} u_{g,t-1} + R_g^{SU} v_{gt} \qquad \forall g, t \tag{C.84}$$

$$p_{g,t-1} - p_{gt} \leq R_g^{hr} u_{gt} + R_g^{SD}(v_{gt} - u_{gt} + u_{g,t-1}) \qquad \forall g, t \tag{C.85}$$

$$\sum_{\forall g} p_{gt} = \sum_{\forall n} D_{nt} \qquad \forall t \tag{C.86}$$

$$-F_l \leq \sum_{\forall n} \Psi_{nl} \left(\sum_{g \in G(n)} p_{gt} - D_{nt} \right) \leq F_l \qquad \forall l, t \tag{C.87}$$

$$\sum_{\forall i} r_{it} \geq r_{gt} + p_{gt} \qquad \forall g, t \tag{C.88}$$

$$p_{gt}, r_{gt} \geq 0 \qquad \forall g, t \tag{C.89}$$

$$u_{gt} \in \{0, 1\} \qquad \forall g, t \tag{C.90}$$

$$0 \leq v_{gt} \leq 1 \qquad \forall g, t \tag{C.91}$$

Equation (C.78) is the objective includes startup cost, no-load coast and generation cost. Equation (C.79) specifies the relation between the startup variable, v_{gt}, and the unit commitment status variable, u_{gt}. Equation (C.80) and (C.81) are the generator minimum up and down time constraint. It restricts that if the generator g is turned on at period t, then it has to be on for the next UT_g periods; similarly if the generator g is turned off at period t, it has to be off for the next DT_g periods. There are many methods to model minimum up and down time constraints. Rajan and Takriti (2005) proved that the given constraints are the facet-defining constraints for u, v projection polytope. Equation (C.82) and (C.83) specify the generation level lower and upper bounds respectively. Reserve r_{gt} is included in this formulation. When the generator is not committed, i.e., $u_{gt} = 0$, then both the generation and reserve are forced to be zero. Equation (C.84) and (C.85) impose the hourly ramp rate limits along with the startup and shutdown ramp rate limits for the generators. Equation (C.86) is the power balance constraint and (C.87) is the network constraint. Equation (C.88) states that the total reserve in the power system must exceed the single largest generator contingency, which is a necessary condition to withhold system security. Equation (C.89) restricts the power generation and reserve to be non-negative. Equation (C.90) restricts the unit commitment status variable to be binary variables. Although startup variable is linearized in (C.91), the optimal solution returned form this MIP for v_{gt} will be either 0 or 1 because (C.79)-(C.81) restrict it to be so given u_{gt} are binary.